Optimum Corona Ring Design for High Voltage Compact Transmission Lines

Using Gaussian Process Model

by

Nihal Mohan

A Thesis Presented in Partial Fulfillment
of the Requirements for the Degree
Master of Science

Approved July 2012 by the
Graduate Supervisory Committee:

Ravi S. Gorur, Chair
Gerald T. Heydt
Vijay Vittal

ARIZONA STATE UNIVERSITY

August 2012

ABSTRACT

Electric utilities are exploring new technologies to cope up with the increase in electricity demand and power transfer capabilities of transmission lines. Compact transmission lines and high phase order systems are few of the techniques which enhance the power transfer capability of transmission lines without requiring any additional right-of-way. This research work investigates the impact of compacting high voltage transmission lines and high phase order systems on the surface electric field of composite insulators, a key factor deciding service performance of insulators.

The electric field analysis was done using COULOMB 9.0, a 3D software package which uses a numerical analysis technique based on Boundary Element Method (BEM). 3D models of various types of standard transmission towers used for 230 *kV*, 345 *kV* and 500 *kV* level were modeled with different insulators configurations and number of circuits. Standard tower configuration models were compacted by reducing the clearance from live parts in steps of 10%. It was found that the standard tower configuration can be compacted to 30% without violating the minimum safety clearance mandated by NESC standards. The study shows that surface electric field on insulators for few of the compact structures exceeded the maximum allowable limit even if corona rings were installed.

As a part of this study, a Gaussian process model based optimization program was developed to find the optimum corona ring dimensions to limit the electric field within stipulated values. The optimization program provides the dimensions of corona ring, its placement from the high voltage end for a given dry arc

length of insulator and system voltage. JMP, a statistical computer package and AMPL, a computer language widely used form optimization was used for optimization program. The results obtained from optimization program validated the industrial standards.

ACKNOWLEDGEMENTS

First and foremost, I would like to offer my sincerest gratitude to my advisor, Dr. Ravi S. Gorur who constantly guided, inspired and supported me at every stage of my research. I want to thank my colleagues in this project for their continuous support. I also want to express my gratitude to Dr. Gerald Heydt and Dr. Vijay Vittal for their time and consideration in being a part of my graduate supervisory committee.

Financial assistance provided by the Western Electricity Coordinating Council (WECC), a regional entity responsible for coordinating and promoting bulk electric system reliability in the Western Interconnection in North America, is greatly acknowledged.

I especially want to thank my father Kumar Bijay Mohan, my mother Rita Mohan and my sisters Shweta, Shivani and Divya for the continual inspiration and motivation to pursue my utmost goals. I also would like to thank my friends from ASU and VNIT and roommates who stood beside me and encouraged me constantly.

TABLE OF CONTENTS

LIST OF TABLES

LIST OF FIGURES

Figure Page

Figure Page

Figure Page

NOMENCLATURE

2D	Two dimensional
3D	Three dimensional
AC	Alternating current
B	Magnetic flux density vector in weber per square meter
BEM	Boundary element method
BIE	Boundary integral solution
CTL	Compact transmission lines
D	Corona ring diameter
d	Conductor diameter
DC	Direct current
D_c	Distance between conductors
D_e	Subdomain in finite element method
D_{flux}	Electric flux density vector in coulomb per square meter
E	Electric field vector in volts per meter
E–field	Electric field
EHV	Extra high voltage
E_{max}	Maximum electric field on the surface of insulator
EPRI	Electric Power Research Institute
FDM	Finite difference method
FDTD	Finite-difference time-domain method
FEM	Finite element method
FRP	Fiberglass reinforced plastics

G	Green function
H	Magnetic field vector in amperes per meter
h	Distance of corona ring from the high voltage end
HPO	High order systems
HTLS	High temperature low sag
J	Electric conduction current density in amperes per square meter
L	Insulator dry arc length
n_e	Total number of triangle elements in finite element method
NESC	National Electrical Safety Code
n_i	Unit normal vector
NIMBY	Not in my backyard
np	Total number of knots in the network
PDE	Partial differential equation
ph-g	Phase to ground
ph-ph	Phase-to-phase
ph–t	Phase-to-tower
R	Corona ring radius
r	Position vector
rms	Root mean square
ROW	Right-of-way
RPS	Renewable Portfolio Standard
RSM	Response surface methodology
S_i	Surface of materials

S_M	Coefficient matrix for finite element method
T	Corona ring tube thickness
T_j	Vector of free terms for finite element method
TML	Transmission line matrix
Vph	Phase to ground voltage
α_e	Computational coefficients for a triangular element ‘e’
ε	Permittivity of material
ρ	Volume charge density in coulombs per cubic meter
ρ_m	Magnetic resistivity of material
σ	Conductivity of material
φ	Electric potential
μ	Permeability of material

Chapter 1. Introduction to High Voltage Compact Transmission Lines and High Order System

1.1 Introduction: Present Constraints in Transmission Grid

As per US Department of Energy, it is projected that electricity demand will increase to 2% in the U.S. in the coming years [1]. While electricity generation has not been posing any issues, the bottlenecks in transmission system is hindering reliable and cost effective power transfer. It has been reported that the energy demand has increased by 25% since 1990 but new construction in transmission infrastructure has decreased by 30%. The annual investment in building new transmission infrastructure has continuously decreased over the last 25 years [1]. This situation has put an enormous pressure on the present transmission infrastructure to meet the load demand. Another issue that has aggravated the present situation is the change in the type of electricity generation. Government regulation of renewable portfolio standard (RPS) calls for addition of renewable generation portfolio in the electric grids [2]. As a result there is a growing focus on installation of large scale renewable plants. The location of the renewable plants is usually far from the load centers when compared to conventional electric generating stations, which were constructed in vicinity of load centers. Hence delivering power from distant generating stations to load centers requires increase in power transfer capacity of existing transmission system. The above mentioned reasons have resulted in congestion in the electric grid and have prevented access to lower-cost electricity generation.

Constructing new transmission lines and increasing voltage ratings have been few of the conventional approaches to address congestion. However, there have been many techno-economic and social issues associated in implementing these methods. A few of them are listed below:

1. *Obtaining new right-of-way (ROW).* High land cost has hindered the process of acquiring new ROW for constructing new lines.
2. *Stringent electric and magnetic field limits.* Government regulation put stringent limits on the maximum allowable electric and magnetic field values near ROW. This issue has particularly inhibited construction of new transmission corridors in densely populated areas.
3. *Public concern of environmental and aesthetics problems.* "Not in my backyard–NIMBY" syndrome in people has forced utilities to explore for aesthetically better designed transmission lines, thereby increasing the cost.
4. *Legislative requirements.* The lead time of transmission lines has been marred by long duration of obtaining legislative and environmental clearance for government departments. It has discouraged investors to build new transmission lines.

Hence utilities are looking for alternate techniques which would help in increasing power transfer capacity in the transmission systems, using existing or reduced ROW. Some of the techniques are listed below:

1. Compact transmission lines (CTL)

2. Higher phase order systems (HPO)
3. High temperature low sag (HTLS) conductors

Compact transmission lines first came into service in 1970s in the USA at Saratoga, New York for delivering power at high voltage transmission system with reduced ROW [3]. High phase order systems (more than 3 phases) were built in late 1970s on experimental basis and were found to be feasible for operation [4]. HTLS conductors with composite core have lower sag, better mechanical strength and current carrying capacity, but are relatively expensive and newer technology [5]. A detailed description of each technology is mentioned in the subsequence sections.

As is the case with every new technology, there are some concerns which need to be investigated and addressed before implementation. A few of the factors governing the safe and reliable operation of transmission lines are mentioned in section 1.2. One of the major factors among them is insulators performance. The performance of insulators depends on the surface electric field (E-field) on it [6]. This thesis investigates the impact on surface E-field on insulators due to compact transmission lines and high phase order system and recommends techniques to mitigate the problems.

1.2 Factors Governing Power Transfer, Transmission Line Design and Performance

In typical extra high voltage (EHV) transmission systems the power transfer capability depends on thermal or sag limits, operational stability limits, volt-

age regulation and economics. The impact of each factor depends on the line length. It is a well-known fact that short transmission lines are usually thermally limited, while long transmission lines are voltage and stability constrained. However, there exist other factors which put a limit on the power transfer capacity of transmission lines. These factors in turn decide the transmission tower dimensions and ROW requirements. Some of these factors are mentioned below [7]:

1. *Conductor's voltage gradient.* High conductor voltage gradient (Electric field) causes audio noise, radio interference and corona discharge. High voltage gradient also causes insulator's long term service performance. The maximum allowable electric field value for limiting the corona activities is recommended to be 2.1kV/mm [6]. Bundled conductors are installed to reduce the conductor voltage gradients, but robust tower structures are needed to bear higher conductor weight.
2. *Switching and lightening surges.* Voltage surges caused by lightening hit or switching operation in transmission lines could cause flashovers and insulator failures, resulting in line outage. Line insulation, air gap insulation, insulator string length must be designed to withstand voltage surges.
3. *Reduced electrical strength due to insulation contamination.* Pollution levels at the location of transmission lines determine the contamination on the surface of insulators. Contamination causes insulators to develop dry band arcing and may cause flashovers. Higher leakage distance ensures that insulators perform well in polluted areas.

4. *Electric and Magnetic field requirements*. Public exposure to high electric and magnetic field due to transmission lines has been always a concern. There are government regulations which mention the maximum allowable electric and magnetic field values in the ROW. To adhere to these values, tower dimensions are properly designed.

To address the above mentioned issues, proper safety clearances are required to be kept between the phase-to-phase (ph-ph), phase to ground (ph-g) and phase-to-tower (ph–t). The minimum clearances are mandated by the National Electrical Safety Code (NESC) standard for safe live line operation and maintenance. Table 1-1 shows minimum safety clearances as stipulated in NESC standard.

Table 1-1 Clearance in any direction from line conductors to support [18]

Maximum Operating Voltage (ph-ph)	Switching surge factor	Switching surge	Computed clearance to supports	
			Fixed	Free swinging at maximum angle
kV	*pu*	*kV*	*m*	*m*
242	3.2	632	1.24	1.22
362	2.5	739	1.84	1.59
550	1.8	808	2.14	1.84

In existing transmission structures, these clearances are kept higher than recommended NESC values for protection against lightening and switching surg-

es, swinging and galloping of conductor, as shown in Figure 1-1 for a 362 *kV* H bridge tower.

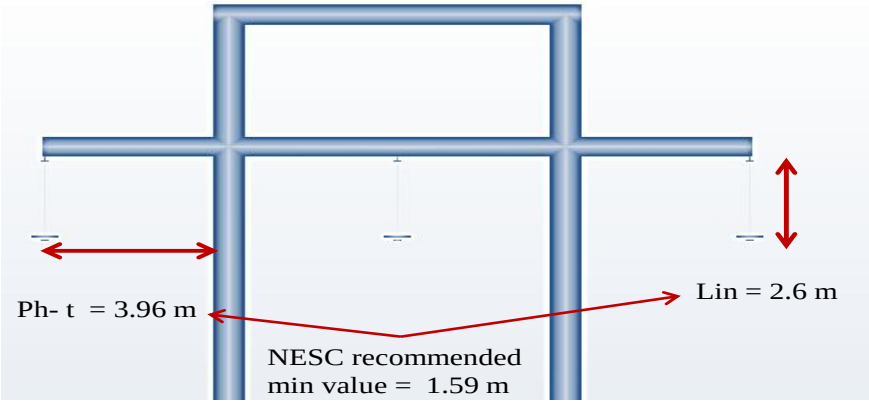

Figure 1-1 Clearances in a typical 362 *kV* H bridge tower

1.3 An Overview of Compact Transmission Lines and High Phase Order System

Compact transmission lines

To deliver power in regions of dense population and limited ROW, electric utilities have installed compact transmission lines, which have reduced clearances compared to a typical line. Figure 1-2 compares the dimensions of a conventional 230 *kV* transmission line tower with different compact structures [3].

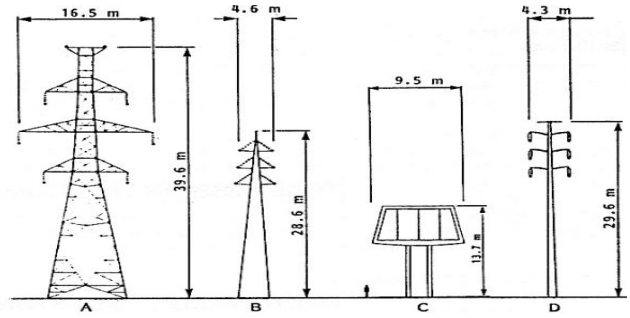

Figure 1-2 Comparative dimensions of conventional and compact 230*kV* tower structures [3]

A: Conventional lattice structure for 240-m spans

B: Twin steel pole structure for 240-m spans

C. Concrete portal structure for 105-m spans

D: Tapered steel pole structure for 240-m spans

High phase order system

A high phase order system is defined by the number of voltages of equal magnitude, equally spaced in time. While in case of a 3-phase system, three equal voltages are spaced 120^{o} in time, for a 12-phase system twelve voltages are spaced by 30^{o}. It is interesting to note that phase–phase voltage in case of a HPO may be equal or less than the phase-ground voltage, as shown in Table 1-2 [19].

Table 1-2 Phase to ground and phase-to-phase voltages for HPO

	Phase - phase (adjacent phase) voltage			
ph-g voltage	3 phase	6 phase	12 phase	24phase
kV	*kV*	*kV*	*kV*	*kV*
80	138	80	41	21
133	230	133	69	35
199	345	199	103	52

This property of HPO helps to build compact transmission system as requirement for different insulations clearance reduces. A comparative figure for tower structures required for different HPO is shown in Figure 1-3.

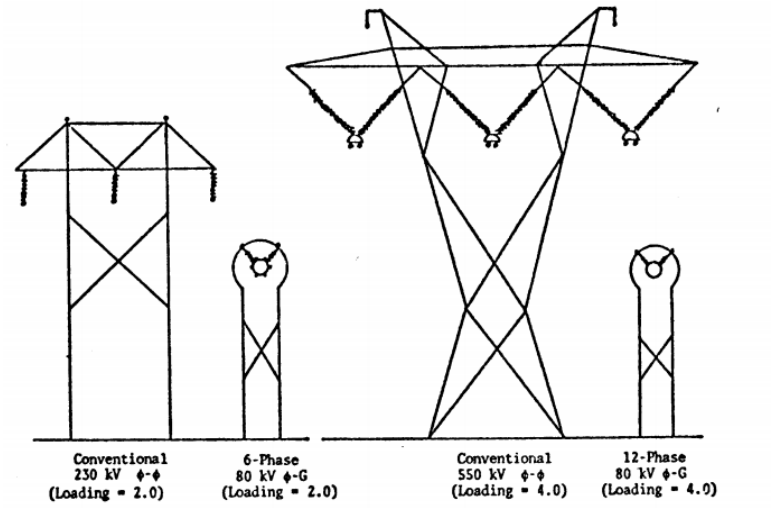

Figure 1-3 Comparison conventions and HPO tower structures [4]

It can be seen from Figure 1-3 that HPO can deliver more power using the same ROW. For HPO it is more convenient to specify system voltages in terms of phase-to-ground voltage levels.

1.4 Research Focus-the Central Objectives of this Research

There are several issues associated with each of the mentioned technologies that need to be addressed. These concerns include corona performance, high conductor gradients, fault analysis and protection schemes, conductor motion control and many more. It is important to study the impact of above mentioned parameters for safe and dependable operation of transmission system. This research examines the impact of compacting transmission lines and high phase order sys-

tem on the surface E-field on insulators, which is a key parameter for service performance of the insulators.

A lot of research has been done on electric field stress control using corona rings on conventional transmission lines. There are several published studies which have mentioned the optimum corona ring dimensions for various voltage levels [8]-[11]. Comparatively, fewer studies have been conducted for determining E-field variation due to compacting transmission line and high phase order system. With present computer power and software available, it is possible to study E-field on complex geometries with different boundary conditions. In this thesis, a method was devised with proper approximations and simplifications, to determine the surface electric field distribution on insulators. The aim was to obtain valid results without requiring excessive computational resources.

As a part of the research, a deterministic computer simulation based experiment was designed to create a multi stage model for finding optimum corona ring dimensions to limit electric field. In first stage, a Gaussian process model was developed to determine the relationship between the electric field and variables such as voltage, insulator length and corona ring parameters. Then an optimization program was written to calculate the optimum corona ring dimensions for given value of voltage and insulator dry arc length.

1.5 Scope of Study

The scope of work in the research is shown in Figure 1-4. Sixteen cases were studied for a three phase system and one case was studied for a 6 phase system.

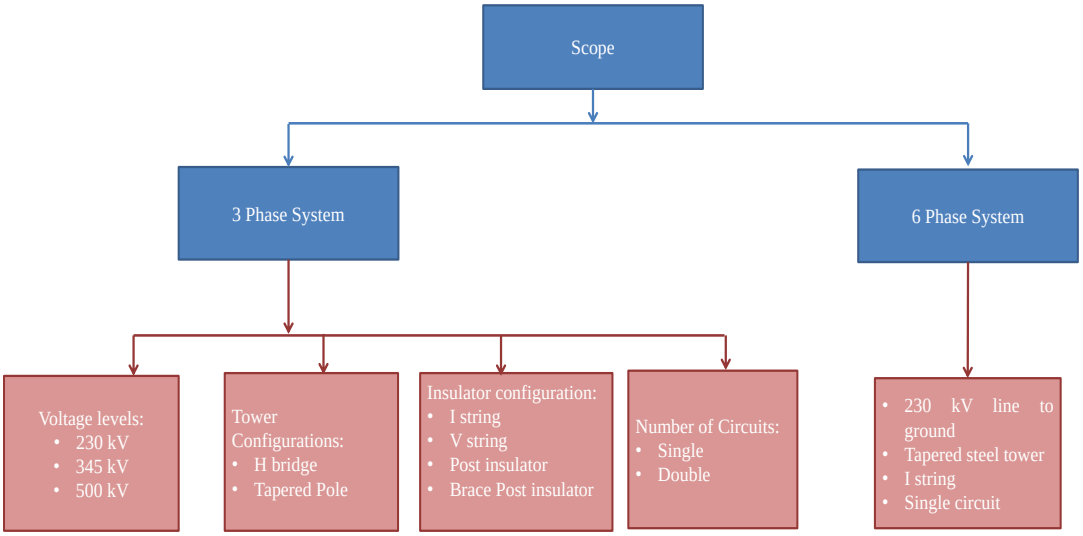

Figure 1-4 Scope of work in the research

1.6 Organization of this Thesis

This thesis consists of seven chapters. Chapter two gives a detailed description of the electric field distribution on the surface of composite insulators. Chapter three describes various methods to evaluate the electric field distribution on the surface of insulators.

Chapter four gives a detailed description of the system under study and 3–dimensional (3D) modeling of the system in COULOMB®, a software package used for determining the electric field distribution.

Results and discussions are presented in Chapter five followed by an illustration in Chapter six, describing the optimization methodology for obtaining the optimum corona ring dimensions to control the electric field. Chapter seven presents the conclusions and the future work deemed necessary.

There are four appendixes namely A, B, C and D. Appendix A contains the dimensions of various tower configurations used in the research. Appendix B and C contain the Gaussian process model based formula representing the electric field in terms of input variables. Appendix D contains a regression model of dry arc length vs. system voltage.

Chapter 2. Electric Field Distribution on the Surface of AC Composite Insulators

2.1. Introduction

A composite insulator is made up of two component systems. The first one consists of an inner rod made up of fiberglass reinforced plastics (FRP) and the second one consists of an outer body of silicone rubber. Use of composite insulators is increasing because of their light weight, superior mechanical strength and better hydrophobicity characteristics. Figure 2-1 shows cross section of a composite insulator.

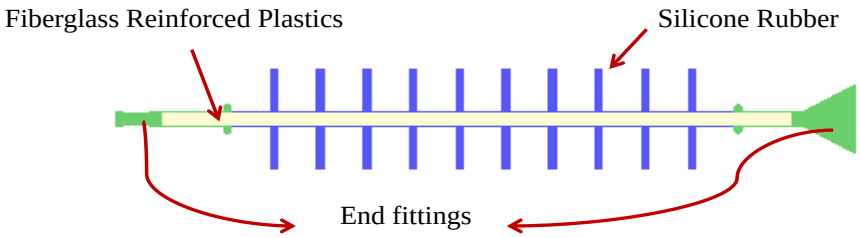

Figure 2-1 Cross section of a composite insulator

2.2. Factors Affecting Performance of Composite Insulators

There are several issues which affect the performance of composite insulators, as listed below:

1. *Handling.* Composite insulators performance can be adversely affected by mishandling during transportation, storage or installation. Any damage or minor crack developed in housing material during storage or transportation can expose the FRP rod to envoirmental conditions such as pollution and moisture ingress. These damages may lead to tracking along the core and cause brittle failure. Improper installation might put extra torsional

strain or cantilever stress on the core which could possibly crack it. Hence the composite insulators should be carefully handled for their durable performance [12].

2. *Manufacturing defects*. Manufacturing defects in composite insulators may also lead to their premature failure. During the manufacturing process, composite insulators end fitting are attached by a process called swaging [12]. This process requires high precision as no damage to the core should take place. This can be achieved by keeping an optimum tolerance between the outside core and inside hardware diameters. Proper preheat temperature for core, mold temperature and moisture control should be done to bond the polymer housing to the core post injection molding [12].
3. *Flashover*. A flashover may be caused by switching or lightning surges, which causes the dielectric breakdown of air due to ionization. Flashovers may also occur at nominal system voltage in insulators, due to dry band arching caused by contaminations. However, the flashover mechanism in composite insulators is different form the ceramic insulators [13]. It is known that composite insulators are hydrophobic in nature. The hydrophobic nature degrades due to high electrical stress and high pollution. Aged insulators lose hydrophobicity and become easily wettable. Consequently, the leakage current of insulators increases and their voltage with-

stand capacity decrease appreciably, leading to flashovers [14]. The flashovers may damage or puncture the insulators.

4. *Corona performance.* One of the major factors deciding the long term performance of insulators is the corona. Corona is caused due to high E-field on the surface of the insulators. Various factors which give rise to high E-field are mentioned in the next section. The high E-field causes electron avalanche and ionizes the air, causing corona discharge. The high speed random motion of ions is capable of causing mechanical damage to insulators. Secondly, formation of acidic water due to hydrated nitrogen oxides produced by corona might lead to corrosion of insulator surface.

   The inception of corona discharge depends on weather conditions. While in dry conditions, the corona discharge may begin at E-fields higher that 1.5 *kV/mm* [15], it might start at much lower values in contaminated conditions. Literature suggests limiting the maximum E-field on the surface of insulators up to 0.45 *kV/mm* to avoid water drop corona [6].

2.3. Factors Affecting E-Field on the Surface of Composite Insulators

The performance of composite insulators depends on E-field distribution along the surface of insulators. It is essential to understand the E-field distribution along the length of composite insulator. Factors which govern the E-field distribution of on the surface of composite insulator are listed below [6]:

1. Geometry of insulators including but not limited to fiber glass rod, end fitting and weather-shed shape

2. Electrical characteristics of polymer weather-shed and fiberglass rod material
3. Dimensions, position and method of attachment of the corona rings
4. Dimensions the attachment hardware for corona ring, conductor bundles, grounded hardware and grounded structure
5. Alignment of the insulator relative to the attachment hardware, corona rings, bundled conductors, grounded structures
6. Magnitude of energized voltage on the insulator
7. Magnitude of energized voltage, location of nearby phase wires
8. Existence of the earth

A typical E-field profile obtained from simulation for a 500 *kV* composite insulator without corona ring (neglecting the geometry of sheds) is shown in Figure 2-2.

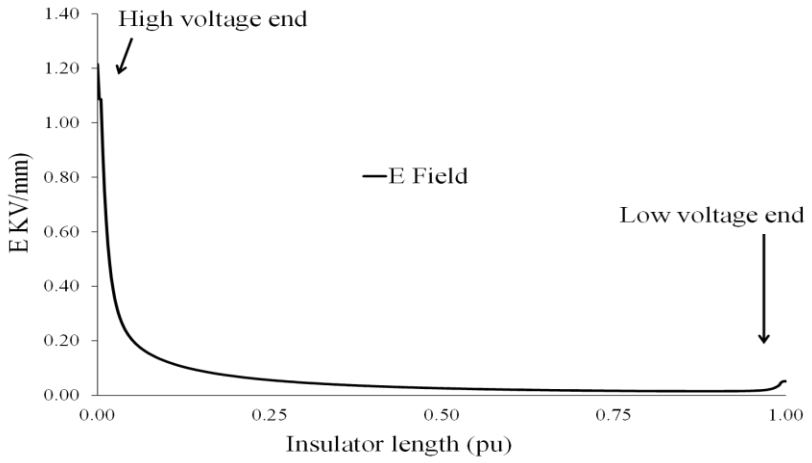

Figure 2-2 E-field distribution along the shank of 500*kV* composite insulator without corona ring

It can be observed that the electrical field stress is maximum at the junction of three media namely air, metal hardware and the insulator sheath. This junction is called a triple point, shown in Figure 2-3. Due to presence of high E-field, electron emission from the metal surface is most favorable and may cause avalanche of secondary electron emissions [17]. The electron avalanche under favorable conditions may result in flashover of insulators [16]-[17]. Thus triple point is usually considered as the location where possibility of flashover is highest in high voltage insulation.

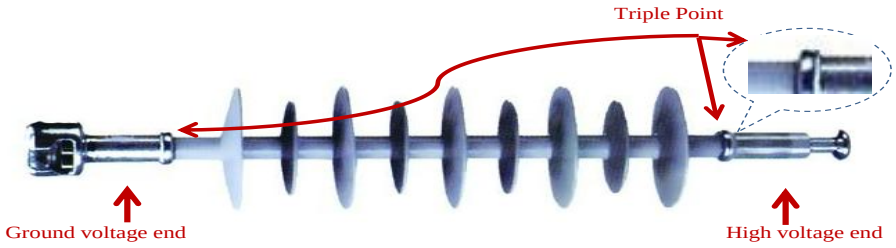

Figure 2-3 Triple point in composite insulators[1]

2.4. Methods for Controlling E-Field on Composite Insulators near Triple Point

The service performance of composite insulators critically depends on controlling the E-field near the triple point. The possible methods to control the E-field are:

1. *End fitting design*. End fitting design affects magnitude and distribution of the E-field distribution on composite insulators. However, the location maximum E-field remains near the triple point.

[1] Image source: Wenzhou Haivo Electrical Co.Ltd, website, available at: http://haivosales.en.busytrade.com

2. *Corona rings.* Conventionally corona ring have been applied to control E-field values under permissible limits. The corona ring alleviates the stress near the triple point of insulators, shifting the location of maximum E-field away from it.

The maximum permissible value of E-field mentioned in literature for the composite insulators to perform satisfactory in field is mentioned below [6]:

1. *Triple point.* 0.45 *kV/mm* (rms) maximum near the triple point measured 0.5 mm above the surface of the sheath
2. *Insulator's material.* 3.0 *kV/mm* internal to the fiberglass rod and rubber weather-shed materials
3. *Metal fittings and corona ring.* 2.1 *kV/mm* on the surface of metal fittings and corona ring. This value should be considered in conjunction with the values of E-field which reduce the radio interference and audio noise to permissible values.

2.5. Impact of Compact Transmission Lines on the E-Field Distribution of Composite Insulators

Compact transmission line has lesser phase-to-phase and phase-to-tower clearances compared to a typical transmission line. Reduced clearance causes higher E-field stress on the surface of insulators [3]. As mentioned earlier, E-field distribution decides the long term performance of insulators. Hence it is necessary to study the E-field distribution of compact structures. In this research, composite

insulators were considered for constructing compact transmission lines as they have lighter weight and better mechanical properties.

Chapter 3. Electric Field Calculation Techniques

3.1 Introduction to Electric Field Calculation Techniques

There are several methods to calculate E-field distributions. However, it has been known that electric field calculation has been a complex issue. There are several reasons for this, such as lack of analytical methods due to the complex geometry of the physical system, boundary conditions and intricate mathematical calculations. The broad categories under which electric field calculation can be categorized are analytical, experimental, analogue methods and numerical methods. Each method is discussed below with their advantages and disadvantages.

3.1.1 Analytical Methods

The analytical approach gives the exact field distribution by solving the mathematical models of simple physical geometries. For example, electric field around a point charge can be easily solved by using simple Gaussian formulae. Due to difficulties arising from the complex geometries and boundary conditions, assessing electric field distribution becomes very problematic using analytical techniques.

3.1.2 Experimental Methods

Experimental methods involve electric field measurement using probes near the physical objects to evaluate electric field. These methods are very useful for measuring electric field on objects in laboratory experiments and field testing. This method has gained popularity particularly in field testing as they provide useful inputs for determining the urgency of carrying out preventive actions or

maintenance activities for any defective equipment such as outdoor composite insulators and high voltage transformers. Experimental methods are very resource intensive and unsafe for high voltage measurements, as can be seen in Figure 3-1. Although with advent of digital probes the experimental methods have become easy to implement, these methods do not provide any information about electric field inside body of the object under investigation.

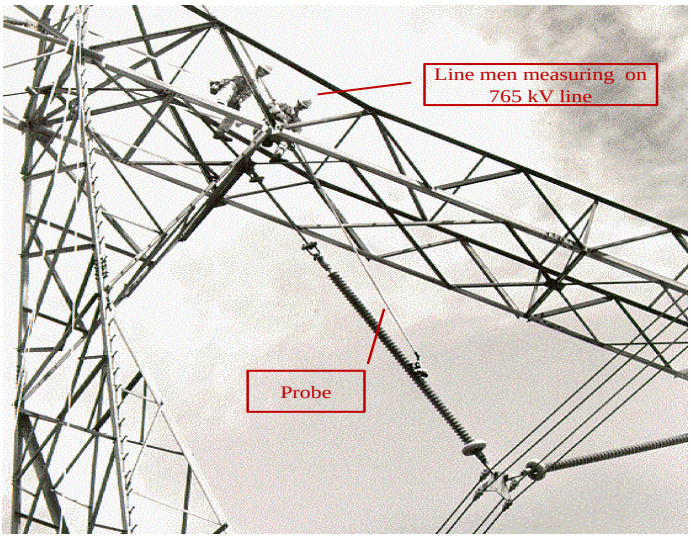

Figure 3-1 Image showing two linemen using probe to measure electric field along the composite insulators on a 735 *kV* line[2]

3.1.3 Analog Methods

Analog techniques are used when a mathematical analogy can be derived between two different objects having same dielectric distribution. For example, the relative change in the permittivity of a cable termination model can be made analogue to an electrolytic tank with different dielectric media. The conduction current between the two electrodes of the tank gives information about the electric

[2] Image source: Hydro-Québec's website, available at: http://www.positronpower.com/en/paper_ill_practical_app/Field.htm

field distribution. This method is simple and is fairly accurate for engineering problems [23].

3.1.4 Numerical Methods

Designing equipment with better electrical properties and optimized dimensions necessitated more sophisticated tools than simple analytical methods. With arrival of massive computing power, numerical methods became much more feasible to implement. It became possible to mathematically model complex geometries having non-homogenous regions, different boundary conditions using numerical methods; and these methods are capable of solving models iteratively. A broad understanding of working of various numerical methods is mentioned below.

The basic principles behind all of the numerical methods are governed by numerical representation of electromagnetic field. The electromagnetic field is governed by Maxwell's equations which are represented in vector calculus as:

$$\nabla . D = \rho_v \tag{3.1}$$

$$\nabla . B = 0 \tag{3.2}$$

$$\nabla \times E = -\frac{\partial B}{\partial t} \tag{3.3}$$

$$\nabla \times H = J + \frac{\partial D}{\partial t} \tag{3.4}$$

$$D_{flux} = \varepsilon E \tag{3.5}$$

$$B = \mu H \tag{3.6}$$

Where the capital characters represent vector quantities and

E is the electric field vector in volts per meter,

D_{flux} is the electric flux density vector in coulombs per square meter,

H is the magnetic field vector in amperes per meter,

B is the magnetic flux density vector in weber per square meter,

J is the electric conduction current density in amperes per square meter.

ρ is the volume charge density in coulomb per cubic meter.

There are various numerical methods to solve the PDE, such as finite difference method (FDM), finite element method (FEM), boundary element method (BEM) and transmission line matrix (TLM) method. The electromagnetic field is usually a time varying field and can be solved by FDM or TLM. Periodically varying fields can be solved by Maxwell equations and can be further simplified to Helmholtz equations [25]. For a static electric or magnetic field (time invariant charge or current), the field equations are governed by Laplace equations and can be solved by FDM, FEM and BEM. In general, for continuous charges in alternating current (AC) or direct current (DC) problems, FEM and FDM are better choices. For the problems where the material boundary is easily defined, BEM is most appropriate [25].

A. Finite Difference Method

In general electromagnetics, the finite difference method is called the finite-difference time-domain method (FDTD) because it is a time-stepping method, where the electromagnetic properties are updated at each time interval to obtain next value of solution. This method divides the object of interest into an interlocking lattice of 3D cubes as shown in Figure 3-2. The electric and magnetic

field components are decided at a particular point on each cube using various algorithms.

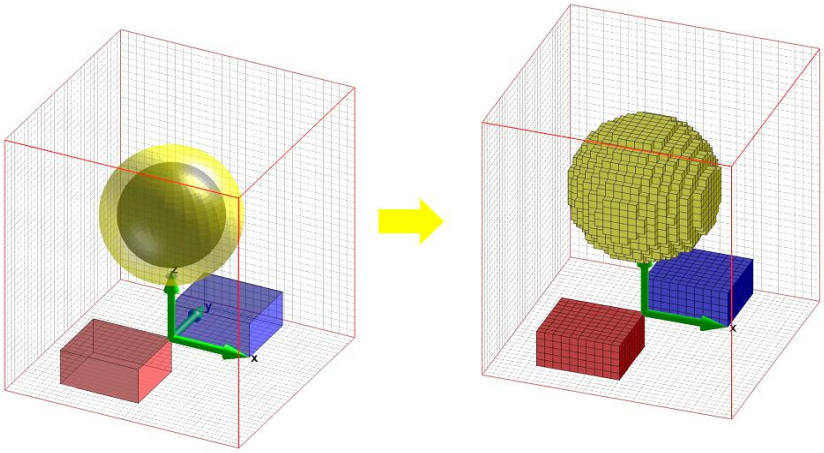

Figure 3-2 FDM formulations in 3D[3]

For materials having field-independent, direction-independent, and frequency-independent electric and magnetic properties, Maxwell's curl equations take the following form:

$$\frac{\partial H}{\partial t} = -\frac{1}{\mu}\nabla XE - \rho_m H \tag{3.7}$$

$$\frac{\partial E}{\partial t} = -\frac{1}{\varepsilon}\nabla XH - \frac{\sigma}{\varepsilon} \quad E \tag{3.8}$$

Where,

H and E are as per previous definition,

μ is the permeability,

ε is the permittivity,

ρ_m is the magnetic resistivity and

σ is the conductivity of the material under investigation.

[3] Image source : R. Bargallo, "Finite Element course for Electrical Engineers," available at: http://www.aedie.org/eeej/webrevista/articulos/librosONLINE/EFRBP2006FULL.pdf

It should be noted that ρ is taken to be zero, however to show the similarity between the two equations, it is demonstrated here. Equations (3.7) and (3.8) can be split into scalar quantities in x, y and x directions as shown below:

$$\frac{\partial H_x}{\partial t} = -\frac{1}{\mu}\left(\frac{\partial E_y}{\partial z} - \frac{\partial E_z}{\partial y} - \rho H_x\right) \qquad \frac{\partial E_x}{\partial t} = -\frac{1}{\varepsilon}\left(\frac{\partial H_y}{\partial z} - \frac{\partial H_z}{\partial y} - \sigma E_x\right)$$

$$\frac{\partial H_y}{\partial t} = -\frac{1}{\mu}\left(\frac{\partial E_z}{\partial x} - \frac{\partial E_y}{\partial x} - \rho H_y\right) \qquad \frac{\partial E_y}{\partial t} = -\frac{1}{\varepsilon}\left(\frac{\partial H_z}{\partial x} - \frac{\partial H_y}{\partial x} - \sigma E_y\right)$$

$$\frac{\partial H_z}{\partial t} = -\frac{1}{\mu}\left(\frac{\partial E_x}{\partial y} - \frac{\partial E_x}{\partial z} - \rho H_z\right) \qquad \frac{\partial E_z}{\partial t} = -\frac{1}{\varepsilon}\left(\frac{\partial H_x}{\partial y} - \frac{\partial H_x}{\partial z} - \sigma E_z\right)$$

This set of coupled six partial differential equation forms the basis of solution for FDTD, which can be solved by many algorithms [26]. The most popular algorithm was proposed by Yee in 1966 [27].

B. Finite Element Method

E-field defined by Poisson's equation is given as:

$$\nabla^2 \varphi(\vec{r}) = -\frac{\rho(\vec{r})}{\varepsilon} \tag{3.9}$$

Where $\varphi(\vec{r})$is electric potential, $\rho(\vec{r})$ is the space charge density, $\vec{r}$ is the position vector. For an isotropic media with constant ε and no space charge density, following holds true:

$$\nabla^2 \varphi(\vec{r}) = 0 \tag{3.10}$$

If distribution of φ is found which satisfies equation (3.10), then electric field can be calculated as negative gradient of electric potential distribution given by:

$$E(\vec{r}) = -\nabla\varphi(\vec{r}) \tag{3.11}$$

and the charge distribution on the conductor surfaces can be determined from sur-

face-charge density [28]

$$\rho_s = \varepsilon E_n, \tag{3.12}$$

To understand the principle for FEM, for assumption mentioned for equation (3.10) that the domain (D) under consideration has constant ε and no space charge density, it can be shown that two-dimensional electrostatic potential function $F(\varphi)$ in the Cartesian system of coordinates can be written as [29]:

$$F(\varphi) = \frac{1}{2}\int_D \left[\varepsilon_x \left(\frac{d\varphi}{dx}\right)^2 + \varepsilon_y \left(\frac{d\varphi}{dy}\right)^2\right] dx \cdot dy \tag{3.13}$$

Where ε_x and ε_y are the x and y components of the dielectric constant in the Cartesian system of coordinates. For isotropic medium ($\varepsilon_x = \varepsilon_y = \varepsilon$), equation (3.13) becomes

$$F(\varphi) = \frac{1}{2}\int_D \varepsilon \left[\left(\frac{d\varphi}{dx}\right)^2 + \left(\frac{d\varphi}{dy}\right)^2\right] dx \cdot dy \tag{3.14}$$

To obtain the solution for φ, the domain is discretized in smaller triangular subdomain D_e, and a linear variation of voltage φ is assumed to be:

$$\varphi_e(x, y) = \alpha_{e1} + \alpha_{e2} * x + \alpha_{e3} y \tag{3.15}$$

Where $\varphi_e(x, y)$ is the electric potential of any arbitrary point inside each subdomain D_e, α_{e1}, α_{e2} and α_{e3} are the computational coefficients for a triangular element "e", and "n_e" is the total number of triangle elements.

To calculate the value of electric potential at every knot in the total domain composed of several triangular elements, the function $F(\varphi)$ is minimized [29]:

$$\frac{dF(\varphi_i)}{d\varphi_i} = 0 \; ; i = 1,2, \ldots n \cdot p \tag{3.16}$$

Where $n \cdot p =$ total number of knots in the network

From equation (3.16), for every knot in the network, a matrix can be formed as [29]:

$$[S_{Mji}][\varphi_i] = \left[T_j\right]\ j, i = 1,2, \ldots n \cdot p \qquad (3.17)$$

Where $[S_{Mji}]$ is the coefficient matrix, $[\varphi_i]$ vector of unknown values of the potential at the knots and $[T_j]$ is the vector of free terms.

The set of matrix mentioned above can be solved using many numerical techniques such as Gauss–Seidel iterative method [29].

C. Boundary Element Method

As discussed in above sections, FEM and FDM require entire domain to be discretized. Hence these methods are better suited for the regions where the potential is bounded, as the total number of equations required to be solved will be proportional to the number of discrete elements in that volume. For an unbounded volume, there will be massive set of equations to be solved, requiring excessive computations resources.

BEM is based on discretization of an integral solution which is formulated such that it is mathematically equivalent to the PDE to be solved. This reformulation of PDE is done such that this integral is defined on the boundary of the domain and integral relates the boundary solution to the solution at points in the domain. This numerical technique is termed as boundary integral solution (BIE) and also popularly known as boundary element method (BEM). Reformulation of PDE in integral equations is limited to only a certain type of PDE. Therefore BEM is applicable only for certain type of PDE solution, unlike FEM or FDM.

The advantage of BEM is that is often results in numerical method which is easier to apply and is computationally more proficient.

To understand concepts underlying the BEM methodology, consider following case. It is known that by using Green's theorem, Laplace's equation can be expressed in integral form [30]. For the assumption that a medium consists of various homogenous materials having only surface charges, mathematical manipulation can give an expression for voltage which can be represented as surface integral over the unknown charges [31].Then an integral equation can be formulated by setting the integral to known values of voltage on the conductors.

These integral equations can be solved for given surface charge densities by approximating the integral as a sum over small surface elements with assumed uniform charge density. The value of the sum is set equal to the value of voltage at the center of each discrete element on the surface. This process results in obtaining a set of linear algebraic equations which can be solved by various numerical techniques.

The computational efficiency of BEM comes from the fact that only the boundary of the domain of the PDE requires discretization, whereas in case of FEM or FDM, the whole domain is required to be discretized. To understand the concepts of BEM consider Figure 3-3 shown below.

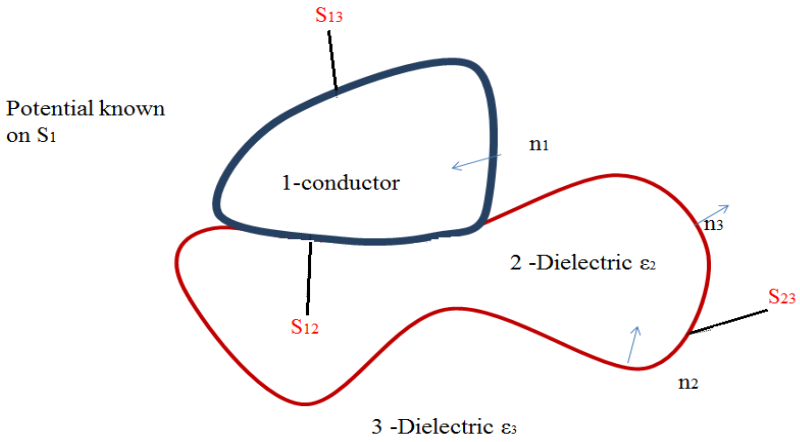

Figure 3-3 Diagram for understanding BEM formulation

Here n_i represent unit normal vector, inward to the surface S_i, where S_i = $(S_{ij} + S_{ik})$. Following boundary conditions are known:

$$\varphi_1 = \varphi_2 = \varphi_{1S} \text{ a known quantity on } S_{12} \tag{3.18}$$

$$\varphi_1 = \varphi_3 = \varphi_{1S} \text{ a known quantity on } S_{13} \tag{3.19}$$

$$\varphi_2 = \varphi_3 \text{ on } S_{12} \tag{3.20}$$

$$\varepsilon_2 \nabla\varphi_2 \cdot n_2 = \varepsilon_2 \frac{\partial\varphi_2}{\partial n_2} = -\varepsilon_3 \frac{\partial\varphi_3}{\partial n_3} = \varepsilon_3 \nabla\varphi_3 \cdot n_3 \text{ on } S_{23} \tag{3.21}$$

$$\varphi_3 = 0 \text{ at the infinite boundary} \tag{3.22}$$

$$\frac{\partial\varphi_1}{\partial n_1} = 0 \text{ on } S_1 \text{ on the conducting surface} \tag{3.23}$$

`For above mentioned boundary conditions and for electrostatic field, the voltage φ_i on i^{th} region satisfies the Laplace equation given by:

$$\nabla^2 \varphi_i(\bar{x}) = 0 \tag{3.24}$$

To solve above equation, consider a Green function which satisfies following condition:

$$-\nabla_x^2 G \quad (\bar{x}, \bar{\xi}) = \delta(\bar{x} - \bar{\xi}) \tag{3.25}$$

Where $$G(\bar{x},\bar{\xi}) = \frac{1}{4\pi R} = \frac{1}{4\pi(\bar{x} - \bar{\xi})} \quad (3.26)$$

The subscript x in equation (3.26) indicates that derivatives are taken with respect to the field coordinates x. To obtain the solution, following steps are followed:

- Add product of equation (3.25) and equation (3.27) to product of equation(3.26) and $\varphi_i(\bar{x})$
- Integrate the obtained equation over volume V_i and apply Green's theorem

Following result is obtained:

$$\int_{S_i} \{ -G(\bar{x},\bar{\xi}).\frac{\partial \varphi_i(\bar{\xi})}{\partial n_i} + \varphi_i.\frac{\partial G(\bar{x},\bar{\xi})}{\partial n_i} \}.dS_i = \begin{cases} \varphi_i(\bar{x}); \text{ for } (\bar{x}) \text{ in } V_i \\ 0; \text{ for } (\bar{x}) \text{ in } V_i \end{cases} \quad (3.27)$$

Equation (3.27) is applicable for all the 3 boundaries, which can be solved numerically using the algorithms proposed in literature [31] [32][33].

Chapter 4. System Modeling in COULOMB

4.1 Introduction to System Modeling

This chapter outlines 3D modeling concepts for the system under study in COULOMB V9.0 software. Following steps give a broad understanding of modeling procedure. Details of the system follow in subsequent sections.

1. At first a 3D geometric model of the physical system was constructed in the software. Dimensions of the physical components were taken from reputed composite insulator manufacturers' catalog, literature and EPRI Red Book [3][7].
2. The model was then assigned physical properties such as voltage and type of material.
3. The 3D model was discretized into two dimensional (2D) small "elements" having triangular shape, as a BEM solver was used.
4. The correctness of the solution was determined by calculating difference between the line integral of electric field along a segment and the voltage drop along that segment. A maximum limit of 5% difference was allowed in this study.

4.2 Description of Physical System

A physical system of transmission tower consisting of many components which are necessary to be modeled, is shown in Figure 4-1. A brief description of each component is provided thereafter.

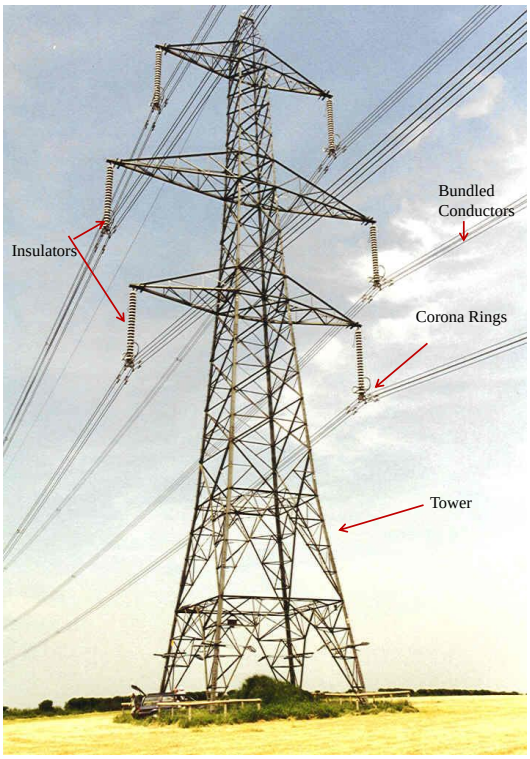

Figure 4-1 A typical transmission tower and installed components[4]

4.2.1 Tower Structure

A tower could be made up of lattice steel structure, tapered steel pole or a wooden pole structure. The basic function of tower is to provide support to conductors. These towers are solidly grounded to protect lines against lightening hits and back flashovers. From the modeling point of view, these towers provide the grounding (zero potential) structures and influence the electric field distribution.

4.2.2 Composite Insulators

Insulators perform the basic function of providing mechanical link for suspending conductors from towers and giving electrical insulation from high

[4] Image source: http://www.eng.uwo.ca/people/esavory/tower.htm

voltage part to towers. The electric field on the surface of composite insulators is the main subject of the study, as its aim is to quantify the impact on electric field due to line compaction.

4.2.3 Conductors

Conductors are the physical medium for energy transfer in transmission lines. As a practice, transmission line use bundled conductors for reducing electric surface gradient on the insulators and metal hardware, radio interference and audio noise. Modeling conductors is very important for achieving correct estimates of electric field values [21].

4.2.4 Metal Hardware

Metal hardware is used to suspend conductors on insulators and connect insulators to towers. The design of metal hardware is vital for transmission lines as it provides the necessary mechanical link and also determines electric field distribution [6].

4.2.5 Corona Rings

Corona rings are metallic toroid, usually attached to the high voltage end of insulators to control the electric field. Corona ring distributes the electric field values such that the maximum electric field value is below corona inception limit of air. Corona rings are recommended to be installed in transmission lines with system voltage of 230 kV or greater [3]. For a 230 kV or below system voltage level, corona ring is required only at the high voltage end of insulators. However,

for extra high voltage systems, corona rings are required at the both ends to control the electric field values, as shown in Table 4-1 [11].

Table 4-1 Corona ring diameter for different voltage levels

System voltage rating	Corona ring	
(*kV*)	Line-end (diameter, in)	Grounded-end (diameter, in)
138	No ring	No ring
230	8	No ring
345	15	8
500	15	15
765	15	15
1000	30	30
1200	30	30

4.3 3D Modeling of Components

This section describes the methodology of modeling each component for simulations. Major dimensions, geometry, material types and assumptions made for of each component are described below.

4.3.1 Tower Structures

A metallic tower structure provides a grounded structure in modeling, thus influencing electric field distribution. The geometry of different towers determines the electric field distribution; hence it is necessary to accurately model the tower structure [21]. Two main types of tower structure were modeled with different insulator configuration and number of parallel circuits, as shown in Table

4-2. Details of each type of tower are provided in APPENDIX A. All the towers modeled were assumed to be steel.

Table 4-2 Tower configurations studied for simulation

Voltage level		H bridge	Tapered steel tower		
230 *kV*	Insulator config.	I	P	I	BP
	No of circuits	○	○ / ○○	○ / ○○	○ / ○○
345 *kV*	Insulator config.	I	V	I	BP
	No of circuits	○	○	○ / ○○	○ / ○○
500 *kV*	Insulator config.	V	x	I	BP
	No of circuits	○		○ / ○○	○

Where

I: I string insulator ○: Single circuit P: Post insulator

V: V string insulator ○ / ○○: Single and double circuit BP: Braced post insulator

4.3.2 Composite Insulators

Insulators perform the basic function of providing mechanical link for suspending conductors from towers and providing electrical insulation between high voltage components and the tower. Typically there are two main types of composite insulators, a) suspension insulators and b) post insulators. While suspension insulators are the most commonly used type of insulator in transmission structures, post insulators are used when a high ratio between strength and weight, pollution resistance, brittle resistance behavior, highly restricted right-of-way re-

quirement and aesthetically better looking transmission lines are required. Interestingly, post insulators are also used in the areas that are highly prone to vandalism [22].

A combination of suspension and post insulators can be designed to cater the mechanical strength and electrical clearance requirements, as shown in Figure 4-2. An I and V insulator string is made up of suspension insulators. Braced post insulators assemblies are categories under "armless" transmission towers, as there is no cross-arm to support the tower structure. Also known as "Horizontal V," these structures have two major components, one a horizontal post type insulator and other a suspension insulator or brace attached to the end of the horizontal post insulator as shown in Figure 4-2. Application of braced post insulators started in 1960s in the USA for developing compact structures in urban areas [40][41].

I String V string Post Insulator Braced Post

Figure 4-2 Types of insulator configuration[5]

Simplified models of composite insulators

In this research a simplified model of the insulator is modeled, which includes only fiberglass rod covered with silicon material, simplified end fittings as

[5] Image sources: http://www.eng.uwo.ca/people/esavory/tower.htm and [41]

shown in Figure 4-3 . No watersheds were modeled because of primary reasons mentioned below:

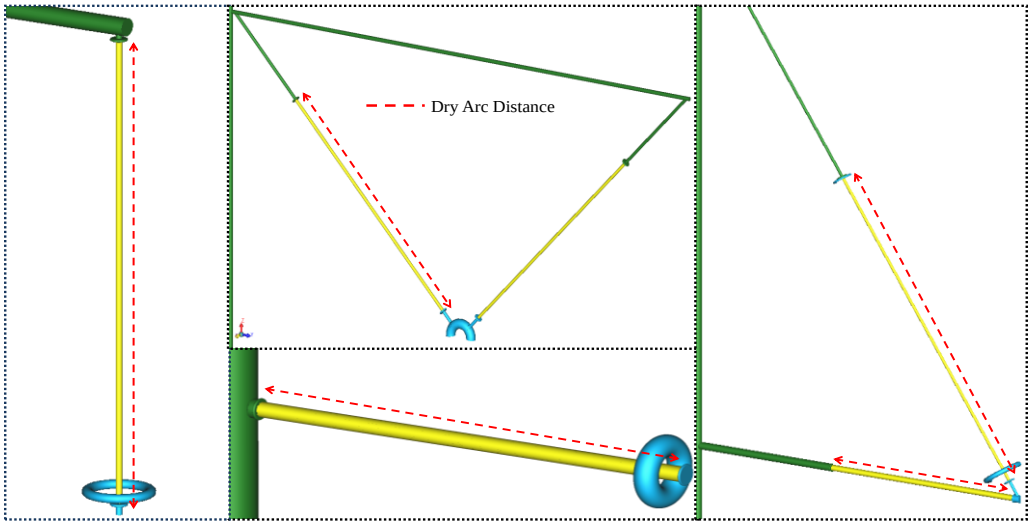

Figure 4-3 Simplified models of composite insulators modeled in COULOMB

a. Since the primary objective of the research is to quantify the maximum surface electric field on insulators due to line compaction and nearby phases, a simplified model of insulator is suitable. Literature indicate that the relative difference between electric field values of two models, one with watersheds and the other without it, is around 1.7% at the high voltage end and 4% at ground end of the insulator. The minor difference in the results indicates that omitting watersheds will not adversely affect the accuracy of the results [21] [35].

b. Computational resources are very high for a model which has conductors, tower, insulators and corona rings as components. The file size for the model was found to be in the range of 20 megabytes and can have more than 80,000 elements in mesh to solve. With Intel Pentium G6950/2.8 GHz processor, 8

GB RAM, it might take more than 8 hours to solve a single model. Hence to minimize the computational requirements, water sheds were not modeled.

The four insulator configurations as shown Figure 4-2 were modeled for different voltage levels. However, for each type of configuration for a particular voltage level, the dry arc distance for suspension and post insulators were kept constant as shown in Table 4-3. The dry arc distance for insulators was taken from the catalogs of reputed manufacturers and literature [11] [36][37][38][39].

Table 4-3 Major dimensions for the insulators

Voltage rating (*kV*)	Dry arc distance *(mm)*		Shank diameter *(mm)*	
	Rod insulator	Post Insulator	Rod insulator	Post Insulator
230	2000	1780.8	16	31.75
345	2600	2045.00	16	31.75
500	5000	3005.00	16	31.75

4.3.3 Conductors

It is very important to include conductors in modeling as the electric field results can vary to a significant extent and can lead to incorrect estimations [21]. Conductors reduce electric surface gradients on the insulators and metal hard-ware, due to their shielding effect. Following cases clearly show the importance of modeling conductors to estimate the correct electric field values:

a. For 345 *kV* and higher voltage level, with standard dimensions of corona ring installed, computer simulations indicated that the maximum value of

electric field was not under the specified limits. However, after conductors were included in the models, maximum electric field fell within the limits.

b. It is known that the post insulators in brace post configuration do not require corona ring for 230 *kV* voltage level. Only the suspension insulators have the corona ring installed on it. In absence of conductors, the maximum electric field on the post insulators was found to be higher than the limiting value, as shown in Figure 4-4. Hence it is very important to model conductors for insulators not having any corona ring, as conductors provide the primary grading effect.

There is no available standard which mentions the length of the conductor required to be modeled for simulation; some studies have explored the effect of modeling conductors as long as twice, four times or even eight times the insulator length [21]. Considering the computational requirements, the conductor length was maintained at twice the dry arc length of insulators for all the simulations. Aluminum made Bluebird conductor having diameter of 1.762" was considered for all models. For 345 *kV* and above, bundled conductors were modeled. A bundle consisted of two conductors separated by a distance of 18" [7].

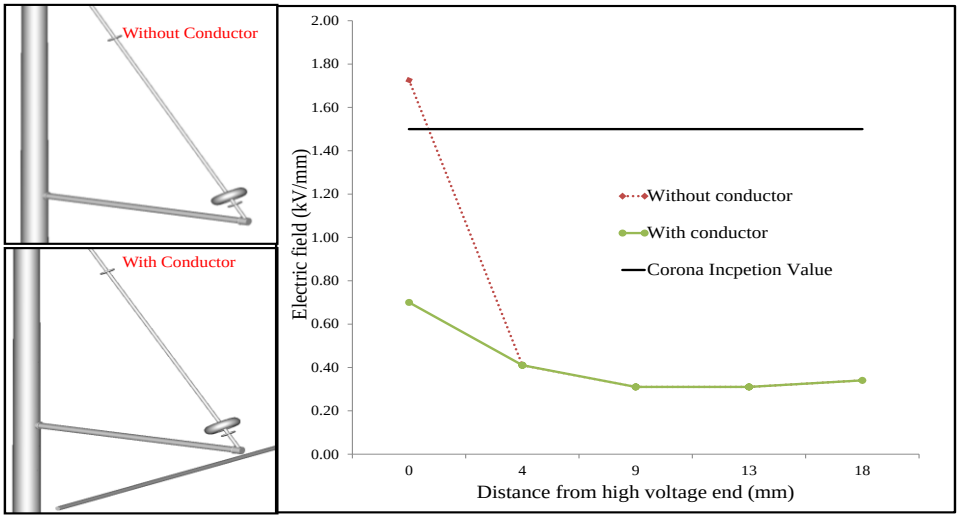

Figure 4-4 E-field values for brace post insulator model with and without conductor

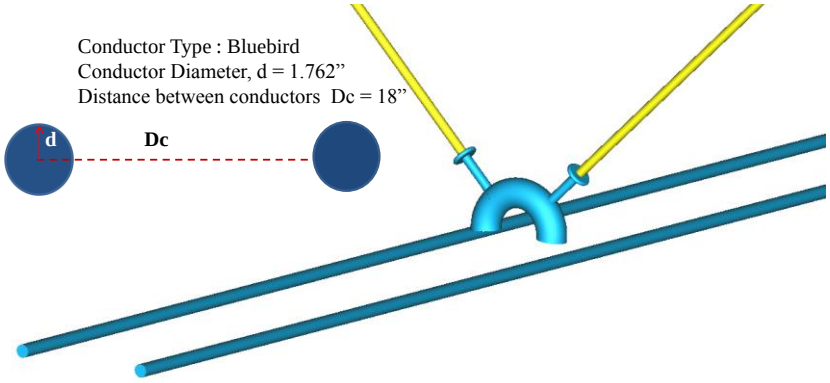

Figure 4-5 conductor modeling

4.3.4 Corona Ring

Corona ring is the most important component to control the electric field on surface of insulators. A corona ring is modeled as a steel toroid whose axis lies along the shank of composite insulators. The three main parameters of a corona ring which determine the magnitude and location of maximum surface electric field are corona ring diameter - *D*, corona ring tube thickness- *T* and distance of corona ring from the high voltage end - *h*, as shown in Figure 4-6. Impact of each factor is studied in detail while building the optimization model.

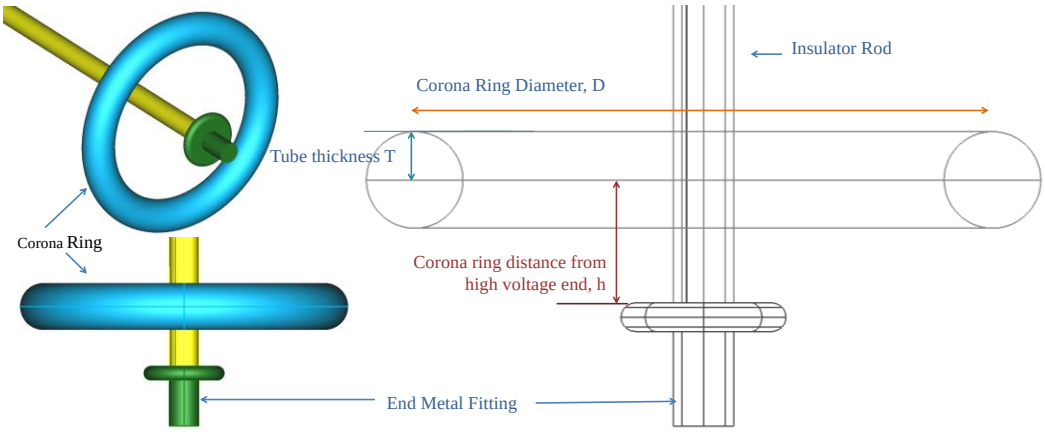

Figure 4-6 Corona ring dimensions

Following table shows the dimensions of corona ring considered for each voltage level in the models.

Table 4-4 Major dimensions for the insulators

Voltage rating *(kV)*	Position of corona ring	Corona ring dimension			
		D(in)	*R (mm)*	*T(mm)*	*h(mm)*
230	High Voltage end	8.35	106	45	90
	Ground end	----	----	----	----
345	High Voltage end	12	152.4	25	60
	Ground end	----	----	----	----
500	High Voltage end	15.75	200	25	100
	Ground end	8	102	10	100

4.3.5 Metal Hardware

Metal hardware was found necessary to be modeled in case of V sting insulators, to get reasonable values of electric field on the surface of insulators. In ab-

sence of metal hardware, computer simulation of V sting insulators showed distorted voltage contours near high voltage end of insulators giving rise to strong electric field.

4.4 Assigning Physical Properties and Boundary Conditions

Each of the components was assigned physical properties such as type of material boundary conditions, as shown in Table 4-5. The material library provided in COULOMB was used to assign the material type. For a 3 phase system, the boundary condition for each phase is shown in Table 4-6.

Table 4-5 Phsycial properties and boundary condition for each component

S. No	Component	Material	Boundary condition (voltage)
1.	Towers	Steel	Zero potential
2.	Composite insulators	End fittings: Steel	High voltage end fittings : Respective line to ground voltage Low voltage end fittings : Zero voltage
		Shank: Silicone rubber	Shank: to be determined by simulation
3.	Conductors	Aluminum	Respective line to ground voltage
4.	Corona Rings	Steel	Respective line to ground voltage

4.5 Discretization of 3D Model- Assigning 2D Elements

Pertaining to explanations provided in Section 3.1.4, all the models are discretized in 2D elements, as shown in Figure 4-7. A higher number of elements

improved the accuracy of the solution, but increased the computational time increases quadratically [34]. A compromise between high accuracy and computational constraint is to be arrived, depending on the area of interest of research.

Table 4-6 Boundary condition on each phase

	Phase voltage magnitude *(Vph* is *Phase to ground Voltage)*		
	A (*kV*)	B (*kV*)	C (*kV*)
System Voltage↓	$1.1 * V_{ph} \angle 120^{o}$	$1.1 * V_{ph} \angle 0^{o}$	$1.1 * V_{ph} \angle -120^{o}$
230 *kV*	-73.03	146.07	-73.03
345 *kV*	-109.55	219.10	-109.55
500 *kV*	-158.77	317.54	-158.77

4.6 Error Validation

In order to validate the results, following error checks were performed using basic principles of electromagnetics,

1. The difference between the line integral of electric field along a segment and the voltage drop along that segment was calculated. Theoretically it should be zero. Suitable assumptions and simplifications were made to limit the difference (error) within 5%.
2. It was verified that the tangential component of the electric field, both inside and outside the boundary of the insulator is equal. Also, the normal component of the electric field along a medium boundary should be in inverse proportions relative to the dielectric constant of the two media.

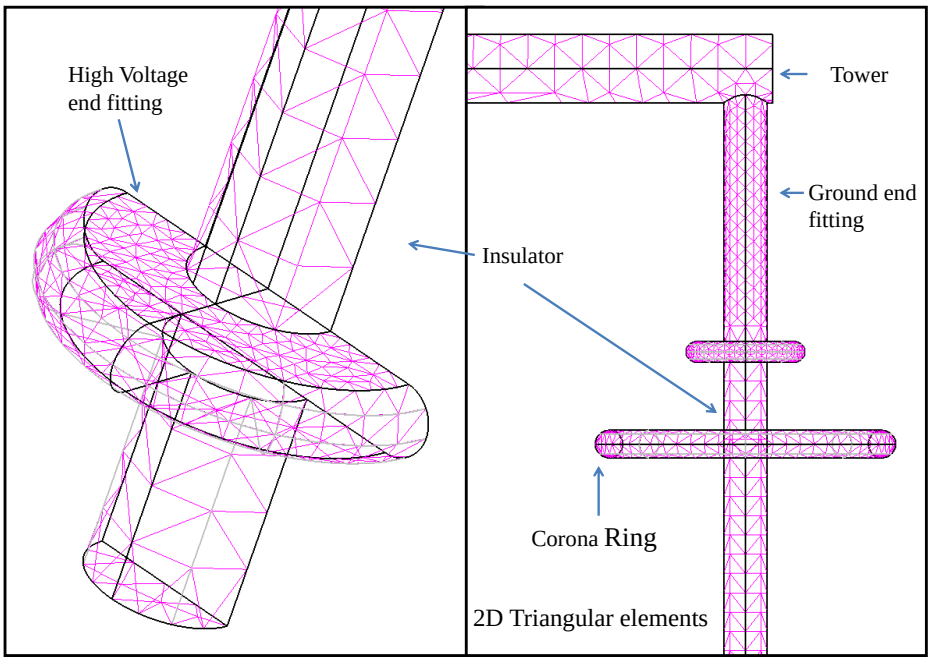

Figure 4-7 2D elements in model

3. The consistency of simulation was verified by increasing the number of 2D mesh elements. It was ensured that the results obtained do not vary to a large extent.

4.7 Methods to Reduce Computation Time

For 500 *kV* simulations, the computational time for solving the 3D model was excessively long. The symmetric nature of the structure along Z axis was used to build computer models, which reduced the computational time to a great extent. Secondly, a 64 bit version of COULOMB was used to reduce the computational time.

Chapter 5. Electric Field Study on Surface of Composite Insulators for Compact Transmission Line

5.1 Introduction

Compact transmission lines came into existence in the USA around 1970s with arrival of transmission class horizontal post insulators [41][42]. The other design popular for the compact transmission lines were braced post insulators. Braced line post insulators, also known as “Horizontal V” structures were first introduced by Lapp Insulator Company, USA. In the initial designs, the post insulator would be made of porcelain insulators. However, with the advent of composite insulators, compact structures were equipped with composite insulators. Composite insulators are better suited for compact transmission lines as they are light weight, have better mechanical properties and have superior hydrophobic characteristic than ceramic insulators. Additionally, composite insulators are less prone to failures due to vandalism and are easier to maintain [40][14]. Composite class post insulators were reported to be used by Florida Power and Light Company for compact transmission lines since 1977 at 138 kV [41]. Figure 5-1 provides a perspective on size of a composite and ceramic insulator under similar condition.

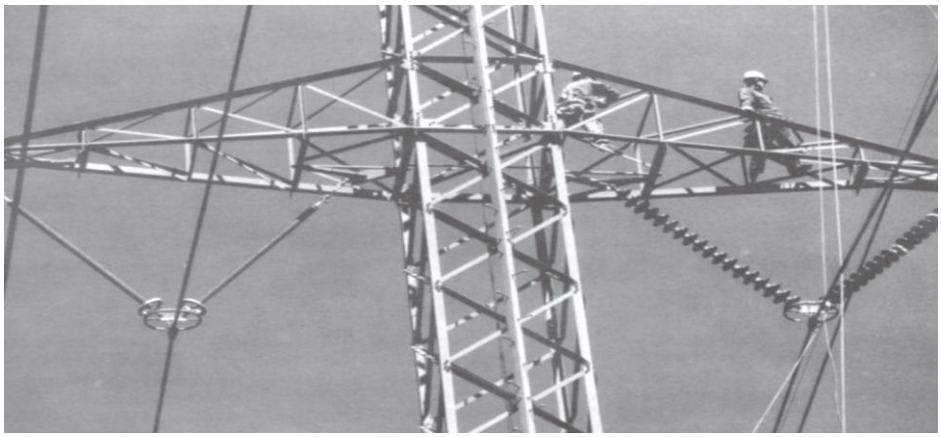

Figure 5-1 A composite insulator and polymer insulator on same tower[6]

Compact transmission lines also require phase-to-phase spacers be placed on the conductors along the mid-span to damp the conductor motion, maintain the clearances and avoid flashovers. Composite insulators are better suited for spacers as they are light weight, have high mechanical strength and possess stable bending behavior under high compressive strength [43].

There are few issues with composite insulators, such as composite insulators undergo greater mechanical and electrical stress when compared to a ceramic insulator. The failure of composite insulators is dependent on stress, temperature and period of service [44]. It is known that with time, the hydrophobic nature of composite insulators degrades due to high electrical stress and environmental factors [44]. Aged insulators lose hydrophobicity and become easily wettable. Consequently, the leakage current of insulators increases and their voltage withstand capacity decrease appreciably [44] [45].

[6] Image source : http://www.supergenameres.org/Other%20Information/OHL%20Meeting%2008/Reliability_of_Composite_Insulators_Seminar.pdf

Compacting transmission line puts a greater electric field stress on the composite insulators as electric field is enhanced due to reduced clearances. Figure 5-2 shows change in voltage profile along the length of insulator with decrease in dry arc length.

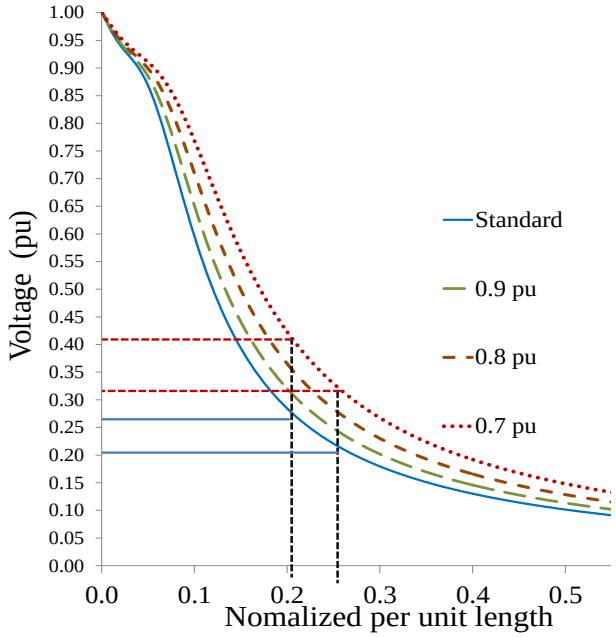

Figure 5-2 Voltage profile for different length of an insulator

It can be observed that reducing the insulator length increases the stress in voltage lines, thus increasing the electric field. Further, compact transmission line also have reduced phase-to-phase clearances, hence electric field could increase to a greater extent. Therefore, it is necessary to quantify the electric field increment on insulators due to line compaction and design suitable corona rings to mitigate the problem. In this chapter, electric field increment on the surface of composite insulators due to line compaction is assessed for various tower configurations, number of circuits and voltage levels.

5.2 Description of Case Study

For the 3 phase system, a total 15 types of models were built with the combination of voltages, tower and insulator configuration and number of circuits. For a 6 phase circuit, only one type of model was considered.

5.3 Case Formulation

Compact transmission lines for each of 15 tower configuration mentioned in Table 4-2 was modeled. Each tower was compacted in following manner:

- The dry arc length of insulator, phase-to-phase distance and tower height was reduced in steps of 10%
- In case of tapered steel tower, the phase-to-tower distance was also reduced in same proportion

Thus 70 % compact tower would mean that all the above mentioned dimensions are 70% of the original tower configuration. Figure 5-3 shows a comparison between a 100% and 70% tower dimensions. All the cases were limited to 70% compaction, as the dry arc length of the insulator reaches to its minimum allowable value stipulated in NESC standards.

5.4 Results of Computer Simulation for 230 *kV* Compact Structures

Results obtained from computer simulations are summarized for each case in the following sections.

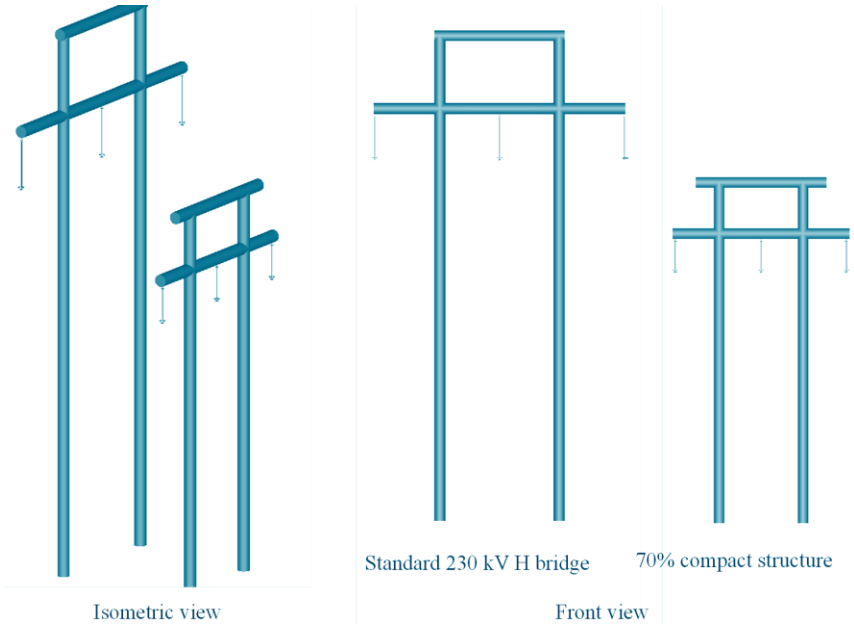

Figure 5-3 A comparative image for 230 kV standard and compact structures

5.4.1 Case-1 Configuration- 230 *kV* H Bride Tower with Single Circuit

3D model built for H Bridge and tapered pole structures for 230 *kV* is shown in Figure 5-4, with phase sequence and the voltage vector on that phase. Phase B was assumed to be at the peak of voltage vector and at the same point of time, phase A and C were at the negative half of voltage vector. This combination gave the worst case scenario for phase B insulator, as it was experiencing the maximum voltage. Voltage magnitude on each tower is shown in Figure 5-4.While assigning the boundary conditions; each phase was assigned voltage magnitude as shown in Table 4-6, which is at the time stamp of the voltage vector shown in Figure 5-4. A 10% overvoltage in each of the phase was considered for all simulations. Simulations were done for 90%, 80% and 70% compact structures for each case.

No conductors were modeled, hence the limiting value of electric field on insulator surface was chosen to be 0.40 *kV/mm.* Simulations were done for 90%, 80% and 70% compact structures for each case.

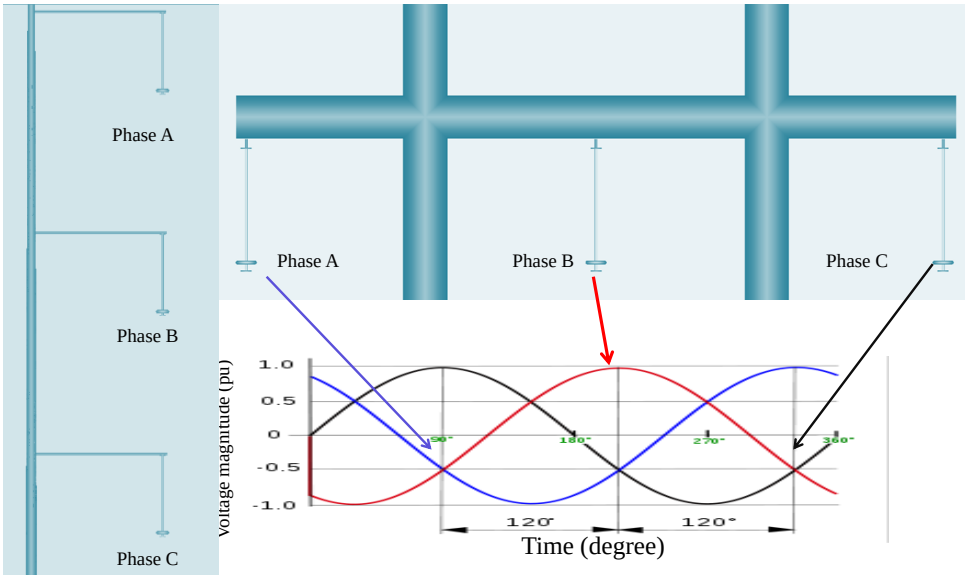

Figure 5-4 Phase sequence on H bridge tower

Table 5-1 Phase voltage magnitude for 230 *kV*

System voltage : 230 *kV*, V_{ph} = 132.8 *kV*			
Phase →	A (*kV*)	B (*kV*)	C (*kV*)
Phase voltage magnitude	-73.03	146.07	-73.03

Figure 5-5 shows the electric field distribution on the three phase insulators for case b) standard configuration. An insulator has been shown to understand the distribution of electric field along the length.

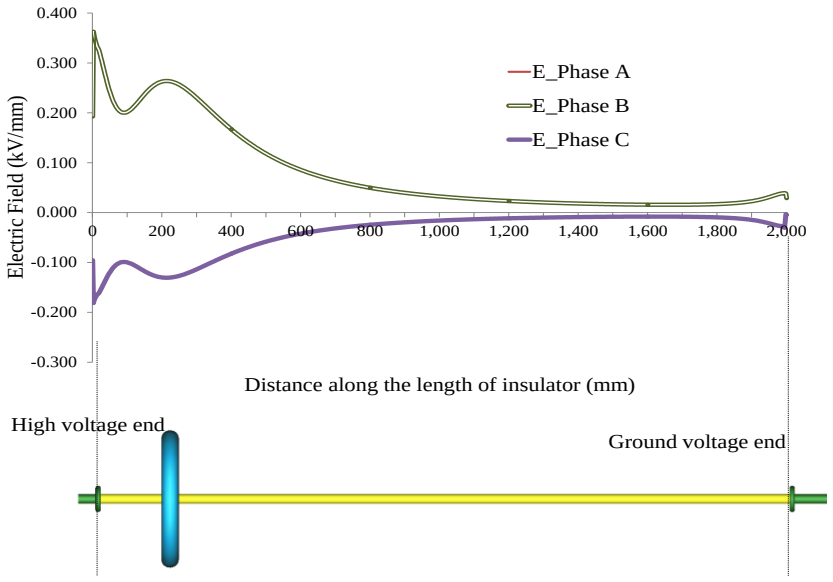

Figure 5-5 E-field distribution along the insulator in case-1 configuration

The results indicated that the maximum electric field occurred in phase B, near the "Triple Point" and another peak was observed near corona ring location. The electric field values were found to be within the limit of 0.40 *kV/mm.*

Figure 5-6 shows the electric field distribution on phase B of each compact structure for different compaction level. The results indicated that maximum electric field value increased with line compaction. While in standard configuration the dimension of corona ring was sufficient to keep the electric field value within the limit, in compact configurations the diameter of corona ring were required to be changed as shown in Table 5-2. The change in corona ring dimension

was done by an educated guess. Later in the research, an optimization program was developed to calculate the optimum value.

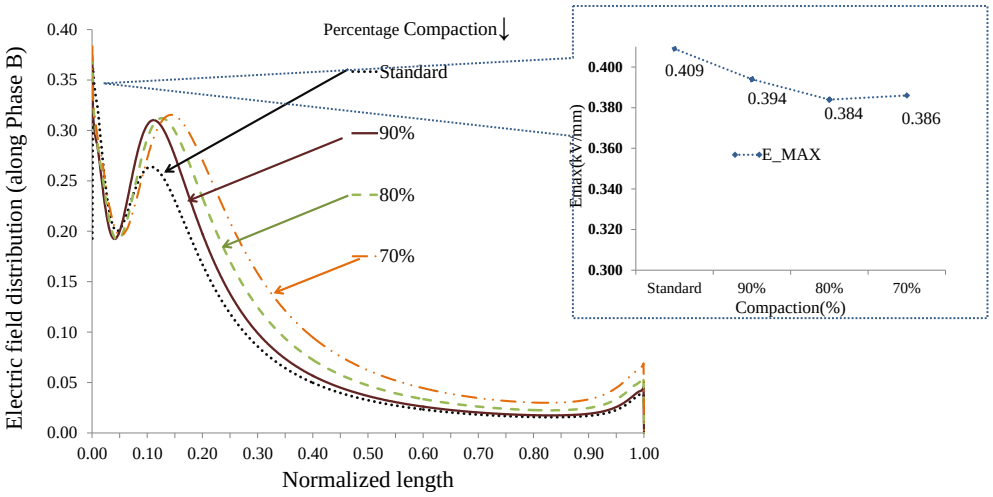

Figure 5-6 E-field distribution on phase B for case-1 configuration

Table 5-2 Corona ring dimensions for 230 *kV* compact structures

Corona Ring dimensions for % Compaction				
Tower compaction →	Standard	90%	80%	70%
T (mm)	45	45	45	45
h (mm)	90	90	90	90
R (mm)	106	115	120	120
D (in)	8.35	9.06	9.45	9.45

Henceforth, for all the simulation for 230 *kV* structures, the upper value of electric field was chosen to be 0.40 *kV/mm* in the results sections. Figure 5-7 shows the maximum electric field on phase B insulator surface vs. the corona ring diameter for each configuration. Similar figures shall be provided to discuss the electric field value and respective corona ring dimensions.

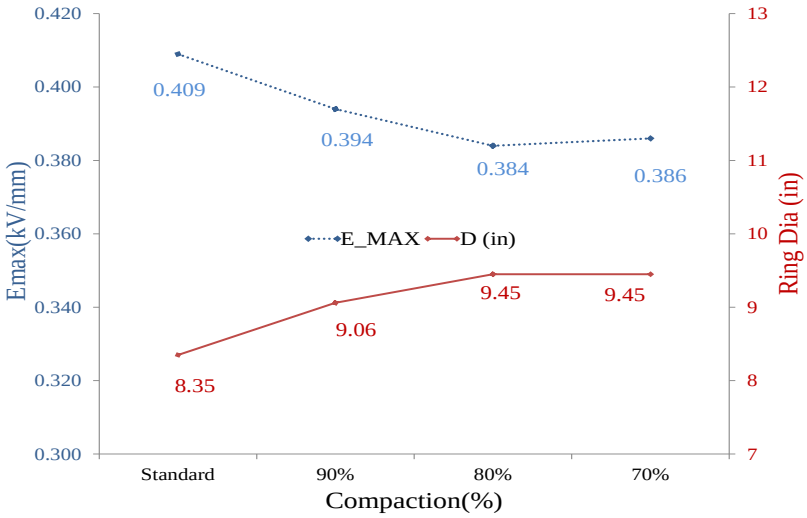

Figure 5-7 E-field distribution on phase B for compact structures for case-1

Error Check:

Error check was done by evaluating the line integral of electric field and comparing the value with the applied boundary condition. This functionality is provided in COULOMB®. The error was found to be less than 1% as shown in Figure 5-8, which was found to be the case for all the other simulations.

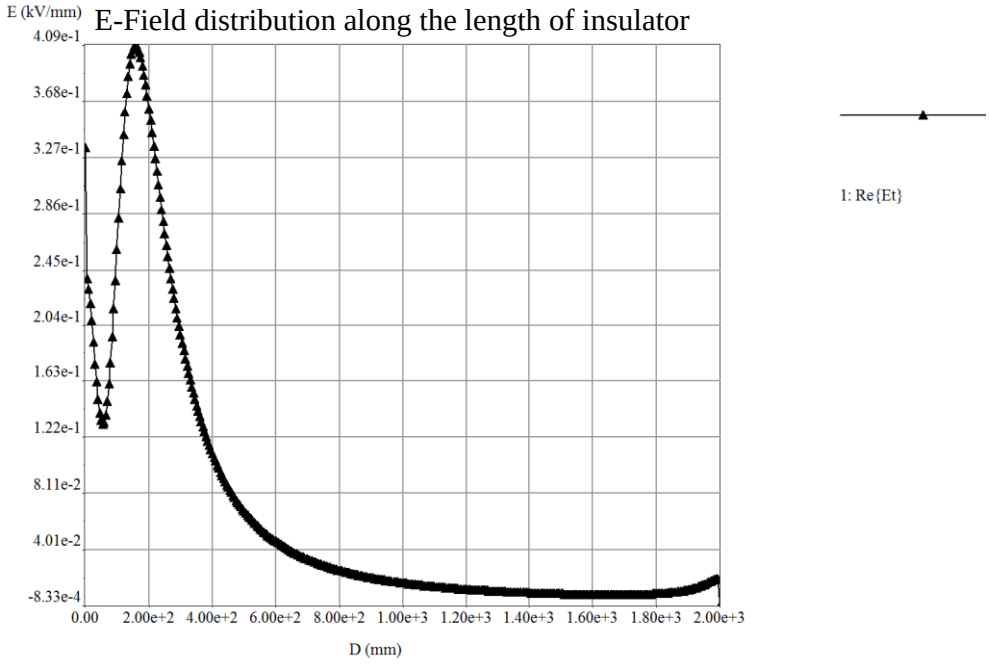

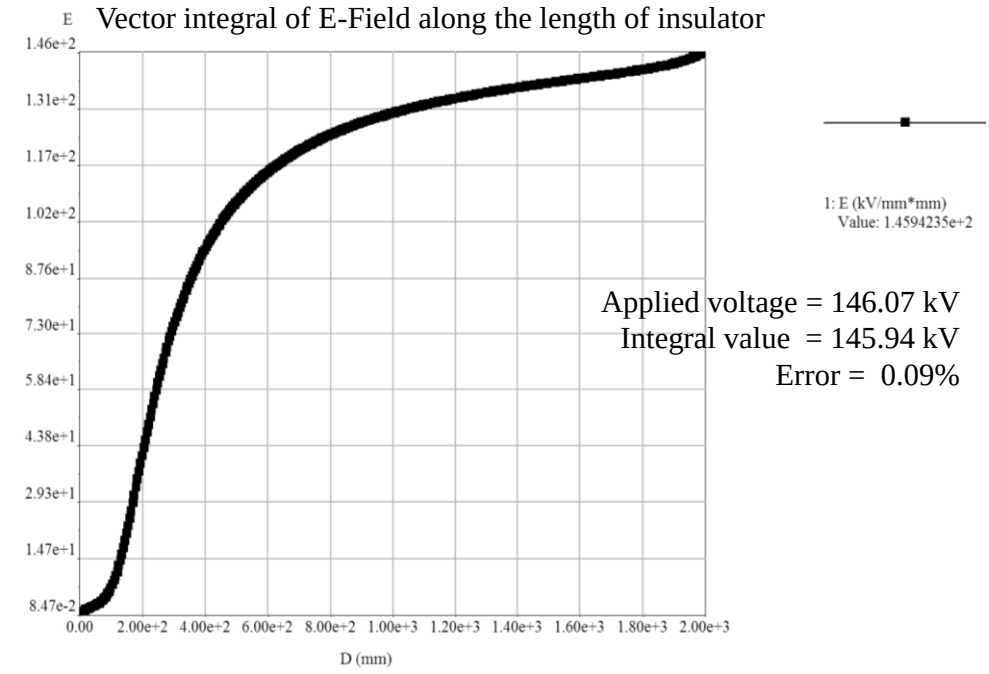

Applied voltage = 146.07 kV
Integral value = 145.94 kV
Error = 0.09%

Figure 5-8 Error check in COULOMB® for simulations

5.4.2 Case-2 Configuration- 230 *kV* Tapered Steel Pole Single Circuit

Simulations were conducted for standard and compact structures for tapered steel poles with I string insulators with single circuit. Corona ring dimensions mentioned in Table 5-2 was modeled in this case. Figure 5-9 shows the electric field distribution for phase B for all configurations.

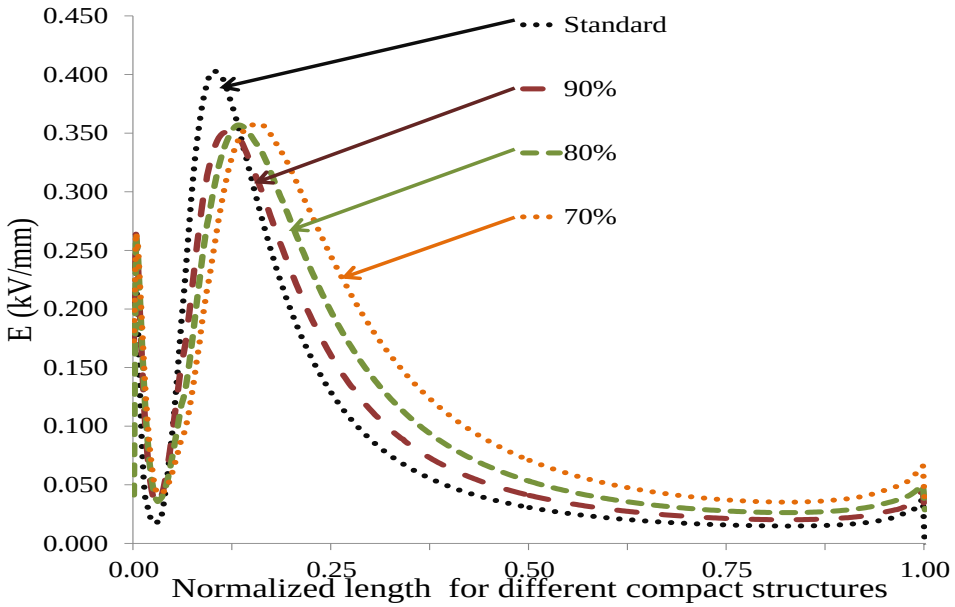

Figure 5-9 E-field distribution on phase B for case-2 configuration

It was found that the corona ring dimension had to be changed to restrict maximum electric field value within limits, as shown in Figure 5-10. The tower configuration and corresponding 3D model in COULOMB® is also shown.

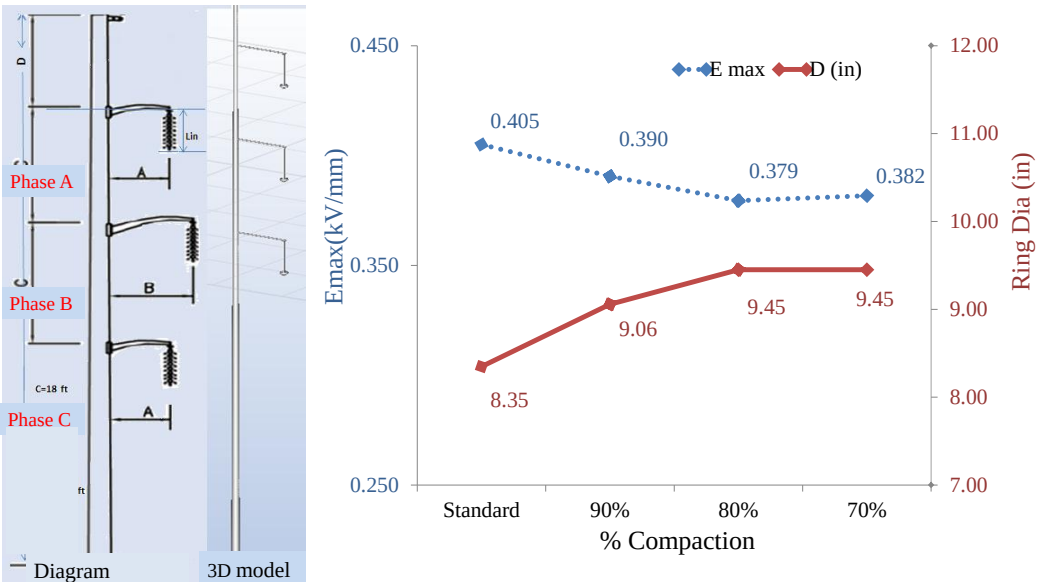

Figure 5-10 E-field vs. corona ring diameter for case-2 configuration

5.4.3 Case-3 Configuration- 230 *kV* Tapered Steel Pole Double Circuit

With all the parameters such as tower dimension, corona ring dimensions kept unchanged as per case-2, simulations were carried out for double circuit configurations to study the effect to nearby phases on compact structures. Figure 5-11 shows the pole configuration and corresponding maximum electric field on phase B of each compact structure in case-3.

The results indicated that the electric field on the surface of insulators rose marginally due to presence of nearby phases. The corona ring dimension which was used in single circuit configuration was adequate to contain the electric field value within the limit.

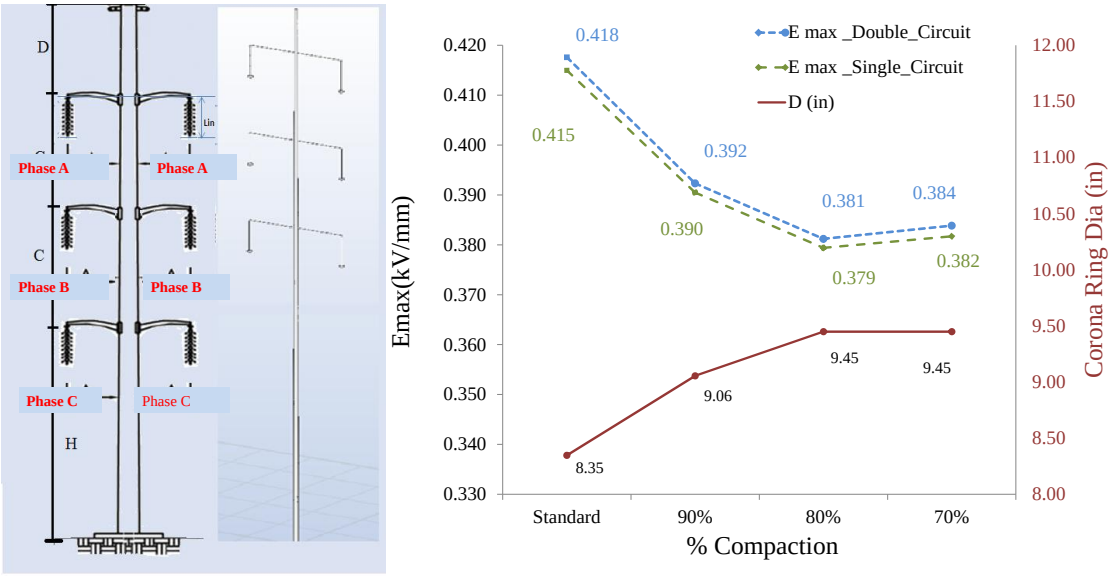

Figure 5-11 E-field vs. corona ring diameter for case-3

5.4.4 Case-4 Configuration- 230 *kV* Tapered Steel Pole Post Insulator Single Circuit (Delta)

A 230 *kV* tapered steel tower with post insulators in delta configuration was modeled. 230 *kV* post insulators may require corona ring to be fitted [47]. In this research, the post insulators were fitted with manufacturer recommended corona rings [36]-[39].Figure 5-12 shows the corroding maximum electric field on phase B and the corona ring diameter for each of the compact structure for case-4.

The results indicated that appropriate dimension of corona ring was necessary to limit the surface E-field on insulators for compact transmission lines. In this case the optimum dimension of corona ring was estimated by an educated guess.

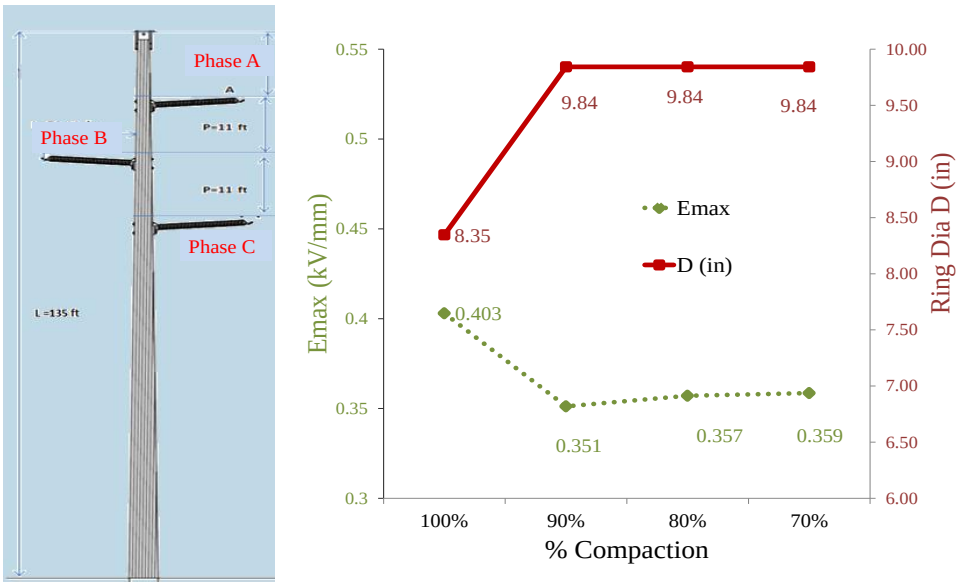

Figure 5-12 E-field vs. corona ring diameter for case-4

Table 5-3 shows overall dimensions of corona ring used for simulation.

Table 5-3 Corona ring dimensions for case-4

% compaction → / Corona ring dimension ↓	Standard	90%	80%	70%
T (mm)	45	45	45	45
h (mm)	90	90	90	90
R (mm)	106	125	125	125
D (in)	8.35	9.84	9.84	9.84

5.4.5 Case-5 Configuration- 230 *kV* Tapered Steel Pole Post Insulator – Double Circuit

A double circuit configuration for a post insulator was modeled as shown in Figure 5-13. Maximum electric field on the surface of phase B insulator for

each compact structure is shown, along with the corona ring dimension. All the parameters such as tower dimension, corona ring dimensions were kept unchanged, as per case-4.

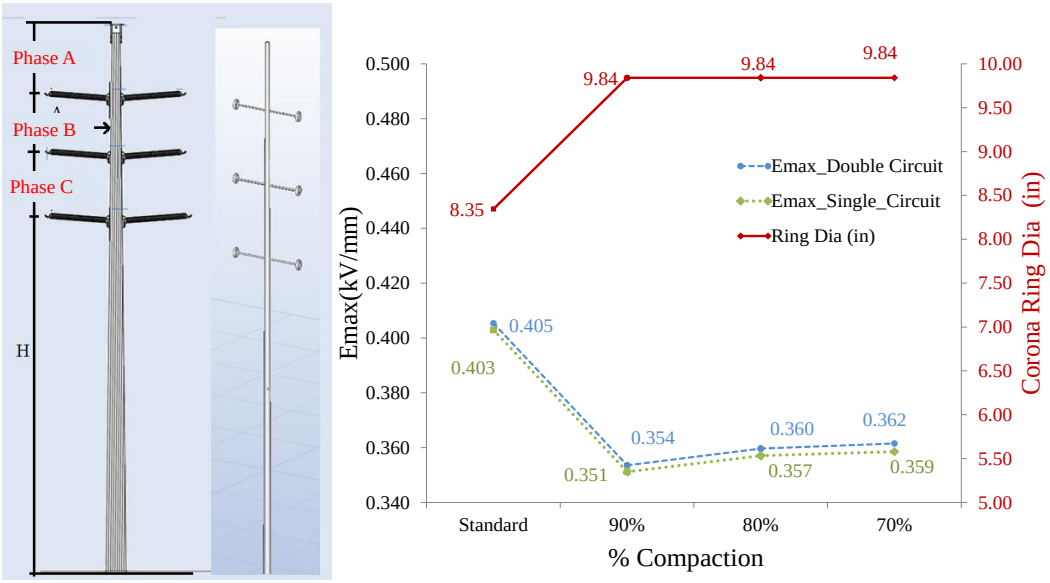

Figure 5-13 E-field vs. corona ring diameter for case -5

Similar to the result for tapered pole double circuit configuration for string insulator, the results indicated that the electric field on the surface of insulators rose marginally due to presence of nearby phases, but were found to be in limits.

5.4.6 Case-6 Configuration- 230 *kV* Tapered Steel Braced Post Insulator–Single Circuit

Study was carried out for braced post insulator for 230 *kV* tower structures. As explained in Section 4.2.3, the Bluebird conductors were also modeled for obtaining correct estimation of electric field. Figure 5-14 shows the electric field line along the length of the suspension type and post type insulator; the corona ring is used only for the brace insulator.

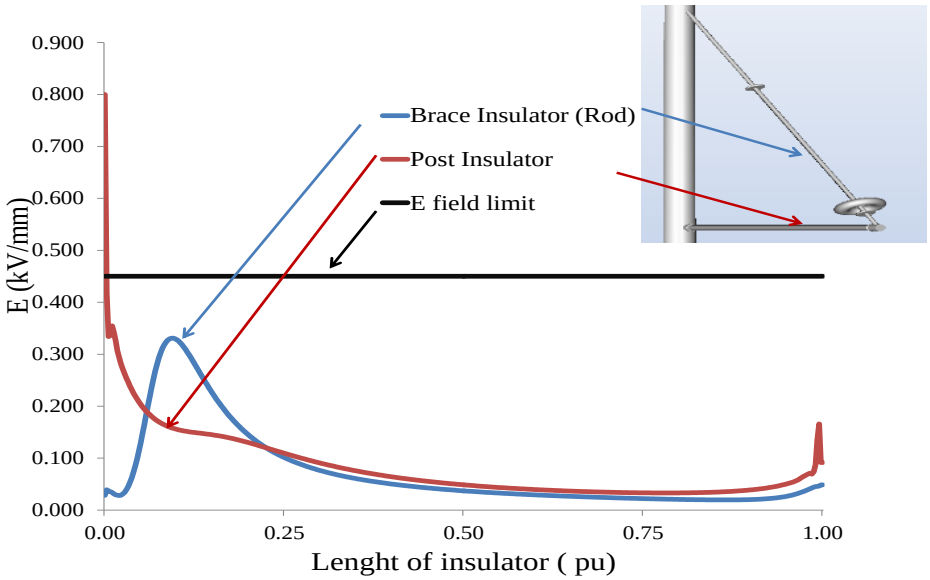

Figure 5-14 E-field lines along the 230 *kV* standard configuration, brace post insulator tower

The results indicated that even though the electric field for the suspension type (brace) insulator within stipulated value, it was much higher at the triple point for the post insulator. Hence electric field value 5 mm from the triple point for the post insulator was also noted for all the simulations, as shown in Figure 5-15.

It was observed that the electric field value 5 mm away from the triple point was within the limit for all configurations. A single conductor was modeled in the simulations. This field can be controlled better by use of bundled conductors. The drop in electric field value in 80% and 70% configuration is due to the fact a larger corona ring was used for these compact transmission towers, which brought down the values of electric field, as shown in Figure 5-16.

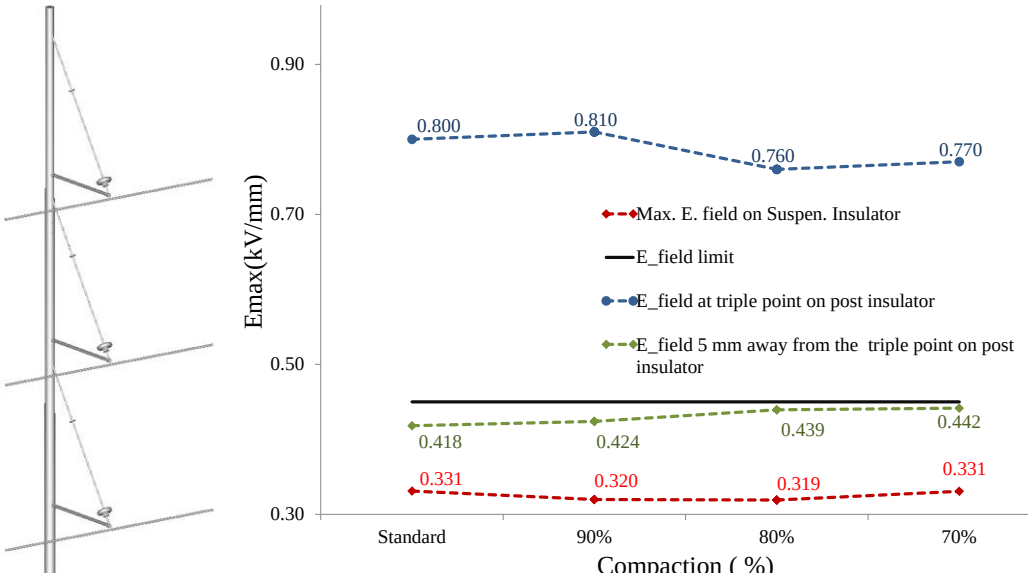

Figure 5-15 E-field values for case-6

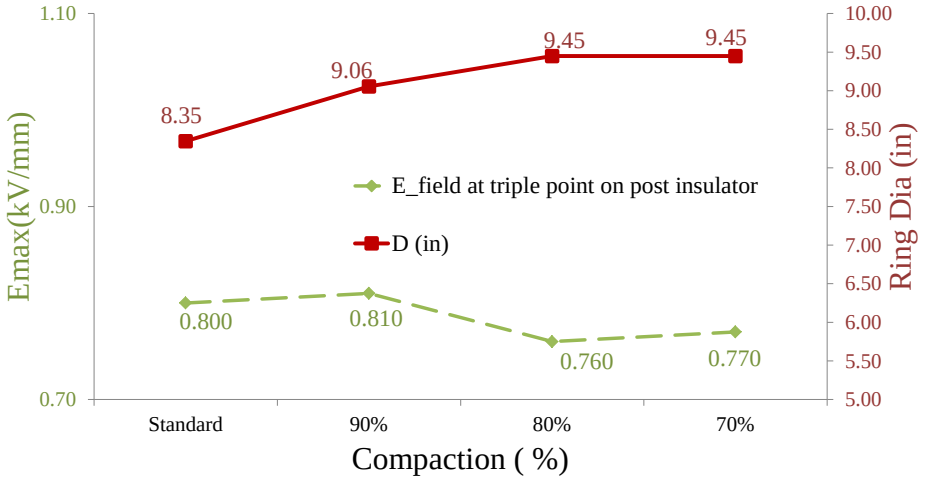

Figure 5-16 E-field vs. corona ring dimensions for case-6

5.4.7 Case-7 Configuration- 230 *kV* Tapered Steel Brace Post Insulator–Double Circuit

A double circuit configuration for braced post insulator model is shown in Figure 5-17 along with the results. The plot contains only the electric field near the triple point on the post insulator, which was found to be highest among all the locations of interest in a single circuit configuration.

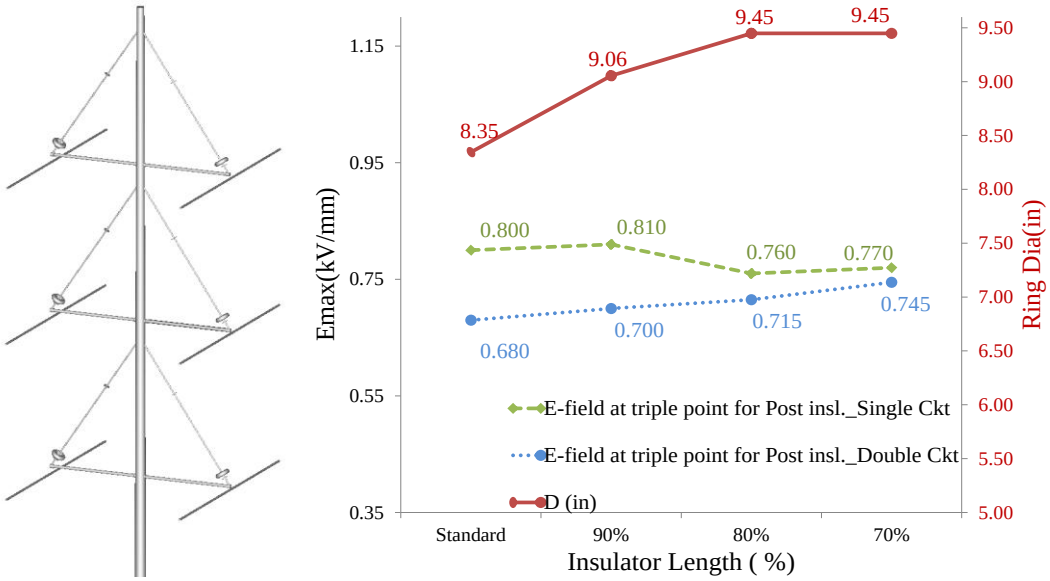

Figure 5-17 E-field vs. corona ring dimensions for case -7

The results indicated that electric field near the triple point on post insulator in this configuration was lesser than single phase configuration, due to phase cancelation effect.

5.4.8 Case-8 Configuration- 345 *kV* Tapered Steel Pole I String Insulator–Single Circuit

Similar to the phase sequence, modeling methods and assumptions made in Section 5.4.1, simulations were done for 345 *kV* tapered steel pole tower. Table 5-4 shows the dimensions of corona ring used for 345 *kV* systems [9].

In case of 230 *kV* compact structures, the conductors were not modeled for similar tower configurations. However, research indicated that the effect of conductors and tower modeling is very important for 345 *kV* and above systems to obtain the correct estimates of electric field values. Figure 5-18 shows the effect

of conductor and tower modeling on the surface electric field distribution of a 345 *kV* insulator.

Table 5-4 Dimensions of corona ring used for the 345 *kV* system

% compaction → / Corona ring dimension ↓	Standard	90%	80%	70%
T (mm)	25	25	25	25
h (mm)	90	90	90	90
R (mm)	152.4	152.4	152.4	152.4
D (in)	12.0	12.0	12.0	12.0

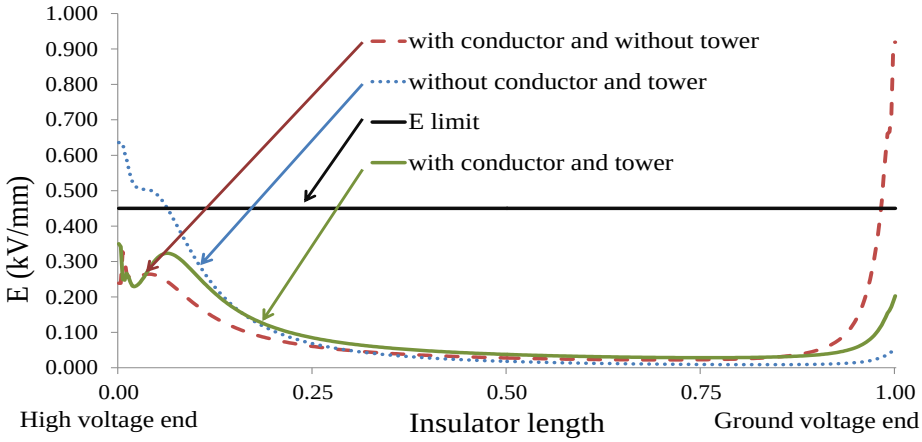

Figure 5-18 Effect of conductor and tower modeling on the surface electric field distribution of 345 *kV* composite insulator

The results indicated that the maximum surface electric field of insulator modeled, only with corona ring installed, was found to be higher that stipulated limit of 0.45 *kV/mm*. In presence of conductors, the electric field at the high voltage end came down within the limits, but the value at the ground end electric field

rose to 0.919 *kV/mm*. However, when the tower was included in the modeling, the electric field ground end voltage was reduced to 0.202 *kV/mm*. The reason of this effect is well explained by the voltage contours as seen in the Figure 5-19.

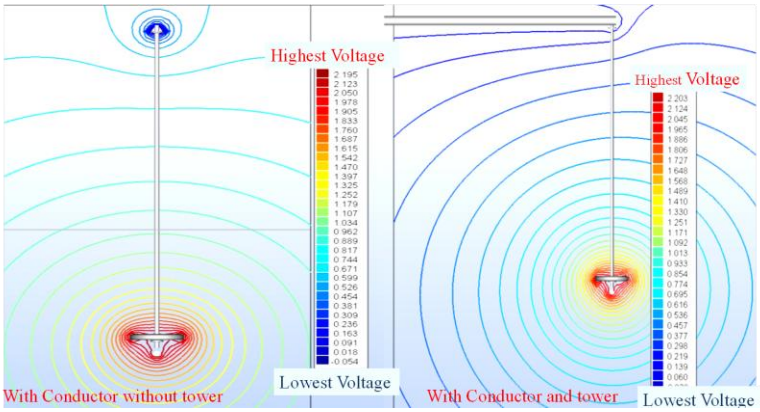

Figure 5-19 Voltage contours showing effect of tower and conductor modeling on the surface electric field of 345 *kV* insulator

It can be observed that in the absence of tower, the live conductor induced a zone of high stress on the ground end of insulator, however, when tower was modeled, the stress on the ground end reduced. Hence modeling of the tower became important to accurately obtain results and simulate the real field conditions. For all the simulations for 345 *kV* and above, a bundle of two Bluebird conductors as described in Section 4.3.3 were modeled.

Figure 5-20 shows the maximum electric field for each tower configuration of case-8. The results indicated that the electric field value for case-8 configurations were found to be within limits.

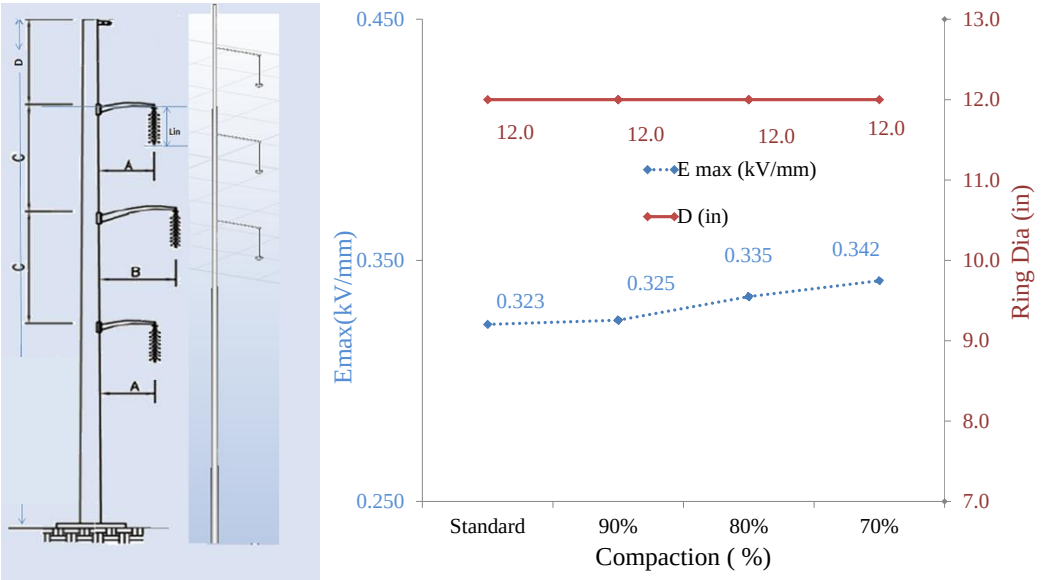

Figure 5-20 E-field vs. corona ring dimensions for case -8

5.4.9 Case-9 Configuration- 345 *kV* Tapered Steel Pole I String Insulator– Double Circuit

Simulations were done for double circuit configurations, keeping the other parameters unchanged as per case 8. The results indicated that electric field was marginally higher than single circuit, but within the limits.

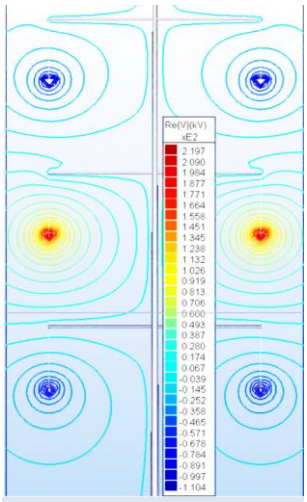

Voltage contours for case -9

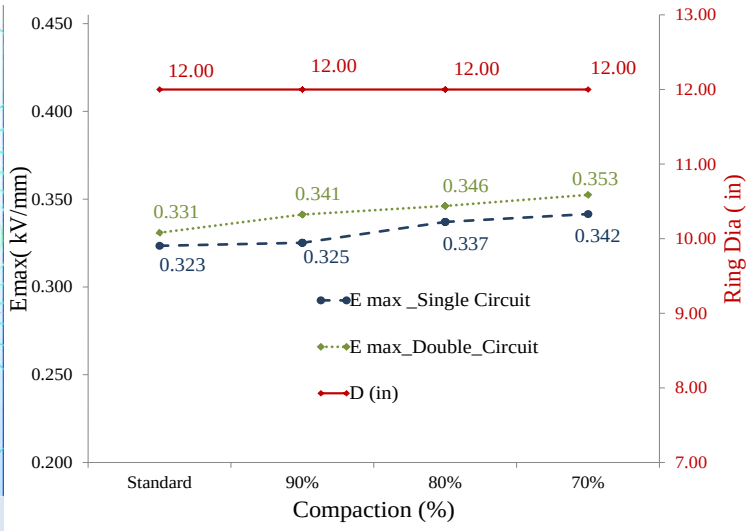

Figure 5-21 Voltage contours; E-field vs. corona ring dimensions for case -9

5.4.10 Case-10 Configuration- 345 *kV* Tapered Steel Pole V String Insulator– Single Circuit

V string insulators are commonly used for 345 *kV* voltage and above [3][7]. Compact structures of tapered steel pole with V string –single circuit were modeled for 345 *kV*. As explained in Section 4.3.5, a simplified metal hardware was also modeled for better estimations of electric field. Figure 5-22 shows the surface electric distribution on one of the suspension insulator of V string for standard and 90% compact structure.

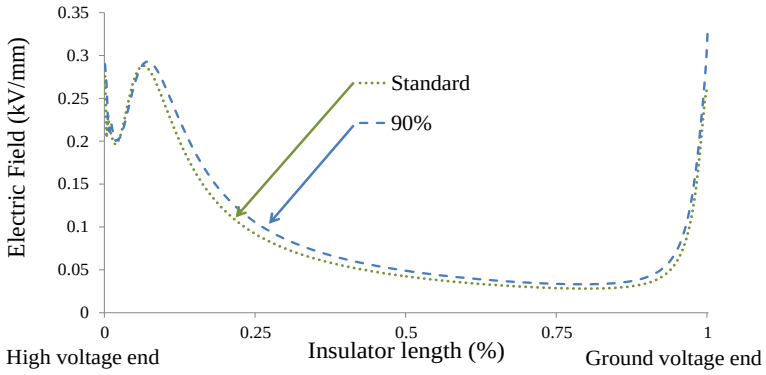

Figure 5-22 E-field distribution of the suspension insulator in V string for case-10

Interestingly, it was noticed that with corona ring at only HV end, the maximum electric field occurred near the ground end of the insulator. However, electric field was within the limits. This phenomenon can be explained by observing the voltage contours around the V string insulator as shown in Figure 5-23. A high electric field near the ground level can be attributed to the fact that high electric field stress may arise from the twisted voltage lines, like the one shown near the ground end in as shown in Figure 5-23.

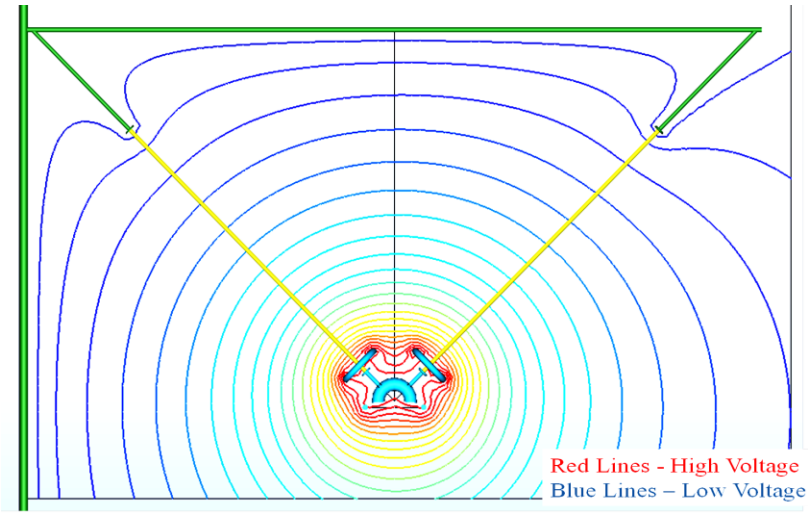

Figure 5-23 Voltage contours around V string insulator of 345 *kV* system

Figure shows the maximum electric field values near the vicinity of high voltage and ground voltage end for case -10 configurations.

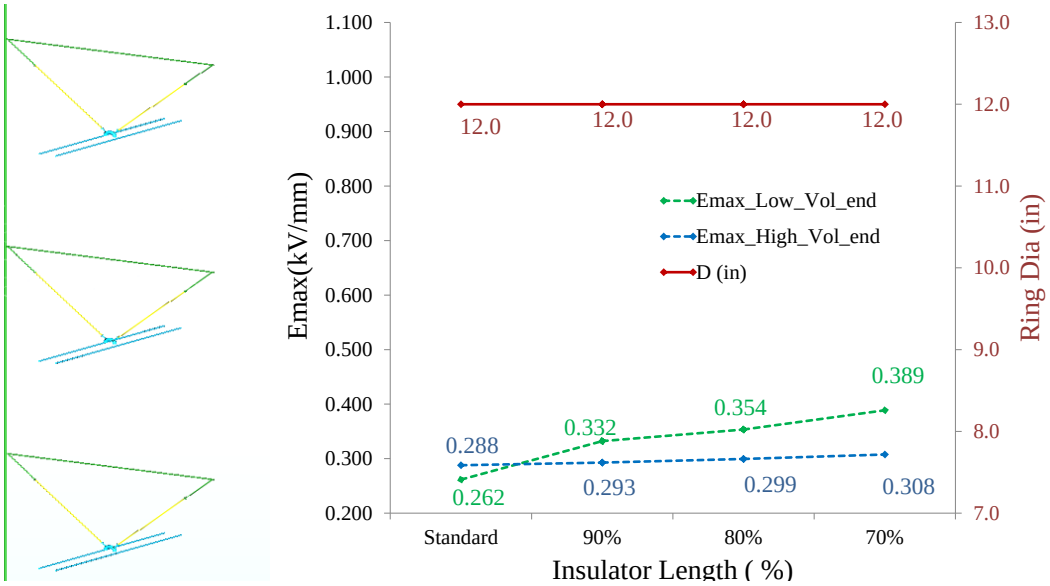

Figure 5-24 E-field vs. corona ring dimensions for case-10

The results indicated that electric field near the ground end voltages were greater than the high voltage end for compact towers. However, the values were

within the limits. A corona ring may be placed near the ground end terminal to limit the electric field values.

5.4.11 Case-11 Configuration- 345 *kV* H Bridge I String Insulator–Single Circuit

An H bridge configuration with I string insulator was modeled for 345 *kV*. Figure 5-25 compares the maximum electric field for all the compact structures and the corona ring diameter used in case -11. The results indicated that the electric field value was found to be within the limit for this case.

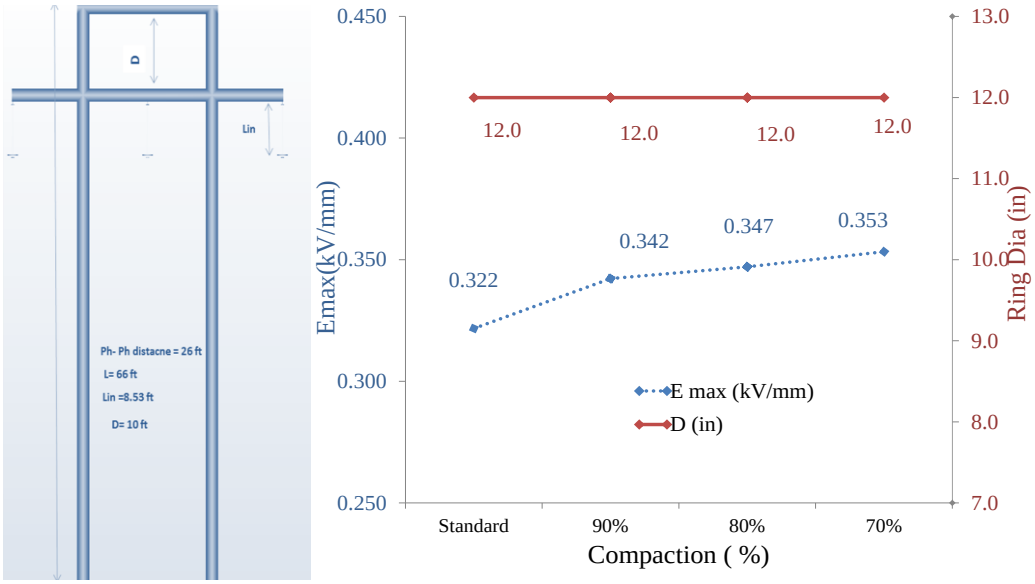

Figure 5-25 E-field vs. corona ring dimensions for case-11

5.4.12 Case-12 Configuration- 345 *kV* Tapered Steel Pole Braced Post Insulator–Single Circuit

A tapered steel tower with braced post insulator was modeled. Bundled conductors were modeled beneath the post insulators. Figure 5-26 shows the maximum electric field on the surface of post and the suspension insulator.

It was found that electric field value on both the insulators remained well within the limits. As can be seen, a uniform region of voltage contour (shown by red color) was produced by the combined effect of the corona ring and the bundled conductors, which effectively controlled the electric field.

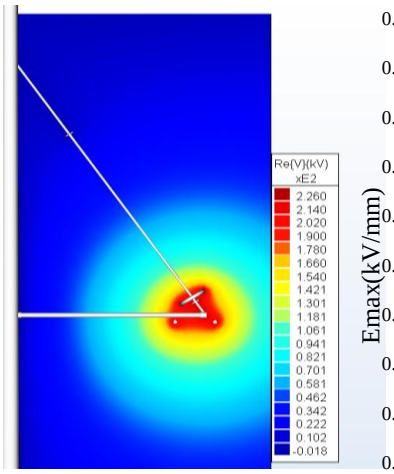

Red Lines - High Voltage
Blue Lines – Low Voltage
Voltage contours for 345 kV Brace post Insulator Tower

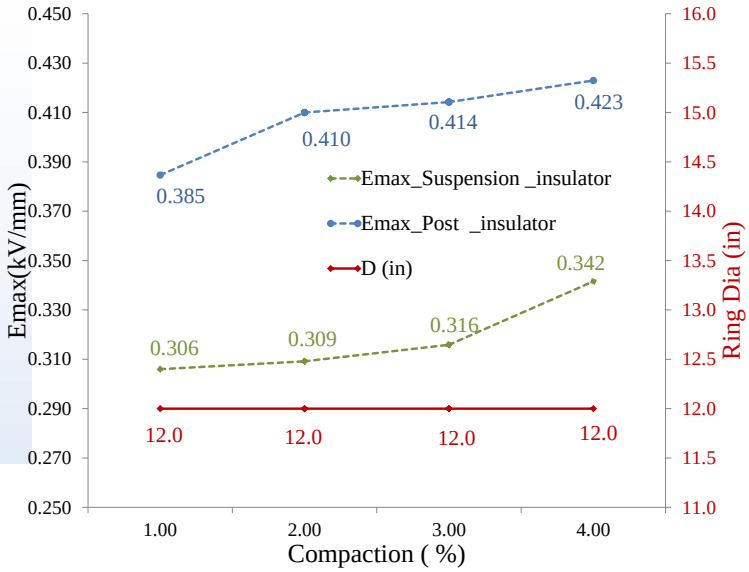

Figure 5-26 E-field on post and suspension insulator for case 12 configurations

5.4.13 Case-13 Configuration- 500 *kV* H Bridge V String- Single Circuit

The EPRI book [7] shows 500 *kV* H bridge tower with a V string insulator configuration. Hence simulations were done for a 500 *kV* H bridge tower with the same configuration. It was found that due to large dimensions of H bridge tower, a full scale 3D model required excessive memory to run the simulation. This issue was overcome by the method described in Section 4.7.

As per the industry practice, the 500 *kV* insulators were equipped with corona ring at both the ends [11]. Figure 5-27 shows the electric field values for ground end and the high voltage end on the insulator surface for this case. In one

of the cases, a model with corona ring placed only at high voltage end is simulated.

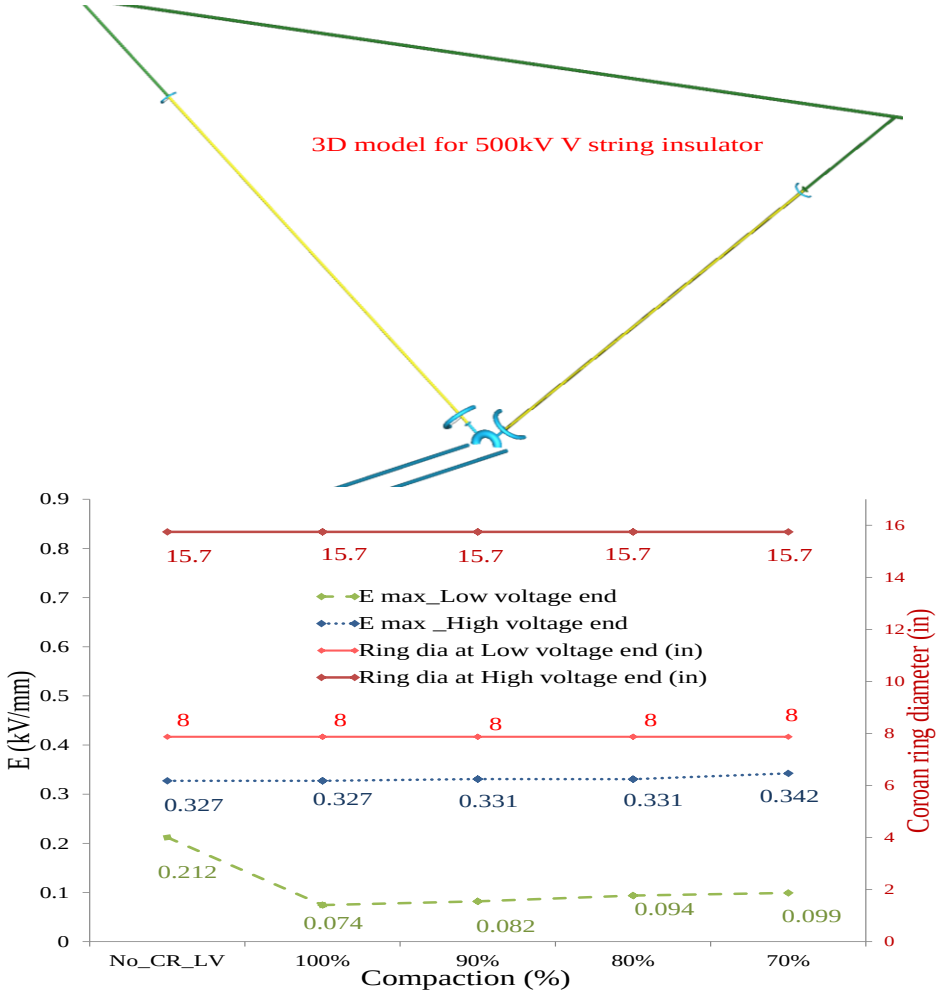

Figure 5-27 E-field on suspension insulators for case 13 configurations

The results indicated that if only corona ring was placed near the high voltage end; the electric field value at low voltage end was high, indicating a possibility of corona discharge in contaminated conditions. However, with corona ring placed at both the ends, electric field values lay within the limits.

5.4.14 Case-14 Configuration- 500 *kV* Tapered Steel Pole I String- Single Circuit

Simulations were done for 500 *kV* tapered steel pole I string towers. Figure 5-28 shows the electric field values obtained from the computer simulations and the 3D model of I string insulators for 500 *kV*. The results indicated that the electric field values were within the stipulated limits for case 14 configurations.

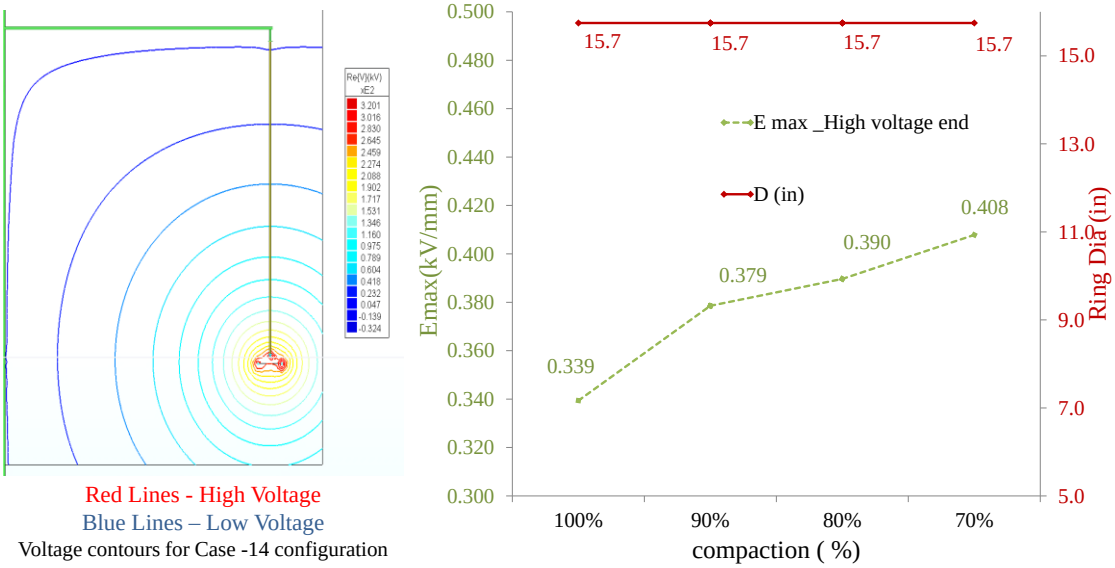

Figure 5-28 E-field on suspension insulators for case-14 configurations

5.4.15 Case-15 Configuration- 500 *kV* Tapered Steel Pole I String-Double Circuit

A double circuit model was also investigated for tapered steel pole I string configuration. Figure 5-29 compares the electric field values for double circuit and single circuit configuration.

The results indicated that maximum electric field values on insulator surface for a double circuit configuration were higher than the single circuit configuration. For 70% compaction, the value was marginally higher than the stipulated value.

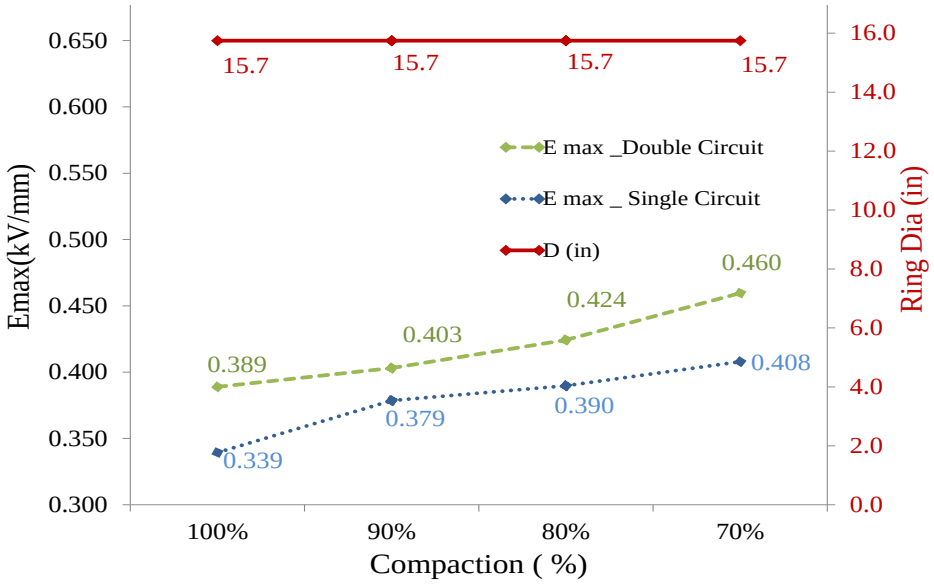

Figure 5-29 E-field –double circuit vs. single circuit values for case 15 configuration

5.4.16 Case-16 Configuration-500 *kV* Tapered Steel Pole Brace Post Insulator Delta Configuration

In accordance with the EPRI book specified tower configurations, a delta configuration for 500 *kV* brace post insulator was modeled. Only the suspension type insulator was provided with the corona ring. Figure 5-30 shows the maximum electric field value on the surface of post insulator near the high voltage end and also near low voltage end.

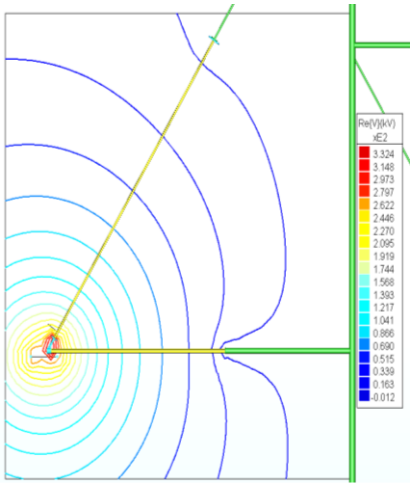

Red Lines - High Voltage
Blue Lines – Low Voltage
Voltage contours for Case -16 configuration

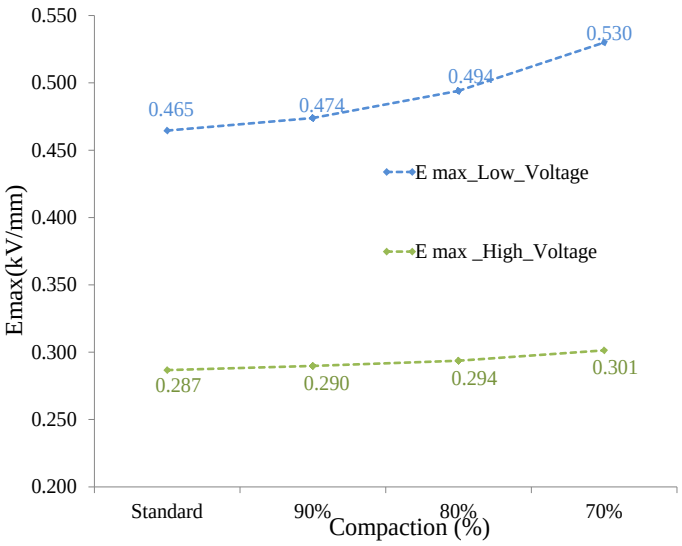

Figure 5-30 E-field on post insulator for case 16 configuration

The results indicated that while the electric field values at the high voltage end were within the limits, the values at ground end were higher than the stipulated limits. The reason for this phenomenon can be explained by the voltage contours shown in Figure 5-30, which indicated that the voltage contours were highly bent near the ground end, giving rise to high electric field stress.

5.4.17 Case-17 Configuration- Tapered Steel Pole with I String Insulators for 230 *kV* (line to line) 6 Phase System

6 phase tower dimensions are comparable to a 3 phase double circuit tower, as the lines to ground voltages are equal for both the systems. For example a 230 *kV* line to line 3 phase system is equivalent to 132 *kV* line to ground 6 phase system. Hence a 3 phase double circuit tower can be converted to a 6 phase tower, without making any major modifications. Figure 5-31 shows the tower configura-

tion, corona ring diameter, phase sequence and voltages for a 6 phase tower used for computer simulations.

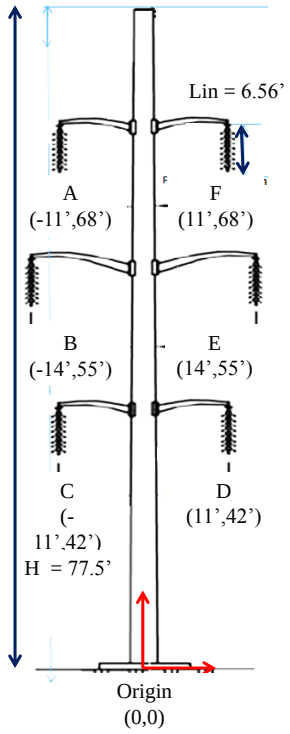

Parameters	Values
Tower Height, H	77.5'
Lin, Insulator dry arc distance	2000 mm
Corona Ring diameter, D	8.35" (120 mm)
Corona Ring thickness, T	45 mm
Corona Ring height , H	90 mm
Phase sequence A B C D E F (*10% over voltage considered for 132 kv system)	 146.07*∠ 0° kV 146.07∠ 120° kV 146.07∠ 240° kV 146.07∠ 60° kV 146.07∠ 180° kV 146.07∠ 300° kV

Figure 5-31 6 phase tower dimensions and 3D model in COULOMB (All dimensions in feet)

For a 6 phase system, the phase sequence was decided in following manner: two 3 phase circuit were created, one comprising of phase A, B, C each 120^0 apart; other comprising phase D, E , F each 120^0 apart. The reason for separating phases in such a manner was to run the system as a single circuit 3-phase line, in case there was a fault in any one of the 6 lines.

Phases A, B, C and phases D, E, F were put on the either sides of the tower. There are 4 possible combinations for arranging the instantaneous voltage vectors on each group, as shown in Figure 5-32. On the either side of tower, the red

color denotes phases experiencing the peak value of voltage vector at an instant of time, while blue color denotes phases displaced by 120^0 to the respective phase. Computer simulations were run to find out which of the four cases has the worst impact on the electric field on the surface of insulators.

Figure 5-33 shows the maximum electric field on the surface of insulator having the maximum voltage, for each of the four configurations shown in Figure 5-32

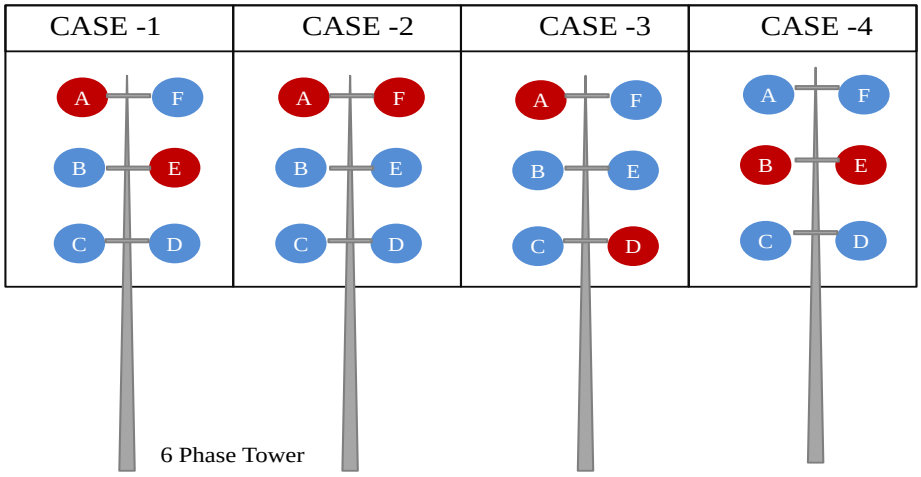

Figure 5-32 Possible voltage phase combination for 6 phase tower

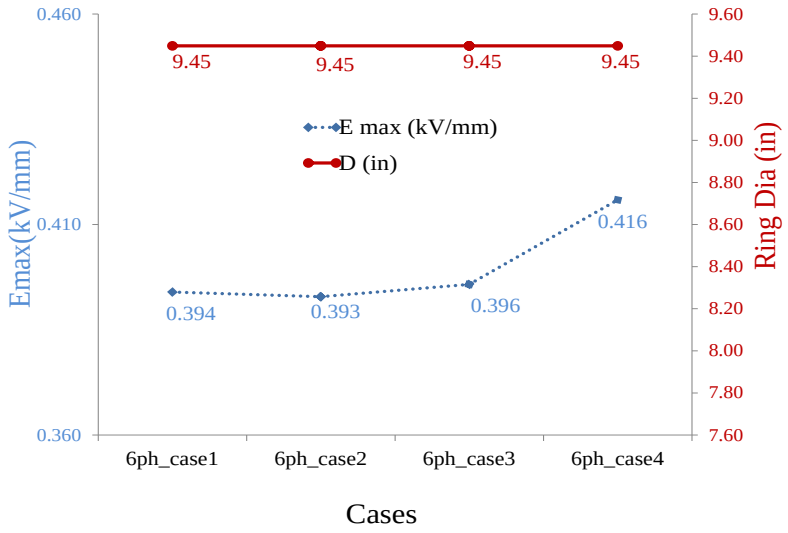

Figure 5-33 Maximum electric field values for case 1, 2, 3 and 4

The results indicated that a configuration shown in 6ph_case-4 caused maximum electric field on the surface of insulators. Thereafter, a study was done for 6 phase compact structure, wherein the phase-to-phase distances, phase-to-tower distance and the insulator dry arc length was reduced in manner stipulated in Section 5.3. For all the compact structures, voltage sequence as per 6p_case-4 was followed. Figure 5-34 shows the maximum electric field on the surface of insulators for all different compaction. The result indicated that surface electric field on 6 phase system was marginally higher than 3-phase double circuits; however the values were found to be in limits.

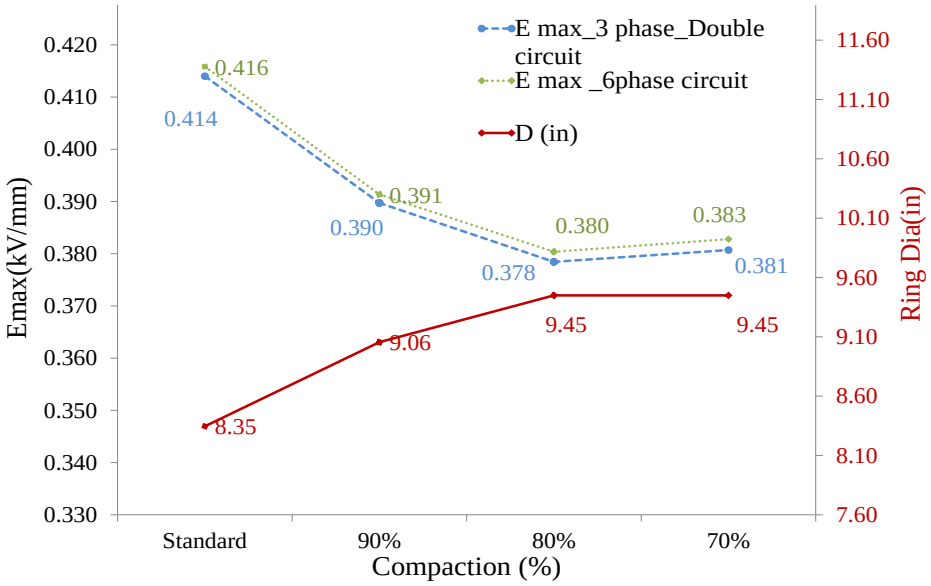

Figure 5-34 Electric field values for compact 6 phase circuits

Chapter 6. Optimization for Corona Ring Dimensions

6.1 Introduction to Corona Ring Dimensions

It has been observed that different insulator manufacturers recommend dissimilar corona ring dimensions for same voltage class insulator. For example, a 400 *kV* composite insulator might be fitted with a 12", 13.8" or a 15" corona ring depending upon the manufacturer's recommendations [6]. There are no set standards which mention corona ring dimensions in industry. The study indicated that the compact structures might require a different corona ring dimension, depending on the level of compaction. This chapter describes a Gaussian process model based on response surface methodology (RSM) to obtain optimum corona ring dimensions for different voltage level.

6.2 Literature Review for Corona Ring Optimization Process

There are many studies conducted on optimization of corona ring dimensions, for various voltage levels [8]-[11]. However, for obtaining optimum corona ring dimension for compact transmission line studied in this research, methodologies described in literature are not sufficient because of the following reasons:

1. Each of these studies discusses the optimum corona ring dimension for one particular voltage. There is no generalized approach to obtain corona ring dimension for different voltage levels.
2. As described in Section 2.1, there are many factors which influence the electric field on the surface of insulators. While some of the studies have considered impact of bundled conductor, tower geometry and in-

sulator configurations [21], the variation in insulator dry arc length, voltage is not investigated in any of the studies. This puts a major limitation for applying these methods in determining optimum dimensions for compact transmission lines.

3. Rather than a scientific approach, a brute force method is applied in many of these studies to arrive at the optimum corona ring dimension [9][11].

6.3 Corona Ring Optimization using Response Surface Methodology

In this research, corona ring optimization was done using RSM is mentioned below.

Introduction to RSM with a focus on computer experiments

In some of the systems involving optimization between a response variable y and set of predictor variable $\boldsymbol{X} = [x_1, x_2, \ldots, x_k]$ the relationship between y and the $\boldsymbol{X}$ might be known exactly, based on the undermining concepts of engineering, physical or chemical principles. In these types of cases, y can be written as:

$$y = f(x_1, x_2, \ldots, x_k) + \varepsilon \tag{6.1}$$

Where x_i is predictor variable, i=1,2,…,k (6.2)

ε is the error in the system

These kinds of relationships are known as mechanistic model [48]. However, there are some cases where the essential principles are not fully understood and the function f cannot be evaluated, then an empirical formula might be required to express the y in terms of $\boldsymbol{X}$. Usually the function f is first order or higher

order polynomial or other types of function. The empirical model is called response surface model. “Response surface methodology (RSM) is collection is a collection of statistical and mathematical techniques useful for developing, improving and optimizing process” [48].

Typically RSM has been applied to a physical process such as chemical process, semiconductor manufacturing and many more. However, RSM can be used for computer simulations models of physical systems, where a model is built using RSM techniques and then optimization is carried out. There are two types of computer simulation models as mentioned below:

a) Stochastic simulation model: A stochastic simulation model has simulation variables as random variables. For example, a computer simulation program which predicts solar wafers quality based upon Monte Carlo simulations is an example of stochastic simulation model. Such computer simulations are used to study complex phenomenon which cannot be expressed by an analytical solution.

b) Deterministic simulation model: In a deterministic simulation model, the output responses are not random variables but their values are entirely determined by a mathematical model which is based on a computer based model. For example, in a power flow file containing thousands of buses, the bus voltages and angles are determined by a computer based power flow program. The bus voltages and angles are totally deterministic value for a particular scenario, which will not change even if the power flow is run a number of times. Hence it is a deterministic computer simulation experiment. Finite element simulations are also an

example of deterministic computer simulation. All the simulations run in this research based on BEM are example of deterministic computer simulation model.

Designs for the computer experiment

RSM is a sequential experiment usually consisting of two phases. In the first phase, an experiment is designed using factorial designs or other methods, to predict the response using a low order polynomial function (usually first order) with the control variables. The gradient of the fitted first order function is used as a search direction for approaching the optimum values. In the second phase of RSM, using other designs such as central composite designs, a higher order (usually a quadratic) function is used to fit the response in terms of control variables, near the neighborhood of the optimum value. This quadratic model is used to find optimal values of the fitted response and corresponding values of the control variables. To obtain a better predicted or fitted response, replicate runs are conducted to eliminate the random error in the experiment.

In a deterministic computer simulation method, the choice of design is done somewhat differently. In computer experiments, since any design point can be practically simulated, space–filling designs have become increasingly popular [48]. Space filling designs have advantage of spreading out the design points somewhat uniformly throughout the region of interest. Secondly they do not contain any replicate runs- major advantage for deterministic computer simulations. There are many space filling designs, some of which are listed below:

1. Latin hypercube design: In a Latin hypercube design, an *n x i* matrix is created where *n* is the number of runs and *i* is the number of variables. The idea behind a Latin hypercube is similar to a 'Sudoku' game; no variable occupies same row and column in the matrix more than once, thus avoiding the replication. An example of Latin hypercube space filling design is shown in Figure 6-1. In this research, a Latin hypercube design was used to create design points.

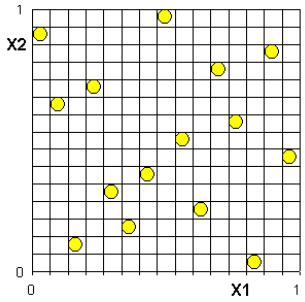

Figure 6-1 Latin hypercube space filling design for two factors

2. Sphere packing design: A sphere packing design minimizes the minimum distance between the two pairs of points.
3. Uniform design: Uniform design attempts to place the design points uniformly through the design space to form a uniform distribution. Further types of design types can be found in [48].

*Modeling: Fitting the response y in terms of **X** using Gaussian process model using JMP*

After a design is chosen, a Gaussian process model is implemented to obtain a mathematical relationship between the control variables and response. Gaussian Process can be used to model the relationship between a continuous response and one or more continuous predictors. The advantage of Gaussian Pro-

cess model is that it often perfectly interpolates the data, hence eliminates the error in prediction [48]. Deterministic computer experimenters like such a feature, as they argue that for given sets of variables, they should obtain same response, if a computer experiment is run a number of times, as there are no random errors in the model.

A computer software called JMP was used to create a Gaussian process model to establish a relation between *y* and ***X***. JMP has been widely used by researches, scientists and engineers to perform complex data analysis, modeling and visualization. It was developed by Statistical Analysis System (better known as SAS) at North Carolina State University, USA. JMP supports a number of design experiments such as classical screening (e.g., fractional factorial), response surface, full factorial, nonlinear and mixture designs, as well as advanced designs such as space-filling, accelerated life tests [49].

As per JMP user manual, "Gaussian Process platform fits a spatial correlation model to the data, where the correlation of the response between two observations decreases as the values of the independent variables become more distant. The Gaussian correlation model uses the product exponential correlation function with a power of 2 as the estimated model" [51]. For this model, it is assumed that *y* has a normal distribution with mean vector μ and covariance matrix $\sigma^2 R(\theta)$, where $R(\theta)$ is a correlation matrix having elements given by r_{ij}.

Where
$$r_{ij} = e^{-\left(\sum_{s=1}^{k} \theta_k (x_{is} - x_{js})\right)^2} \qquad (6.2)$$

μ is normal distribution mean,

σ^2 is normal distribution parameter,

r_{ij} is the correlation between the responses at two design points.

The parameters μ and θ are estimated using the method of maximum likelihood.

The Gaussian process model for y is given by:

$$y = \mu + z(x) \tag{6.3}$$

Where $z(x)$ = Gaussian stochastic process with covariance matrix $\sigma^2 R(\theta)$

The predicted formula for the response y is given by

$$\hat{y}(x) = \hat{\mu} + \acute{r}(x)R\left(\hat{\theta}\right)^{-1}(y - j\,\hat{\mu}) \tag{6.4}$$

$\hat{\mu}$ and $\hat{\theta}$ are maximum likelihood estimates of model parameter μ and θ

$$\acute{r}(x) = [r(x_1, x), r(x_2, x), \dots, r(x_n, x),] \tag{6.5}$$

The prediction formula given by JMP contains one term for each design point. Gaussian process platforms give us and advantage of obtaining a prediction formula which is highly accurate and could be used for optimization and analysis.

Optimization of corona ring dimensions

As explained in the previous section, the Gaussian process model gives a complex non–linear prediction formula between *y* and ***X***. JMP can be used to get an optimum value for the Gaussian process model. However, A Mathematical Programming Language (AMPL) and KNITRO were used to obtain the optimum values of corona ring dimensions.

AMPL is computer language used for describing large-scale mathematical computation, typically large-scale optimization and scheduling-type problems. It

can do linear, nonlinear, and integer programming and supports various solvers to obtain the results [52].

KNITRO is an AMPL supported solver used for nonlinear optimization. KNITRO provides has 3 types of algorithms (solvers) for solving problems, namely a) Interior-point Direct algorithm, b) Interior-point CG algorithm and c) Active Set algorithm. Each of the algorithms can handle a full range of nonlinear optimization issues [53].

6.4 Corona Ring Optimization Case Study for 230 *kV* Corona Ring

For the optimization of corona ring, the control variables as mentioned in the literature [9][10][11] have been corona ring radius (R), tube thickness (T) and the height (h) from the high voltage end as shown in Figure 6-2. However, as indicated by this research, dry arc length (L) also impacts the maximum electric field. Hence R, T, h and L were chosen as four control variables. The maximum electric field (E_{max}) on surface of insulator was chosen as the response variable (y).

The variables were coded in per unit values as shown in Table 6-1. The maximum and minimum allowable values of variables were chosen considering the practical limits [50].

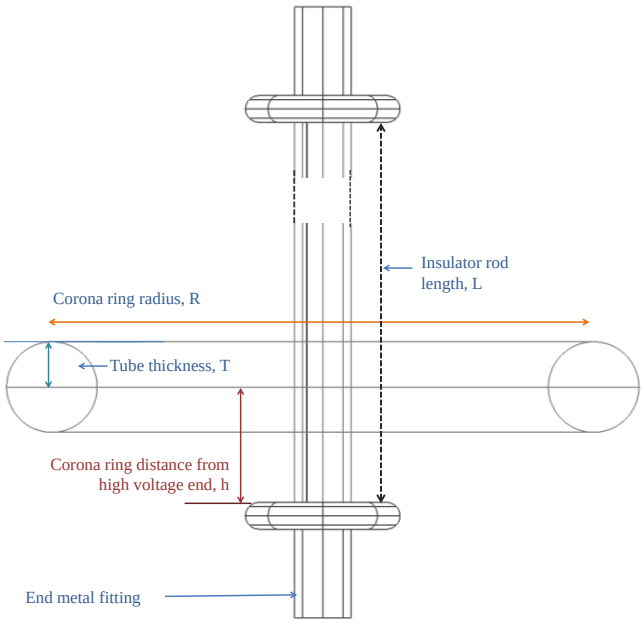

Figure 6-2 Corona Ring optimization variables for 230 *kV*

Table 6-1 Per unit coding of control variables for 230 *kV*

Variables	Min value *(mm)*	Max value *(mm)*	Coded values for	
			Min value	Max value
R	75	150	1	8
T	10	30	1	4
h	-10	100	1	8
L	1400	2000	1	4

As a rule of thumb, 8-10 design points per variable should be used for constructing a design space. Considering four variables, a Latin hypercube design of 30 runs were done, as shown in Table 6-2. Corresponding value of y (E_{max} in

kV/mm), was noted down from the computer simulations. Figure 6-3 shows an example the computer model used in simulations.

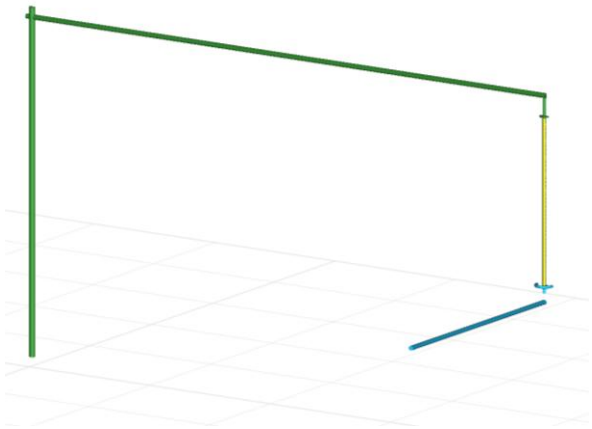

Figure 6-3 Computer simulation model for 230 *kV*

Table 6-2 Latin hypercube design with corresponding Y, Y prediction and error

S. No	*R (pu)*	*T (pu)*	*h (pu)*	*L (pu)*	*Emax* *kV/mm*	$Y_{prediction}$ by JMP	Error($x10^{-11}$)
1	3.414	2.759	7.276	1.103	0.303	0.303	-1.09
2	5.586	1.103	3.897	1.414	0.364	0.364	-0.57
3	2.690	1.931	3.655	1.207	0.332	0.332	0.35
4	4.862	3.793	2.690	1.828	0.285	0.285	-0.50
5	1.966	2.966	3.414	2.655	0.344	0.344	-1.70
6	3.655	1.000	4.621	2.862	0.311	0.311	-0.65
7	3.897	1.310	6.793	1.724	0.281	0.281	-0.38
8	6.069	2.862	7.759	2.552	0.248	0.248	0.30
9	2.448	3.379	3.172	4.000	0.328	0.328	-0.04
10	3.172	1.414	8.000	3.172	0.292	0.292	0.85
11	4.379	2.345	1.483	3.690	0.397	0.397	0.27

12	5.103	4.000	4.379	3.483	0.270	0.270	0.22
13	7.517	1.621	7.517	1.931	0.296	0.296	-0.22
14	7.034	3.483	1.724	3.069	0.328	0.328	0.20
15	1.483	3.172	1.241	1.517	0.392	0.392	-1.05
16	6.310	2.552	5.345	1.310	0.252	0.252	0.29
17	6.793	1.724	6.069	3.379	0.279	0.279	-0.14
18	1.724	3.586	5.103	1.621	0.348	0.348	0.77
19	4.621	3.069	7.034	3.897	0.273	0.273	-0.55
20	2.931	2.138	4.862	3.793	0.313	0.313	-0.03
21	4.138	1.828	1.000	2.241	0.471	0.471	0.81
22	1.241	2.241	6.552	2.345	0.361	0.361	0.31
23	6.552	1.207	2.207	3.276	0.431	0.431	2.64
24	8.000	2.034	2.931	2.138	0.356	0.356	3.64
25	7.759	3.276	5.828	3.586	0.228	0.228	0.04
26	7.276	3.897	5.586	2.034	0.238	0.238	0.76
27	5.345	2.655	4.138	2.759	0.270	0.270	1.31
28	2.207	3.690	6.310	2.966	0.332	0.332	-0.03
29	5.828	2.448	1.966	1.000	0.367	0.367	-2.61
30	1.000	1.517	2.448	2.448	0.405	0.405	-0.54

Model analysis for E_{max} as obtained from JMP

The Gaussian process prediction formula for E_{max} in terms of *R*, *T*, *h* and *L* was obtained from JMP. It consisted of one term for each of the design points, given in APPENDIX B. Figure 6-4 shows the surface generated by the prediction formula given by the JMP. The prediction formula has a very high accurately,

with error in the range of 10^{-11}, as shown in Table 6-2. The adequacy of the model was checked by a jackknife process done by JMP as shown in Figure 6-5.

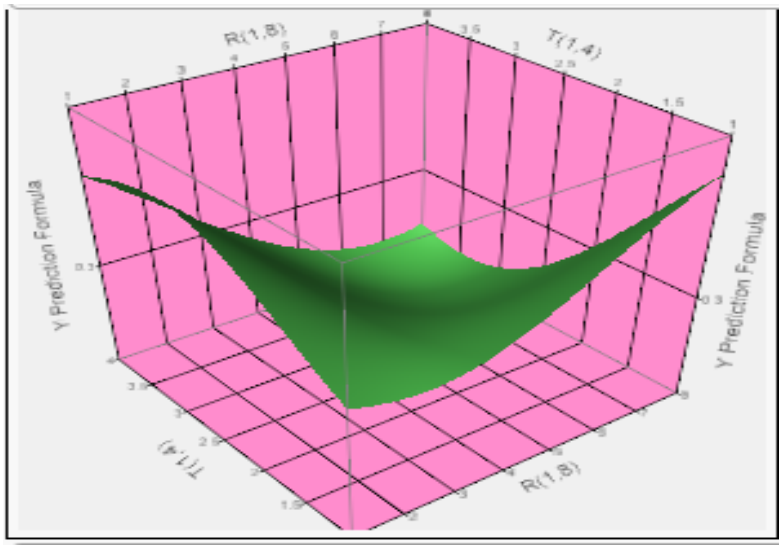

Figure 6-4 Y prediction surface for 230 *kV* case obtained from JMP

The analysis indicated that model is a good fit, since the jackknife process yields a diagonal line at an angle of 45^0 to x axis. The model is a good approximation to the true function that generated the data, if points lie along the 45^0 diagonal line [51].

Theta for *R*, *T*, *h*, and *L* denotes the curvature along response surface along that the parameters. For example, theta is highest for *T*, which means that curvature along *T* axis and *Y* is the maximum, while it is least case of *L*.

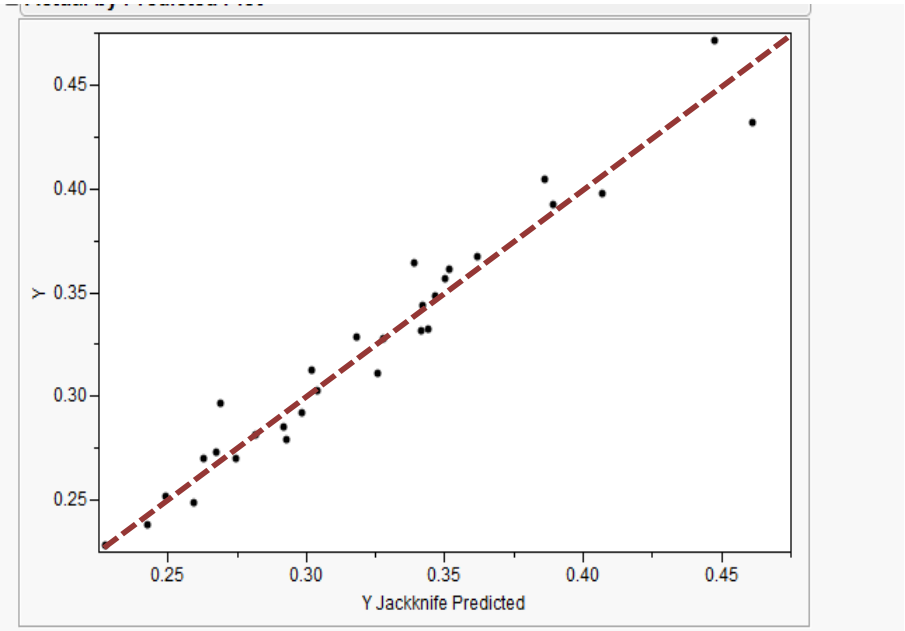

Model Report

Column	Theta	Total Sensitivity	Main Effect	R Interaction	T Interaction	h Interaction	L Interaction
R	0.0269902	0.2442788	0.151275	.	0.0670039	0.025639	0.0003609
T	0.165724	0.2919855	0.144661	0.0670039	.	0.0800801	0.0002405
h	0.053373	0.620014	0.5140539	0.025639	0.0800801	.	0.0002411
L	0.0009997	0.0009204	7.7839e-5	0.0003609	0.0002405	0.0002411	.

μ	σ²
0.3732159	0.005666

-2*LogLikelihood

-143.5887

Fit using the Gaussian correlation function.

Figure 6-5 Jackknife analysis for 230 *kV* prediction model given by JMP

Figure 6-6 shows the marginal plot of all the parameters vs. *Y*. These plots show the average value of each factor across all other factors [51]. The figure qualitatively indicates the variation of *Y* with respect to each variable.

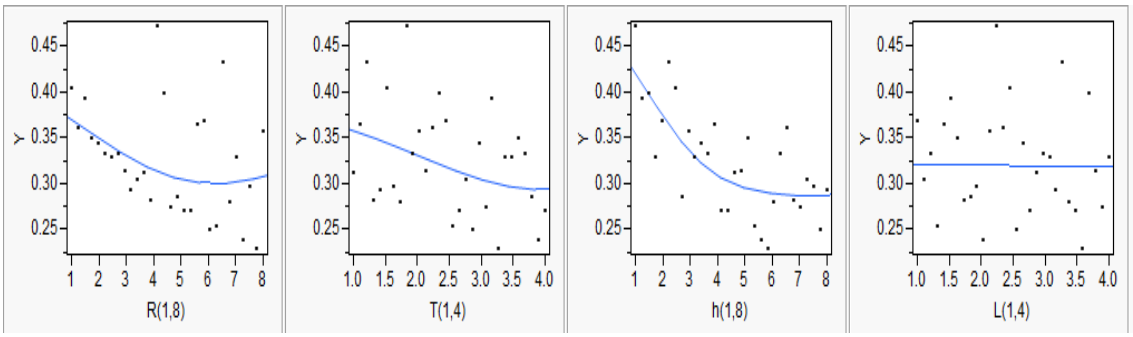

Figure 6-6 marginal plot of control variables against Y obtained from JMP

As per the design, *h* has the main impact on the distribution on *Y*. The main effect for *h* is highest among all parameters, as listed in Figure 6-5.

Case-1:Optimization code for 230 kV

Following optimization code was written in AMPL and JMP

Let $$Emax = f\ (R, L, T, h) \quad (6.6)$$

Where *f* is the objective function given in APPENDIX B

Minimize E_{max}, subject to:

$$1 \leq T \leq 4 \quad (6.7)$$

$$1 \leq h \leq 8 \quad (6.8)$$

$$L = 1,2,3,4 \text{ (For 4 cases)} \quad (6.9)$$

The four cases for L =1, 2, 3 and 4 was considered because the compaction process was done in step of 10%. A comparison between the JMP and AMPL results are shown in Table 6-3.

Table 6-3 JMP and AMPL results for optimization case-1 for 230 *kV*

L (mm)	1400		1600		1800		2000	
	JMP	AMPL	JMP	AMPL	JMP	AMPL	JMP	AMPL
R (mm)	146.1	146.1	146.5	146.5	146.9	146.8	147.2	147.2
D (in)	11.5	11.5	11.5	11.5	11.6	11.6	11.6	11.6
T (mm)	26.2	26.2	26.1	26.1	25.9	25.9	25.7	25.7
h (mm)	78.2	78.2	77.7	77.7	77.1	77.1	76.6	76.6
E_{max} *kV/mm*	0.226	0.226	0.226	0.226	0.226	0.226	0.226	0.226

The results obtained by both the software match closely. The ring diameter obtained by optimization process is around 11.5", which is on the higher side, considering that the usual value of 8" [6]. The reason for the higher values is that the electric field was minimized for absolute minima in the design space. Hence a new optimization was performed considering a limit of 0.45 *kV/mm* on E_{max}. This optimization was done using AMPL as the limit on E_{max} cannot be put in JMP.

The optimization code was written as:

$$Emax = f_1\ (R, L, T, h) \tag{6.10}$$

Where f_1 is the objective function given in APPENDIX B

Minimize E_{max}, subject to:

$$0.449 \leq Emax \leq 0.45 \tag{6.11}$$

$$1 \leq T \leq 4 \tag{6.12}$$

$$1 \leq h \leq 8 \tag{6.13}$$

$$L = 4 \tag{6.14}$$

The results obtained from the optimization for limiting value of Emax is summed in Table 6-3.

Table 6-3 Results obtained for optimization process for 230 *kV* for Emax = 0.45 *kV/mm*

R *(mm)*	D *(in)*	T *(mm)*	h *(mm)*	L *(mm)*	E_{max} *kV/mm*
102.07	8.04	10.06	3.84	2000	0.45

The result indicated that the corona ring diameter was 8.04", for limiting Emax = 0.45 *kV/mm*, which was very close to the industrial standards. A computer simulation in COULOMB was run to verify the corona ring dimension obtained from the optimization results as shown in Figure 6-7.

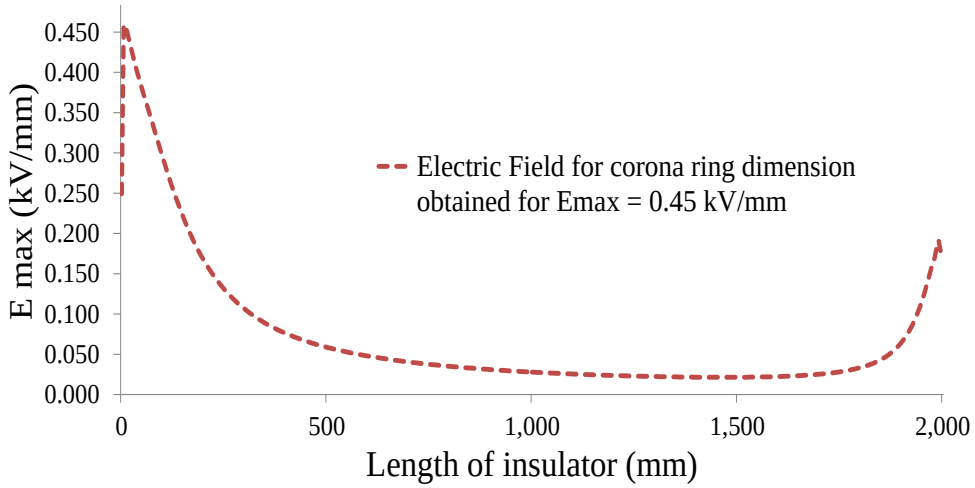

Figure 6-7 Computer simulation verification for AMPL results for E_{max} =0.45 *kV/mm* for 230 *kV*

6.5 Corona Ring Optimization for 330 *kV to* 550 *kV*

230 *kV* was a base case for implementing the corona ring optimization. A generalized model which could give the corona ring dimension for a particular range of voltage range (345 *kV* -550 *kV*, line to line) and level of compaction (up to 70% of standard configuration) was developed. A few modifications were done for the computer simulation model, as listed below:

1. The computer simulation model was fitted with an 8" corona ring dimension at the ground end, as it is practiced for the voltage range chosen [11].
2. A bundle conductor of two conductors per phase was modeled.

The variables were coded in per unit values are shown in Table 6-4.

Table 6-4 Coded values of control variables for 345- 550 *kV* level

Parameter	Min value	Max value	Code for	
			Min	Max
R *(mm)*	75	300	1	8
T *(mm)*	5	40	1	8
h *(mm)*	-10	120	1	8
L *(mm)*	1800	5200	1	8
V (*kV*)	200	330	1	8

Table 6-5 shows the Latin hypercube space fitting design with 50 design points and 5 variables (*R*, *T*, *h*, *L*, *V*). The corresponding values of E_{max} were obtained from the computer simulations.

Table 6-5 Latin hypercube design for 345-550 *kV* and corresponding E_{max} from computer simulation

S. No.	*R* *(mm)*	*T* *(mm)*	*h* *(mm)*	*L* *(mm)*	*V* *(kV)*	E_{max} *(kV/mm)*
1	198.98	28.57	0.61	4991.84	274.29	0.533
2	171.43	37.14	21.84	2077.55	200	0.279
3	281.63	6.43	106.73	2355.1	266.33	0.742
4	290.82	13.57	11.22	2979.59	284.9	0.774
5	162.24	11.43	27.14	3881.63	215.92	0.499
6	263.27	35.71	19.18	2563.27	311.43	0.578
7	97.96	35	64.29	3118.37	298.16	0.541
8	139.29	30.71	51.02	4922.45	319.39	0.449
9	166.84	10	-4.69	3048.98	271.63	0.782
10	125.51	12.86	16.53	4644.9	290.2	0.643
11	272.45	17.86	96.12	4853.06	261.02	0.520
12	254.08	20	-7.35	3395.92	221.22	0.554
13	194.39	31.43	-10	2632.65	258.37	0.539
14	153.06	32.86	90.82	2008.16	250.41	0.338
15	221.94	33.57	109.39	4297.96	287.55	0.366
16	143.88	8.57	66.94	2285.71	231.84	0.507
17	134.69	7.14	112.04	4714.29	218.57	0.468
18	102.55	25	3.27	4783.67	223.88	0.424
19	277.04	32.14	40.41	4367.35	314.08	0.559
20	231.12	12.14	45.71	3673.47	330	0.784
21	203.57	36.43	93.47	2493.88	324.69	0.379

22	116.33	5	72.24	4089.8	308.78	0.698
23	217.35	19.29	24.49	1869.39	322.04	0.732
24	93.37	34.29	-2.04	2146.94	300.82	0.591
25	235.71	17.14	98.78	2424.49	205.31	0.416
26	88.78	15.71	35.1	2771.43	306.12	0.614
27	212.76	7.86	101.43	3812.24	282.24	0.671
28	157.65	16.43	80.2	5130.61	279.59	0.437
29	176.02	27.14	5.92	3534.69	316.73	0.609
30	180.61	14.29	88.16	1938.78	295.51	0.581
31	208.16	27.86	114.69	3951.02	207.96	0.293
32	79.59	21.43	13.88	2216.33	237.14	0.523
33	120.92	39.29	77.55	4436.73	239.8	0.371
34	111.73	25.71	69.59	3257.14	202.65	0.335
35	249.49	9.29	74.9	4159.18	210.61	0.514
36	300	23.57	58.98	3326.53	234.49	0.488
37	148.47	20.71	85.51	3465.31	327.35	0.446
38	226.53	22.14	43.06	1800	245.1	0.501
39	130.1	18.57	120	3187.76	253.06	0.391
40	185.2	26.43	53.67	3604.08	263.67	0.387
41	244.9	10.71	32.45	4575.51	268.98	0.677
42	189.8	24.29	56.33	5061.22	213.27	0.324
43	258.67	5.71	37.76	2702.04	226.53	0.678
44	295.41	30	48.37	5200	242.45	0.441
45	84.18	29.29	117.35	4506.12	292.86	0.587
46	240.31	40	29.8	3742.86	229.18	0.348

47	75	15	61.63	4020.41	255.71	0.553
48	267.86	37.86	104.08	2840.82	247.76	0.353
49	286.22	22.86	82.86	2910.2	303.47	0.607
50	107.14	38.57	8.57	4228.57	276.94	0.472

A Gaussian process prediction model was obtained from JMP to express E_{max} in terms of R, L, T, h and V. Model adequacy was checked using JMP jack-knife process as shown in Figure 6-8.

Figure 6-8 shows that the model was quite accurate as the line is making angle of 45^0 with the x axis. Theta in this case is the maximum for *R*, which is intuitive, as the ring diameter changes for each voltage level.

Figure 6-9 shows the marginal plot as obtained by JMP. It can be seen that that there is a local minimum for *R* and *h*. *T* and *V* are the main factors which contain the maximum electric field value below 0.45 *kV/mm.*

Optimization code for 345-550 kV case

The optimization code for 345-550 *kV* range was written in a manner similar to the 230 *kV* case. There were 5 voltage points for which the optimum corona ring dimensions were calculated, namely 380 *kV*, 400 *kV*, 440 *kV*, 495 *kV* and 550 *kV*. The line to ground voltages was taken as input variables for above mentioned system voltages. The corresponding length of insulator for each *kV* level from obtained from a regression model given in APPENDIX D.

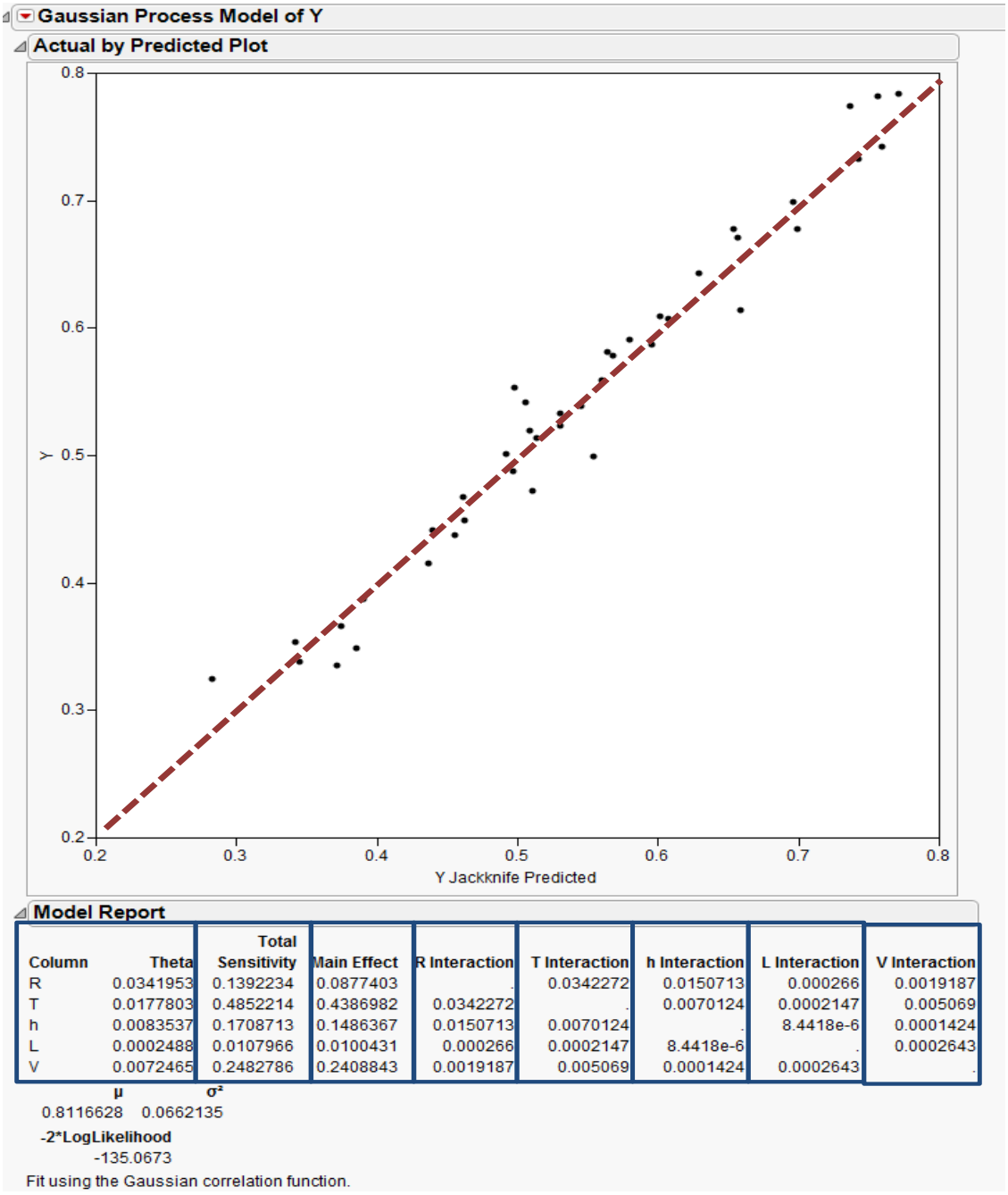

Model Report

Column	Theta	Total Sensitivity	Main Effect	R Interaction	T Interaction	h Interaction	L Interaction	V Interaction
R	0.0341953	0.1392234	0.0877403	.	0.0342272	0.0150713	0.000266	0.0019187
T	0.0177803	0.4852214	0.4386982	0.0342272	.	0.0070124	0.0002147	0.005069
h	0.0083537	0.1708713	0.1486367	0.0150713	0.0070124	.	8.4418e-6	0.0001424
L	0.0002488	0.0107966	0.0100431	0.000266	0.0002147	8.4418e-6	.	0.0002643
V	0.0072465	0.2482786	0.2408843	0.0019187	0.005069	0.0001424	0.0002643	.

μ	σ²
0.8116628	0.0662135

-2*LogLikelihood

-135.0673

Fit using the Gaussian correlation function.

Figure 6-8 Jackknife for 345-550 *kV* model and model parameters obtained from JMP

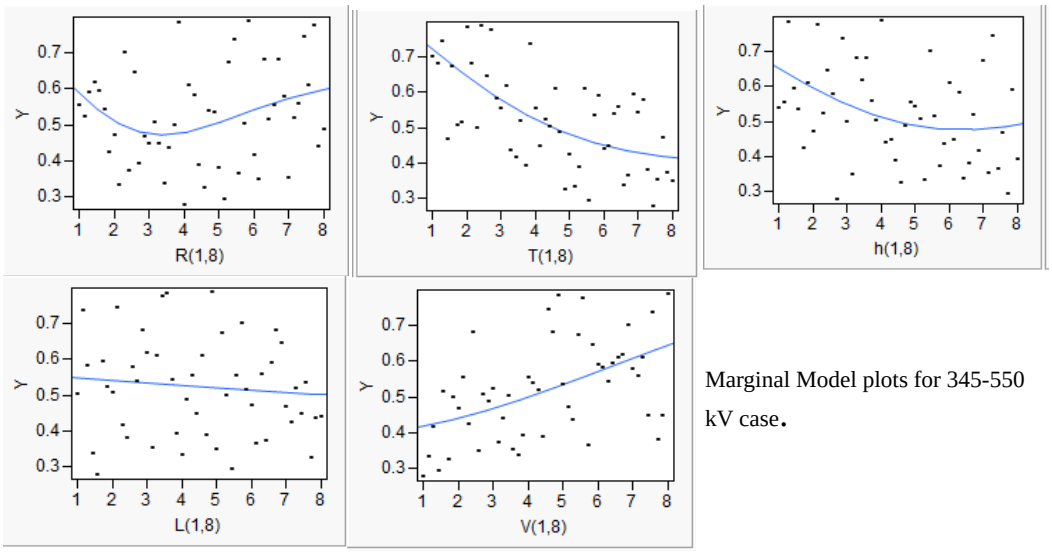

Marginal Model plots for 345-550 kV case.

Figure 6-9 Marginal model plots for 345-550 *kV* case

Optimization model:

Given, $$Emax = f_2\ (R, L, T, h, V) \quad (6.15)$$

Where f_2 is the objective function given in APPENDIX C

Minimize *T*, subject to constraints:

$$0.449 \leq Emax \leq 0.45 \quad (6.16)$$

$$1 \leq T \leq 6 \quad (6.17)$$

$$1 \leq h \leq 7 \quad (6.18)$$

$$1 \leq R \leq 5 \quad (6.19)$$

$$\begin{aligned} &1.04 \leq L \leq 2.7; && \text{\# for 380 } kV \\ &1.4 \leq L \leq 3.2; && \text{\# for 400 } kV \\ &2.12 \leq L \leq 4.2; && \text{\# for 440 } kV \\ &3.15 \leq L \leq 5.7; && \text{\# for 495 } kV \\ &4.16 \leq L \leq 7.7; && \text{\# for 550 } kV \end{aligned} \quad (6.20)$$

$$
\left.
\begin{array}{l}
2.027 \le V \le 2.2; \text{ \# for 380 } kV \\
2.58 \le V \le 2.8; \quad \text{\# for 400 } kV \\
3.80 \le V \le 4.20; \text{ \# for 440 } kV \\
5.57 \le V \le 5.75; \text{ \# for 495 } kV \\
6.16\ V \le 7.50; \text{ \# for 550 } kV
\end{array}
\right\} \qquad (6.21)
$$

T was minimized in for this case to get a correct trend in the solution. This can be explained from the fact that T has maximum impact on variation of E as given in model analysis in Figure 6-8. The results obtained from the optimization model are tabulated in Table 6-6.

Table 6-6 Optimization results obtained for 345-550 *kV* case

V (kV)	*D (in)*	*T(mm)*	*h(mm)*	*L(mm)*	E_{max}*	Difference (%)
380	10.5	13.8	42.9	2600.0	0.423	5.71%
400	10.6	14.9	45.8	2850.0	0.424	5.51%
440	10.6	17.2	51.9	3350.0	0.416	7.32%
495	11.0	20.5	60.2	4066.0	0.411	8.55%
550	11.4	23.6	69.2	5000.0	0.432	3.75%

E_{max}*: Value of maximum electric field obtained from computer simulations. Figure 6-10 shows the trend of various parameters vs. *V (kV)* level. Computer simulations were carried out to verify the correctness of the results, as shown in Figure 6-11.The results indicated that corona ring diameter and tube thickness increased for higher *kV*, which was practically observed. Computer simulations results indicated that the electric field was within the limits, however deviations in the range of 3-8 % were observed, as tabulated in Table 6-6. The

results indicated that corona ring optimization was successfully obtained through the Gaussian process model with acceptable error tolerance.

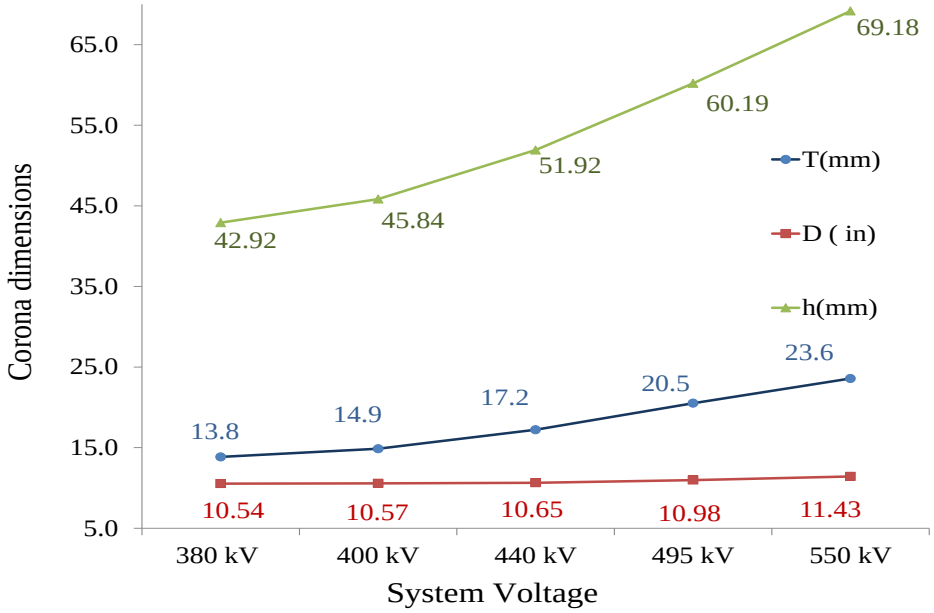

Figure 6-10 Results from optimization for 345-550 *kV* system voltage

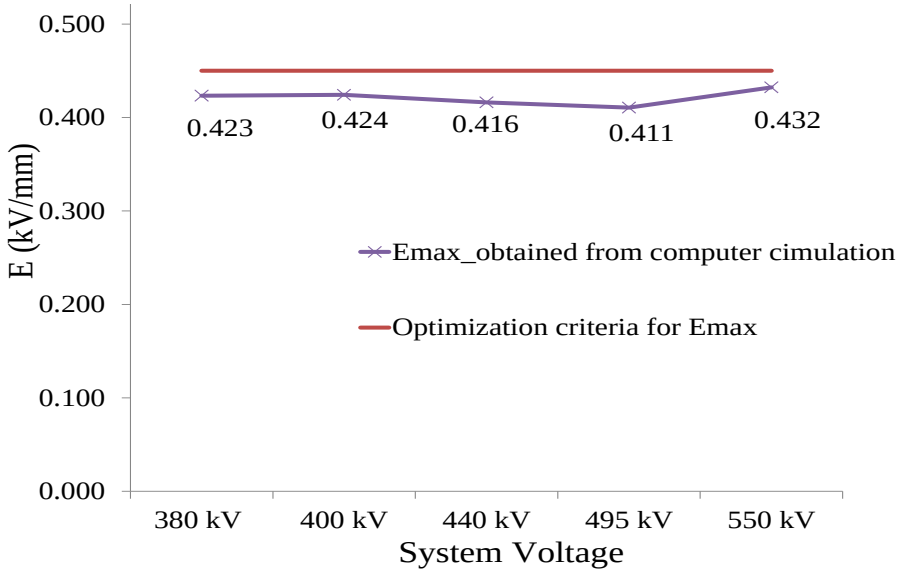

Figure 6-11 Results from the computer simulations carried out for optimization process output

Chapter 7. Conclusions and Future Work

7.1 Conclusions and Main Contributions

The effect of line compaction on the surface electric field of the composite insulators was studied and quantified. A case study on impact of compacting high phase order system on the surface electric field of insulators was also studied. An optimization program based on Gaussian process model was developed for obtaining the corona ring dimensions for compact transmission lines over a range of voltages. From the research conducted, following conclusions can be made:

- The dry arc lengths of insulators for different voltage levels can be compacted up to 70% of length stipulated in NESC standard. The phase-to-phase and phase-to-tower distance can be compacted in same proportion. The electric field on the surface of insulators rises due to the line compaction. In case of 230 *kV*, a higher corona ring diameter is required to contain the electric field within the limits. For 345 *kV* and 500 *kV*, the corona rings used in field are found to be adequate for 70% compact structures.
- It is necessary to model conductors, grounding structures and number of circuits to get a correct estimation on the surface electric field of insulators.
    - In absence of conductor modeling, electric field obtained from 3D computer simulation on braced post insulators, 345 *kV* and above *kV* level suspension insulators is incorrect.

- For 345 *kV* and above voltage levels, for braced post and V string insulators configurations, the electric field values near the ground end might be higher than the high voltage end. Hence corona ring is recommended to be installed at the both end.
- The electric field due to double circuit configurations is marginally higher than the single phase circuits for all the voltage levels

- The electric field on the surface of insulators for 6 phase system is highest when the phase sequence is in a particular order, as shown in Figure 5-32. The surface electric field on the surface of insulators for compact 6 phase structures was found to be within the limits.
- The optimization program for 230 *kV* voltage level based on Gaussian process modeling indicated an 8.04" corona ring to be installed on the insulators. This value is in line with the industry practice.
- The optimization model was extended for 345 *kV* to 550 *kV* voltage levels. The results indicate that a corona ring with diameter of 10.5", 10.6", 10.6", 11.0" and 11.4" are required for 380 *kV*, 400 *kV*, 440 *kV*, 495 *kV* and 550 *kV* respectively to limit the electric field within stipulated values.

Contributions:

- Methods for reducing computational time, factors necessary for obtaining getting correct have been explored and discussed
- A Gaussian process based optimization program was modeled and successfully implemented.

7.2 Future Work

In this research, the impact of line compaction technique on the surface electric field was investigated. Simplified insulators model was used. There are a few concerns which could be addressed:

- The effect of contamination on insulators should be explored as it can increase the corona
- Laboratory testing of hardware should be done to verify the computer simulation results for compact transmission lines
- New technologies such as integrated cross arm insulators [54] should be studied for compact transmission lines

REFERENCES

[1] United States Department of Energy-Office of Electric Transmission and Distribution, "GRID 2030 –A National Vision for Electricity," [online], available at: http://www.climatevision.gov/sectors/electricpower/pdfs/electric_vision.pdf, July 2003

[2] United States Environmental Protection agency, "Renewable Portfolio Standards Fact Sheet," [online], available at: http://www.epa.gov/chp/state-policy/renewable_fs.html, April 2009

[3] Electric Power Research Institute, "Transmission Line Reference Book: 115-138 kV Compact Line Design," First edition, Palo Alto, California, 1978

[4] Stewart, J.R.; Grant, I.S.; , "High Phase Order - Ready for Application," IEEE Transactions on Power Apparatus and Systems, vol. PAS-101, no. 6, pp. 1757-1767, June 1982

[5] Alawar, A.; Bosze, E.J.; Nutt, S.R.; , "A Composite Core Conductor for Low Sag at High Temperatures," IEEE Transactions on Power Delivery, vol. 20, no. 3, pp. 2193- 2199, July 2005

[6] Phillips, A.J.; Kuffel, J.; Baker, A.; Burnham, J.; Carreira, A.; Cherney, E.; Chisholm, W.; Farzaneh, M.; Gemignani, R.; Gillespie, A.; Grisham, T.; Hill, R.; Saha, T.; Vancia, B.; Yu, J.; , "Electric Fields on AC Composite Transmission Line Insulators," , IEEE Transactions on Power Delivery, vol. 23, no. 2, pp. 823-830, April 2008

[7] Electric Power Research Institute, "Transmission Line Reference Book, 345 kV and Above," Second Edition Revised , Palo Alto, California, 1982

[8] Sima, W.; Espino-Cortes, F.P.; Cherney, E.A.; Jayaram, S.H.; , "Optimization of Corona Ring Design for Long-Rod Insulators using FEM based Computational Analysis," IEEE Conference Record of the 2004 International Symposium on Electrical Insulation, pp. 480- 483, 19-22 Sept. 2004

[9] Ilhan, S.; Ozdemir, A.; , "380 *kV* Corona Ring Optimization for AC Voltages," IEEE Transactions on Dielectrics and Electrical Insulation, vol. 18, no. 2, pp. 408-417, April 2011

[10] Li, J.; Peng, Z.; Feng, Y.; Fu, X.; Xie, T.; , "Electric Field Calculation and Grading Ring Optimization of Composite Insulator for 500*kV* AC Transmission Lines," 10th IEEE International Conference on Solid Dielectrics, pp. 1-4, 4-9 July 2010

[11] Doshi, T.; Gorur, R.S.; Hunt, J.; , " Electric Field Computation of Composite Line Insulators up to 1200 *kV* AC," IEEE Transactions on Dielectrics and Electrical Insulation, vol. 18, no. 3, pp. 861-867, June 2011

[12] Gorur, R.S.;. Cherney, E.A.; Burnham, J.T; , "Outdoor Insulators," Ravi S. Gorur Inc., Phoenix, Arizona, USA, 1999

[13] Karady, G.G.; Shah, M.; Brown, R.L.; , "Flashover Mechanism of Silicone Rubber Insulators used for Outdoor Insulation-I," IEEE Transactions on Power Delivery, vol.10, no.4, pp.1965-1971, Oct 1995

[14] Naito, K.; Izumi, K.; Takasu K.; Matsuoka, R.; " Performance of Composite Insulators under Polluted Conditions", CIGRE Session Paper No.33-301, 1996

[15] Looms, J.S.T.; , "Insulators for High Voltage," Peter Peregrinus Ltd, London, U. K., 1988.

[16] Jordan, N.M.; Lau, Y.Y.; French, D.M.;Gilgenbach, R.M.; Pengvanich, P; , "Electric Field and Electron Orbits near a Triple Point," Journal of Applied Physics, vol. 102, Issue 3, 2007

[17] Bergeron, K. D. ; , "Theory of the Secondary Electron Avalanche at Electrically Stressed Insulator Vacuum Interfaces," Journal of Applied Physics, vol. 48, Issue 7, Aug 1977

[18] National Electrical Safety Code, "National Electrical Safety Code (NESC) Handbook," Seventh Edition, pp. 802, Aug. 2011

[19] Stewart, J.R.; Wilson, D.D.; , "High Phase Order Transmission-A Feasibility Analysis Part I-Steady State Considerations," IEEE Transactions on Power Apparatus and Systems , vol. PAS-97, no. 6, pp. 2300-2307, Nov. 1978

[20] North American Electric Reliability Corporation, "High Voltage Transmission Circuit Miles by Voltage (230kV and above)-All NERC Regions and Sub regions (2004)," [online], accessed on 05/14/2012, available at : http://www.nerc.com/page.php?cid=1%7C9%7C119

[21] Zhao, T.; Comber, M.G ; , "Calculation of Electric Field and Potential Distribution along Nonceramic Insulators considering the Effects of Conductors and Transmission Towers," IEEE Transactions on Power Delivery, vol. 15, no. 1, pp. 313-318, Jan. 2000

[22] Papailiou, K.O.; , "Composite Insulators are gaining Ground-25 Years of Swiss Experience," IEEE Transmission and Distribution Conference, vol. 2, pp. 827-833, 11-16 April 1999

[23] Alston, L.L.; , “High-Voltage Technology,” Oxford University Press, UK, 1968

[24] Wang, B.Z.; Mittra, R.; Wei, S.; , "A Domain Decomposition Finite-Difference Method Utilizing Characteristic Basis Functions for Solving Electrostatic Problems," IEEE Transactions on, Electromagnetic Compatibility, vol.50, no.4, pp.946-952, Nov. 2008

[25] Computational Methods in Electromagnetics,[online], available at: http://www.electromagnetics.info/comp.htm

[26] Wang, B.Z.; Mittra, R.; Shao, W.; , "A Domain Decomposition Finite-Difference Method Utilizing Characteristic Basis Functions for Solving Electrostatic Problems," IEEE Transactions on Electromagnetic Compatibility, vol. 50, no. 4, pp. 946-952, Nov. 2008

[27] Yee, K.; ,"Numerical Solution of Initial Boundary Value Problems Involving Maxwell's Equations in Isotropic Media," IEEE Transactions on Antennas and Propagation, vol. 14, no. 3, pp. 302-307, May 1966

[28] Liao, Y.S.; Chyuan, S.Y.; Chen, J.T. ; , "FEM versus BEM," Circuits and Devices Magazine, IEEE , vol. 20, no. 5, pp. 25- 34, Sept.-Oct. 2004

[29] Kim, C.N.; Jang, J.B. ; Huang, X.Y.; Jiang, P.K.; Kim, H. ; , “Finite Element Analysis of Electric Field Distribution in Water Treed XLPE Cable Insulation (1): The Influence of Geometrical Configuration of Water Electrode for Accelerated Water Treeing Test”, Journal of Polymer Testing, vol. 26, pp. 482 – 488, 2007

[30] Stratton, J. A, ; , “Electromagnetic Theory,” McGraw-Hill Book Company, Inc., New York, 1941

[31] Daffe, J.; Olsen, R.G. ; , "An Integral Equation Technique for Solving Rotationally Symmetric Electrostatic Problems in Conducting and Dielectric Material," IEEE Transactions on Power Apparatus and Systems, vol. PAS-98, no. 5, pp. 1609-1616, Sept. 1979

[32] Olsen, R.G.; Einarsson, O. ; , "Boundary Element Methods for Weakly Three Dimensional Quasi-Electrostatic Problems," IEEE Transactions on Power Delivery, vol. 2, no. 4, pp. 1276-1284, Oct. 1987

[33] Rasolonjanahary, J.L.; Krahenbuhl, L.; Nicolas, A.; , "Computation of Electric Fields and Potential on Polluted Insulators using a Boundary Element Meth-

od," IEEE Transactions on Magnetics, vol. 28, no. 2, pp. 1473-1476, Mar 1992

[34] Integrated Engineering Software, "COULOMB® ," [online], available at: http://www.integratedsoft.com/products/coulomb

[35] Olsen, R.G.; Zhao, T.; Comber, M.G.; , "Discussion of "Calculation of Electric Field and Potential Distribution along Nonceramic Insulators considering the Effects of Conductors and Transmission Towers" [Closure to Discussion]," IEEE Transactions Power Delivery, vol. 15, no. 4, pp. 1353-1354, Oct. 2000

[36] NGK-Locke Polymer Insulators Inc, "Polymer Post Insulators for 46 to 500kV Applications"; "Polymer Braced Post Insulators," Virginia Beach, Virginia, June 2012

[37] MacLean Power System Franklin Park , "APEX™ Insulators," Franklin Park, Illinois , June 2012

[38] Lapp Insulators , "Rodurflex® Advanced technology insulator," LeRoy, New York, June 2012

[39] Ohio Brass , "Hi*Lite XL Transmission Insulators," AIKEN, South Carolina, June 2012

[40] Gustek, M.P.; Grisham, T.M.; Crino, A.D.; , "Practical Considerations for The Applications of Polymer Post Insulators in Transmission Class Switch Installations," Proceedings of Seventh International Conference on Transmission and Distribution Construction and Live Line Maintenance.,pp. 94-100, 29 Oct-3 Nov 1995

[41] Baker, A.; , "Design and Application of Braced High Voltage Insulator Assemblies," , IEEE Electrical Insulation Magazine,vol. 26, no. 2, pp. 26-34, March-April 2010

[42] Bernstorf, R.A., "Braced Line Post Ratings," IEEE/PES Transmission and Distribution Conference and Exposition, pp. 1-6, 21-24 April 2008

[43] Sun, B.; Hou, L.; Zhang, C.; Guan, Z. ; Wang, L.; Macalpine, M.; , "Extreme Bending of Composite Insulators on 750 kV Compact Transmission Lines," IEEE Transactions on Dielectrics and Electrical Insulation, vol. 17, no. 6, pp. 1781-1786, Dec. 2010

[44] Cherney, E.A.; , "Long-Term Mechanical Life Testing of Polymeric Post Insulators for Distribution and A Comparison to Porcelain," IEEE Transactions on Power Delivery, vol. 3, no. 3, pp. 1141-1145, Jul 1988

[45] Vlastos, A.E.; Sherif, E., "Natural Ageing of EPDM Composite Insulators," IEEE Transactions on Power Delivery, vol. 5, no. 1, pp. 406-414, Jan 1990

[46] Gorur, R.S.; Chemey, E.A.; Hackam, R. ; , "The AC and DC Performance of Polymeric Insulating Materials Under Accelerated Aging in a Fog Chamber", IEEE Transaction on Power Delivery, Vol. 3,NO. 4, pp. 1892-1902, Oct. 1988

[47] IEEE Standards, "IEEE Guide for Application of Composite Line Post Insulators," 1572-2004 , vol., no., pp.0_1-16, 2004

[48] Myers, R.H. ; Montgomery, D.C. ; Anderson-Cook, C.M. ; , "Response Surface Methodology: Process and Product Optimization Using Designed Experiments," John Wiley & Sons, 2009

[49] JMP, "JMP 10 Fact Sheet," [online] , available at: http://www.jmp.com/software/jmp10/pdf/jmp10_fact_sheet.pdf

[50] Sima, W.; Espino-Cortes, F. P.; Cherney, E. A.; Jayaram, S. H.; , "Optimization of Corona Ring Design for Long-Rod Insulators using FEM Based Computational Analysis," IEEE International Symposium on Electrical Insulation, pp. 480- 483, 19-22 Sept. 2004

[51] JMP user manual, "Modeling and Multivariate Methods - JMP ," [online], available at: http://www.jmp.com/support/downloads/pdf/jmp9/modeling_and_multivariate_methods.pdf

[52] AMPL, available at: www.ampl.com

[53] KNITRO, available at: www.ziena.com/knitro.htm

[54] EMC Pacific insulators , "Product Sheets," Melbourne, Australia, [online], available at : http://www.emcpacific.com.au/product_sheets/EMC_IXI.pdf

APPENDIX A

TOWER DIMENSIONS FOR SIMULATION IN COULOMB

Major dimensions for all the tower configurations were referred from EPRI Red book and Blue Book [3]. Dimension of each type of tower is mentioned below.

A. H bridge Tower:

H bridge tower were considered for simulation as there are number of lines operating on this configuration. Typically this configuration has the highest ph-ph distance; hence investigation for extent of compaction becomes important. The major dimensions of H bridge tower are summed up in Table A-1

Table A-1 Dimensions of H bridge tower

H Bridge Tower (all dimensions in feet)			
Data	230 *kV*	345 *kV*	500 *kV*
ph –ph clearance, D	18	26	35
Tower height	73.3	76	85
Horizontal span, S	36	52	105
Insulator string type	I	I	V
Material type	Steel	Steel	Steel[7]

[7] Steel's material properties was chosen from the available library in COULOMB®

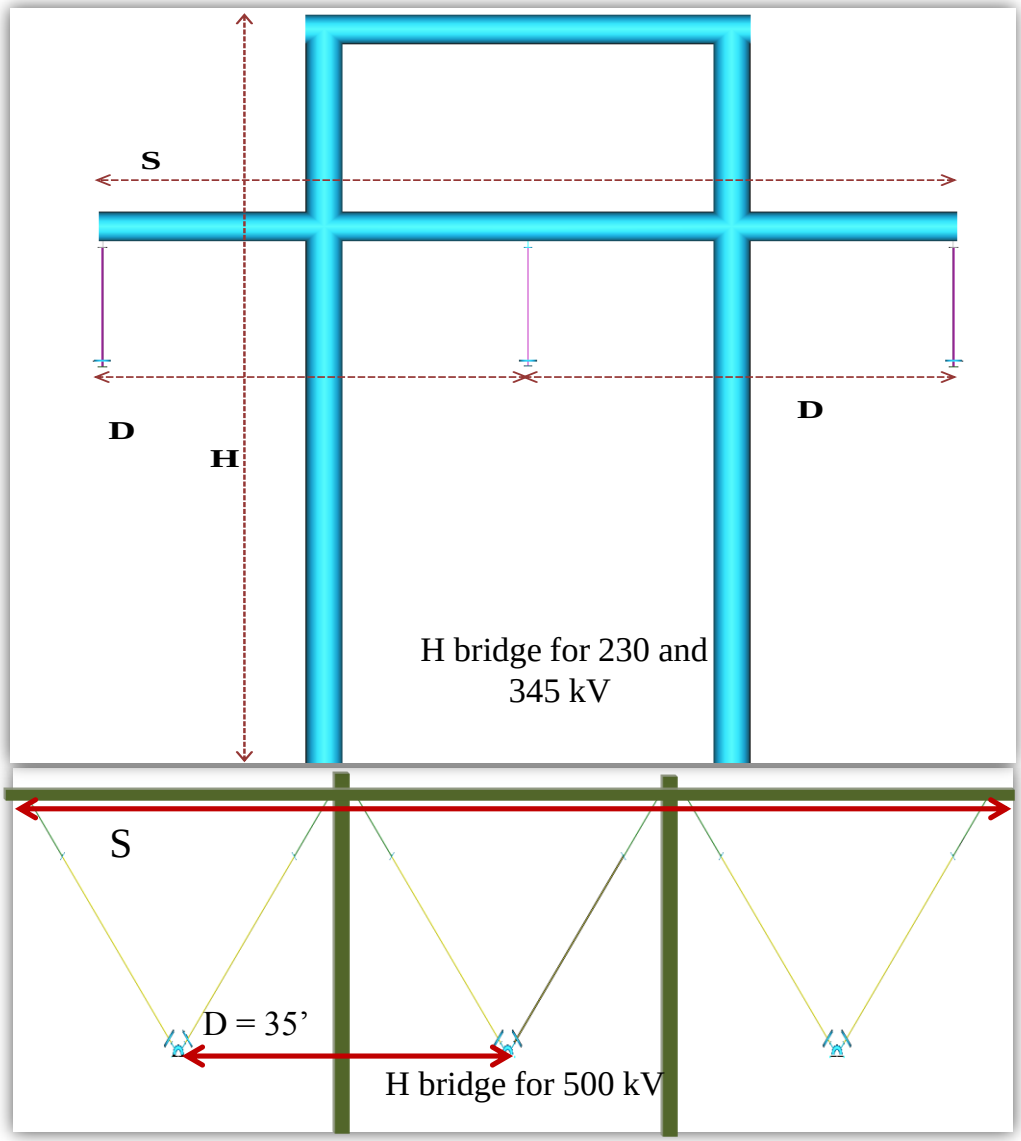

Figure 1 Dimensions for 230 *kV*, 345 *kV* H bridge I string and 500 *kV* V string tower

B. Tapered steel pole tower with string insulator

Table A-2 Dimensions of Tapered Steel Pole Tower with string insulator single and double circuit

Tapered Steel Pole Tower with string insulator (all dimensions in feet)			
Data	230 *kV*	345 *kV*	500 *kV*
ph –t clearance, A	10	14	37
ph –ph clearance, C	18	22	30
Ground wire clearance, D	10	12	15
Tower height, H	135	135	135
Insulator string type	I	I	I
Material type	Steel	Steel	Steel
Insulator dry arc length (L_{in})	6.56	8.53	16.40

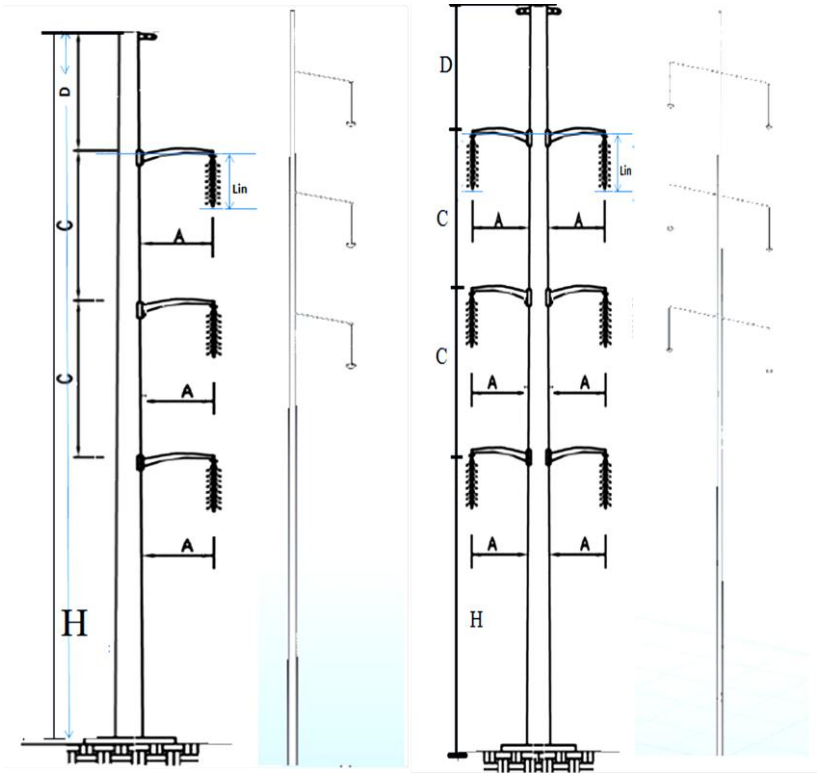

Figure 2 Tapered steel pole tower with string insulator dimensions, modeled in COULOMB®

C. Tapered steel pole tower with brace post insulator

Tapered steel pole for 230 kV and 345 kV were modeled for single and double circuit as shown in Figure 3 . For 500 kV, delta configuration of the tower was modeled, as mentioned in EPRI Red book.

Table A-3 Dimensions of Tapered Steel Pole Tower with brace post insulator; single and double circuits

Tapered Steel Pole Tower with brace post insulator (all dimensions in feet)			
Data	230 *kV*	345 *kV*	500 *kV*
Post Insulator dry arc length L_{post}	6.58	6.71	9.86
ph –t clearance, A	6.58	6.71	17
Rod Insulator dry arc length (L_{in})	6.56	8.43	16.40
ph –ph clearance, C	18	22	25
Ground wire clearance, D	10	12	15
Tower height, H	120	120	120
Material type	Steel	Steel	Steel

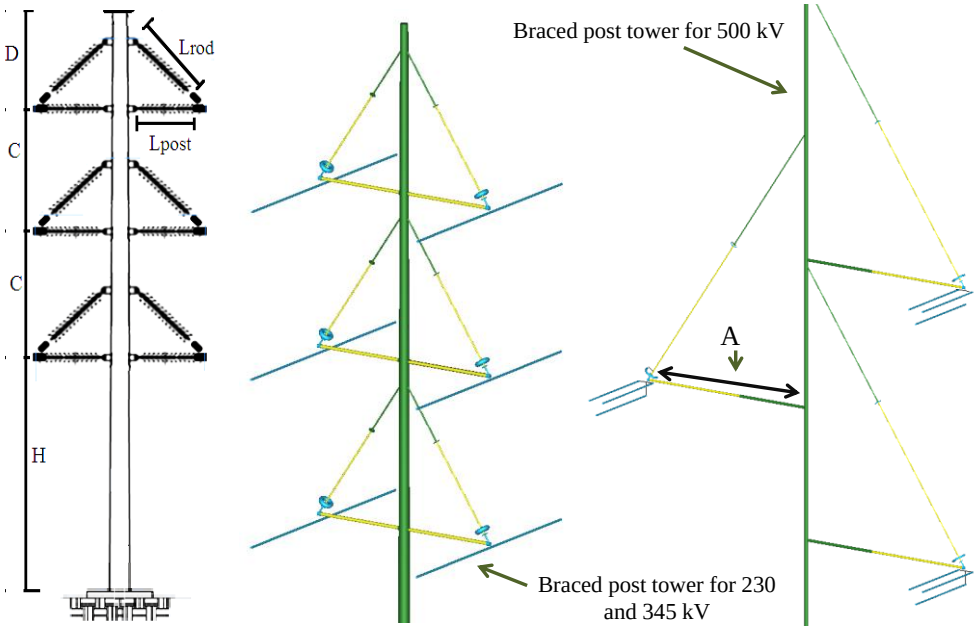

Figure 3 Brace post tower dimensions

D. Tapered steel pole tower with post insulator

Tapered steel pole with post configuration for 230 *kV* is modeled. For 345 *kV* and 500 *kV*, no mention of towers with post insulators is found in EPRI Red book. The most probably reason could be the weight of conductor bundles which necessitates use of brace post insulators.

Table A-4 Dimentions for tapered steel tower for post insulators

Tapered Steel Pole Tower with post insulator (all dimensions in feet)		
Data	230 *kV*	345 *kV*
Post Insulator dry arc length L_{post}	5.88	6.71
ph –ph clearance, C	11	22
Ground wire clearance, D	10	12
Tower height, H	135	135
Material type	Steel	Steel

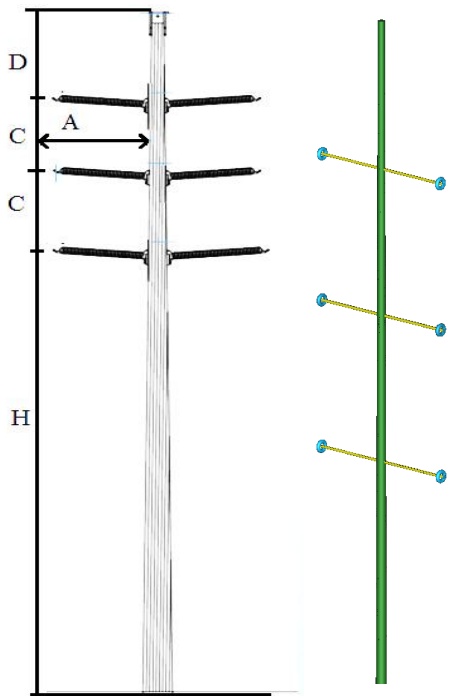

Figure 4 Tapered steel tower with post insulators for 230 *kV* and 345 *kV*

E. Tapered steel pole tower with V string for 345 *kV*

Tapered steel pole with V string configuration is investigated for 345 *kV*. The dimensions of tower is mentioned in table

Table A-5 Dimensions for tapered steel tower for V string insulators

Data	345 *kV*
ph –t clearance, A	18
ph –ph clearance, C	23
Ground wire clearance, D	12
Tower height, H	135
Material type	Steel

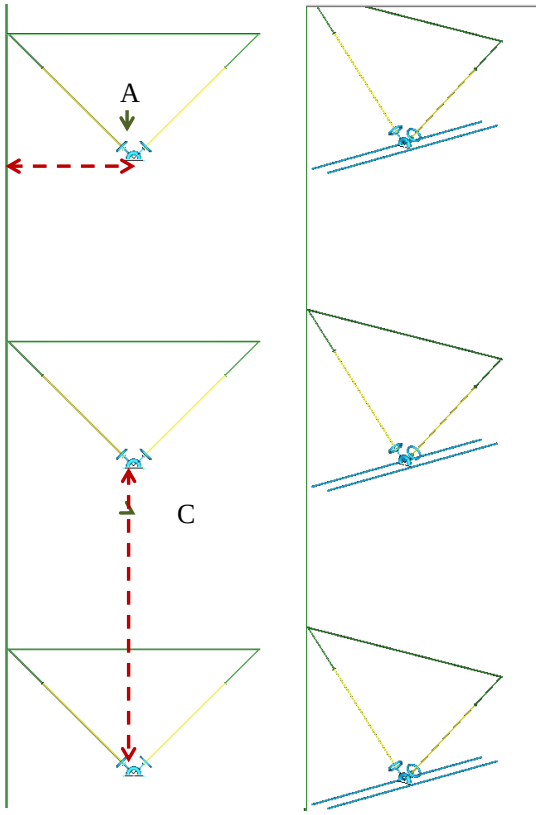

Figure 5 Tapered steel tower with V string for 345 *kV* tower

APPENDIX B

Y (Emax) PREDICTION FORMULA FOR 230 k*V* CASE

The prediction formula for maximum surface electric field for 230 *kV* model is given by:

```
Y = 0.373215923745387 + -0.090255077195868 * 2.7182818^(-
(0.026990234904265 * (R - 3.41379310344828) ^ 2 +0.165723980831553 *
(T -2.75862068965517) ^ 2 + 0.0533730224616919 * (h -
7.27586206896552) ^ 2+0.000999725330962188 * (L     -
1.10344827586207) ^ 2)) + 1.53036620141281 * 2.7182818^(-
(0.026990234904265 * (R - 5.58620689655173) ^ 2 + 0.165723980831553 *
(T -1.10344827586207) ^ 2 + 0.0533730224616919 * (h -
3.89655172413793) ^ 2 +0.000999725330962188 * (L - 1.41379310344828)
1.20689655172414)^2)) + -0.370936537279077 * 2.7182818^(-
(0.026990234904265 * (R - 4.86206896551724) ^ 2 + 0.165723980831553 *
(T -         3.79310344827586) ^ 2 + 0.0533730224616919 * (h -
2.68965517241379) ^ 2 +0.000999725330962188 * (L - 1.82758620689655)
^ 2)) + 0.338861734588035 * 2.7182818^(-(0.026990234904265 * (R -
1.96551724137931) ^ 2 + 0.165723980831553 * (T -2.96551724137931) ^ 2
+ 0.0533730224616919        * (h - 3.41379310344828) ^ 2
+0.000999725330962188 * (L - 2.6551724137931) ^ 2)) + -
0.739817965872073 * 2.7182818^(-(0.026990234904265 * (R -
3.6551724137931) ^ 2 + 0.165723980831553 * (T - 1) ^2 +
0.0533730224616919 * (h - 4.62068965517241) ^ 2 +
0.000999725330962188 * (L - 2.86206896551724) ^ 2)) + -
0.0337507166166394 * 2.7182818^(-(0.026990234904265 * (R -
3.89655172413793) ^ 2 + 0.165723980831553 * (T -1.31034482758621) ^ 2
+ 0.0533730224616919 * (h - 6.79310344827586) ^ 2
+0.000999725330962188 * (L - 1.72413793103448) ^ 2)) + -
0.480663592774934 * 2.7182818^(-(0.026990234904265 * (R -
6.06896551724138) ^ 2 + 0.165723980831553 * (T -2.86206896551724) ^ 2
+ 0.0533730224616919 * (h - 7.75862068965517) ^ 2
+0.000999725330962188 * (L - 2.55172413793103) ^ 2)) + -
0.00361906426848968 * 2.7182818^(-(0.026990234904265 * (R -
2.44827586206897) ^ 2 + 0.165723980831553 * (T -3.37931034482759) ^ 2
+0.0533730224616919 * (h - 3.17241379310345) ^ 2
+0.000999725330962188 * (L - 4) ^ 2)) + -0.145513187267454 *
2.7182818^(-(0.026990234904265 * (R - 3.17241379310345) ^ 2 +
0.165723980831553 * (T -1.41379310344828) ^ 2 + 0.0533730224616919 *
(h - 8) ^ 2 +          0.000999725330962188 * (L - 3.17241379310345) ^ 2)) +
-0.928381076937402 * 2.7182818^(-(0.026990234904265 * (R -
4.37931034482759) ^ 2 + 0.165723980831553 * (T -2.3448275862069) ^ 2 +
0.0533730224616919 * (h - 1.48275862068966) ^ 2 +
          0.000999725330962188 * (L - 3.68965517241379) ^ 2)) +
0.402318942362071 * 2.7182818^(    -(0.026990234904265 * (R -
```

```
5.10344827586207) ^ 2 + 0.165723980831553 * (T - 4) ^ 2 +
0.0533730224616919 * (h - 4.37931034482759) ^ 2 +
0.000999725330962188 *(L - 3.48275862068965) ^ 2)) +
0.565498771911774 * 2.7182818^(-(0.026990234904265 * (R -
            7.51724137931034) ^          2 + 0.165723980831553 * (T -
1.62068965517241) ^ 2 + 0.0533730224616919 * (h - 7.51724137931034) ^
2 +0.000999725330962188  *(L - 1.93103448275862) ^ 2)) +
0.152002988807503 * 2.7182818^(-(0.026990234904265 * (R -
7.03448275862069) ^ 2 + 0.165723980831553 * (T -3.48275862068965) ^ 2
+ 0.0533730224616919 * (h - 1.72413793103448) ^ 2
+0.000999725330962188 * (L - 3.06896551724138) ^ 2)) +
0.0264512506193638 * 2.7182818^(-(0.026990234904265 * (R -
1.48275862068966)            ^ 2 + 0.165723980831553 * (T -
3.17241379310345) ^ 2 + 0.0533730224616919 * (h - 1.24137931034483) ^
2 +0.000999725330962188 * (L - 1.51724137931034) ^ 2)) +
0.301036593989002 * 2.7182818^(-(0.026990234904265 * (R -
            6.31034482758621)            ^ 2 + 0.165723980831553 * (T -
2.55172413793103) ^ 2 + 0.0533730224616919 * (h - 5.3448275862069) ^ 2
+0.000999725330962188     * (L - 1.31034482758621) ^ 2)) + -
0.991859453097413 * 2.7182818^(-(0.026990234904265 * (R -
6.79310344827586) ^ 2+0.165723980831553 * (T -1.72413793103448) ^ 2 +
0.0533730224616919 * (h - 6.06896551724138) ^ 2
+0.000999725330962188 * (L           - 3.37931034482759) ^ 2)) +
0.146946126197706 * 2.7182818^(-(0.026990234904265 * (R -
1.72413793103448) ^ 2 + 0.165723980831553 * (T -3.58620689655172) ^ 2
+ 0.0533730224616919 * (h - 5.10344827586207) ^ 2
+0.000999725330962188 * (L -          1.62068965517241)            ^ 2)) +
0.659379946693516 * 2.7182818^(-(0.026990234904265 * (R -
4.62068965517241) ^ 2 + 0.165723980831553 * (T -3.06896551724138) ^ 2
+ 0.0533730224616919 * (h - 7.03448275862069) ^ 2
+0.000999725330962188 * (L -          3.89655172413793) ^ 2)
) + 1.22389847083972 * 2.7182818^(-(0.026990234904265 * (R -
2.93103448275862) ^ 2 + 0.165723980831553 * (T -2.13793103448276) ^ 2
+ 0.0533730224616919 * (h - 4.86206896551724) ^ 2
+0.000999725330962188 * (L - 3.79310344827586) ^ 2)) +
1.06339338311103 *           2.7182818^(-(0.026990234904265 * (R -
4.13793103448276) ^ 2 + 0.165723980831553 * (T -1.82758620689655) ^ 2
+0.0533730224616919         * (h - 1) ^ 2 + 0.000999725330962188 * (L -
2.24137931034483) ^ 2)) + 0.195646375570189 * 2.7182818^(-
(0.026990234904265 * (R -1.24137931034483) ^ 2 + 0.165723980831553 *
(T -2.24137931034483) ^ 2 + 0.053373022461691 9 * (h -
6.55172413793104) ^ 2 +0.000999725330962188 * (L - 2.3448275862069) ^
2)) + -0.768582385459232 * 2.7182818^(-(0.026990234904265 * (R -
6.55172413793104)            ^ 2 + 0.165723980831553 * (T -
```

```
1.20689655172414) ^ 2 + 0.0533730224616919 * (h - 2.20689655172414) ^
2 + 0.000999725330962188 * (L - 3.27586206896552) ^ 2)) +
0.127433446954132 * 2.7182818^(-(0.026990234904265 * (R - 8) ^ 2
+0.165723980831553 * (T - 2.03448275862069)^ 2 + 0.0533730224616919
* (h - 2.93103448275862) ^ 2 + 0.000999725330962188*(L -
2.13793103448276) ^ 2)) + 0.0422263881720368 * 2.7182818^(-
(0.026990234904265 * (R - 7.75862068965517) ^ 2 + 0.165723980831553 *
(T -3.27586206896552) ^ 2 + 0.0533730224616919 * (h -
5.82758620689655) ^ 2 +0.000999725330962188 * (L - 3.58620689655172)
            2.03448275862069) ^ 2)
) + -0.630977241395947 * 2.7182818^(-(0.026990234904265 * (R -
5.3448275862069) ^ 2 + 0.165723980831553 * (T -2.6551724137931) ^     2
+ 0.0533730224616919 * (h - 4.13793103448276) ^ 2
+0.000999725330962188 * (L - 2.75862068965517) ^ 2)) + -
0.581990948651797 * 2.7182818^(-(0.026990234904265 * (R -
2.20689655172414) ^ 2 + 0.165723980831553 * (T -3.68965517241379)^2+
2.44827586206897) ^ 2 + 0.0533730224616919 *          (h -
1.96551724137931) ^ 2 +0.000999725330962188 * (L - 1) ^ 2)) +
0.248959773754466 * 2.7182818^(-(0.026990234904265 * (R      - 1) ^      2
+ 0.165723980831553 * (T - 1.51724137931034) ^ 2 + 0.0533730224616919
* (h - 2.44827586206897) ^ 2 +  0.000999725330962188 *(L -
2.44827586206897) ^ 2));
```

APPENDIX C

Y (EMAX) PREDICTION FORMULA FOR 345-550 k*V* CASE

The prediction formula for maximum surface electric field for 345-550 *kV* model is given by:

```
Y=  0.811662787244785 + 1.09693151651989 * 2.71828183^(-
    (0.0341952559501701 * (R - 4.85714285714286) ^ 2 +
    0.0177803313628377 * (T -5.71428571428571) ^ 2 +
    0.00835368531666321 * (h - 1.57142857142857) ^ 2 +
    0.000248841071006035 * (L - 7.57142857142857) ^ 2 +
    0.00724650933494119 * (V - 5) ^ 2)) + -1.07554945567888 *
    2.71828183^(-(0.0341952559501701 * (R - 7.42857142857143) ^ 2 +
    0.0177803313628377 * (T -1.28571428571429) ^ 2 +
    0.00835368531666321 * (h - 7.28571428571429) ^ 2
    +0.000248841071006035 * (L - 2.14285714285714) ^ 2 +
    0.00724650933494119 * (V -4.57142857142857) ^ 2)) +
    2.80805832231064 * 2.71828183^(-(0.0341952559501701 * (R -
    7.71428571428572) ^ 2 + 0.0177803313628377 * (T -2.71428571428571) ^
    2 + 0.00835368531666321 * (h - 2.14285714285714) ^ 2
    +0.000248841071006035 * (L - 3.42857142857143) ^ 2 +
    0.00724650933494119 * (V -5.57142857142857) ^ 2)) + -
    6.48198565818126 * 2.71828183^(-(0.0341952559501701 * (R -
    3.71428571428571) ^ 2 + 0.0177803313628377 * (T -2.28571428571429) ^
    2 + 0.00835368531666321 * (h - 3) ^ 2 + 0.000248841071006035 * (L -
    .28571428571429) ^ 2 + 0.00724650933494119 * (V - 1.85714285714286)
    ^ 2)) + 1.89489906476866 * 2.71828183^(-(0.0341952559501701 * (R -
    6.85714285714286) ^ 2 + 0.0177803313628377 * (T -
                7.14285714285714) ^ 2 + 0.00835368531666321 * (h -
    2.57142857142857) ^ 2 +0.000248841071006035 * (L -
    2.57142857142857) ^ 2 + 0.00724650933494119 * (V - 7) ^ 2)) +
    6.67355574817552 * 2.71828183^(-(0.0341952559501701 * (R -
    1.71428571428571) ^ 2 + 0.0177803313628377 * (T - 7) ^ 2 +
    0.00835368531666321 * (h - 5) ^ 2 + 0.000248841071006035 * (L -
    3.71428571428571) ^ 2 + 0.00724650933494119 * (V -
    6.28571428571429) ^ 2)) + -3.64965694677345 * 2.71828183^(-
    0.0341952559501701 * (R - 3) ^ 2 + 0.0177803313628377 * (T -
    6.14285714285714) ^ 2 + .00835368531666321 * (h - 4.28571428571429)
    ^ 2 + 0.000248841071006035              * (L - 7.42857142857143) ^ 2 +
    0.00724650933494119 * (V - 7.42857142857143) ^ 2)) +
    4.65691558292103 * 2.71828183^(    -(0.0341952559501701 * (R -
    3.85714285714286) ^ 2 + 0.0177803313628377 * (T - 2) ^ 2 +
    0.00835368531666321 * (h - 1.28571428571429) ^ 2 +
    0.000248841071006035 * (L - 3.57142857142857) ^ 2 +
    0.00724650933494119 * (V - 4.8571428571286) ^ 2)) +
    4.67864838696887 * 2.71828183^(-(0.0341952559501701 * (R -
```

```
2.57142857142857) ^ 2 + 0.0177803313628377 * (T -
            2.57142857142857) ^ 2 + 0.00835368531666321 * (h -
2.42857142857143) ^ 2 +0.000248841071006035 * (L -
6.85714285714286) ^ 2 + 0.00724650933494119 * (V -5.85714285714286)
^ 2)) + 3.22799277266754 * 2.71828183^(-(0.0341952559501701 * (R -
7.14285714285714) ^ 2 + 0.0177803313628377 * (T -3.57142857142857) ^
2 + 0.00835368531666321 * (h - 6.71428571428572) ^ 2
+0.000248841071006035 * (L - 7.28571428571429) ^ 2 +
0.00724650933494119 * (V -4.28571428571429) ^ 2)) + -
1.51435212791477 * 2.71828183^(-(0.0341952559501701 * (R -
4.71428571428571) ^ 2 + 0.0177803313628377 * (T -6.28571428571429) ^
2 + 0.00835368531666321 * (h - 1) ^ 2 + 0.000248841071006035 * (L -
2.71428571428571) ^ 2 + 0.00724650933494119 * (V -
4.14285714285714) ^ 2)) + -1.01824960839501 * 2.71828183^(-
(0.0341952559501701 * (R - 3.42857142857143) ^ 2 +
0.0177803313628377 * (T - 6.57142857142857) ^ 2 +
0.00835368531666321 * (h - 6.42857142857143) ^ 2
+0.000248841071006035 * (L - 1.42857142857143) ^ 2 +
0.00724650933494119 * (V -3.71428571428571) ^ 2)) + -
0.80311254694726 * 2.71828183^(-(0.0341952559501701 * (R -
5.57142857142857) ^ 2 + .0177803313628377 * (T -6.71428571428572) ^
2 + 0.00835368531666321 * (h - 7.42857142857143) ^ 2
+0.000248841071006035 * (L - 6.14285714285714) ^ 2 +
0.00724650933494119 * (V -5.71428571428571) ^ 2)) + 0.2204066945589
* 2.71828183^(-(0.0341952559501701 * (R - 2.85714285714286) ^ 2 +
0.0177803313628377 * (T -1.42857142857143) ^ 2 +
0.00835368531666321 * (h - 7.57142857142857) ^ 2
+0.000248841071006035 * (L - 7) ^ 2 + 0.00724650933494119 * (V - 2) ^
2)) + -0.733619450998502 * 2.71828183^(-(0.0341952559501701 * (R -
7.28571428571429) ^ 2 + 0.0177803313628377 * (T -6.42857142857143) ^
2 + 0.00835368531666321 * (h - 3.71428571428571) ^ 2
+0.000248841071006035 * (L - 6.28571428571429) ^ 2 +
0.00724650933494119 * (V -7.14285714285714) ^ 2)) +
3.06030943327587 * 2.71828183^(-(0.0341952559501701 * (R -
5.85714285714286) ^ 2 + 0.0177803313628377 * (T -2.42857142857143) ^
2 + 0.00835368531666321 * (h - 4) ^ 2 + 0.000248841071006035 * (L -
4.85714285714286) ^ 2 + 0.00724650933494119 * (V - 8) ^ 2)) +
0.0821664677226655 * 2.71828183^(          -(0.0341952559501701 * (R
- 2.28571428571429) ^ 2 + 0.0177803313628377 * (T - 1) ^ 2 +
0.00835368531666321 * (h - 5.42857142857143) ^ 2 +
0.000248841071006035 * (L - 5.71428571428571) ^ 2 +
0.00724650933494119 * (V - 6.85714285714286) ^ 2)) + -
5.53736420388543 * 2.71828183^(-(0.0341952559501701 * (R -
5.42857142857143) ^ 2 + 0.0177803313628377 * (T -
```

3.85714285714286) ^ 2 + 0.00835368531666321 * (h - 2.85714285714286) ^ 2 +0.000248841071006035 * (L - 1.14285714285714) ^ 2 + 0.00724650933494119 * (V -7.57142857142857) ^ 2)) + 1.51669291114801 * 2.71828183^(-(0.0341952559501701 * (R - 1.57142857142857) ^ 2 + 0.0177803313628377 * (T -6.85714285714286) ^ 2 + 0.00835368531666321 * (h - 1.42857142857143) ^ 2 +0.000248841071006035 * (L - 1.71428571428571) ^ 2 + 0.00724650933494119 * (V -6.42857142857143) ^ 2)) + -3.99059629419728 * 2.71828183^(-0.0341952559501701 * (R - 6) ^ 2 + 0.0177803313628377 * (T - 3.42857142857143) ^ 2 + 0.00835368531666321 * (h - 6.85714285714286) ^ 2 + 0.000248841071006035 * (L - 2.28571428571429) ^ 2 + 0.00724650933494119 * (V - 1.28571428571429) ^ 2)) + -7.39523376913684 * 2.71828183^(-(0.0341952559501701 * (R - 1.42857142857143) ^ 2 + 0.0177803313628377 * (T -3.14285714285714) ^ 2 + 0.00835368531666321 * (h - 3.42857142857143) ^ 2 + 0.000248841071006035 * (L - 3) ^ 2 + 0.00724650933494119 * (V - 6.71428571428572) ^ 2)) + 2.62489809661433 * 2.71828183^(-(0.0341952559501701 * (R - 5.28571428571429) ^ 2 + 0.0177803313628377 * (T -1.57142857142857) ^ 2 + 0.00835368531666321 * (h - 7) ^ 2 + 0.000248841071006035 * (L - 5.14285714285714) ^ 2 + 0.00724650933494119 * (V - 5.42857142857143) ^ 2)) + -7.56485341042804 * 2.71828183^(-(0.0341952559501701 * (R - 3.57142857142857) ^ 2 + 0.0177803313628377 * (T -3.28571428571429) ^ 2 + 0.00835368531666321 * (h - 5.85714285714286) ^ 2 +0.000248841071006035 * (L - 7.85714285714286) ^ 2 + 0.00724650933494119 * (V -5.28571428571429) ^ 2)) + 4.36941425118207 * 2.71828183^(-(0.0341952559501701 * (R - 4.14285714285714) ^ 2 + 0.0177803313628377 * (T -5.42857142857143) ^ 2 + 0.00835368531666321 * (h - 1.85714285714286) ^ 2 +0.000248841071006035 * (L - 4.57142857142857) ^ 2 + 0.00724650933494119 * (V -7.28571428571429) ^ 2)) + 5.06227274127653 * 2.71828183^(-(0.0341952559501701 * (R - 4.28571428571429) ^ 2 + 0.0177803313628377 * (T -2.85714285714286) ^ 2 + 0.00835368531666321 * (h - 6.28571428571429) ^ 2 +0.000248841071006035 * (L - 1.28571428571429) ^ 2 + 0.00724650933494119 * (V -6.14285714285714) ^ 2)) + -0.558436584369335 * 2.71828183^(-(0.0341952559501701 * (R - 1.14285714285714) ^ 2 + 0.0177803313628377 * (T -4.28571428571429) ^ 2 + 0.00835368531666321 * (h - 2.28571428571429) ^ 2 +0.000248841071006035 * (L - 1.85714285714286) ^ 2 + 0.00724650933494119 * (V - 3) ^ 2)) + -2.72378527157696 * 2.71828183^(-(0.0341952559501701 * (R - 2.14285714285714) ^ 2 +

```
0.0177803313628377 * (T -5.14285714285714) ^ 2 +
0.00835368531666321 * (h - 5.28571428571429) ^ 2
+0.000248841071006035 * (L - 4) ^ 2 + 0.00724650933494119 * (V -
1.14285714285714) ^ 2)) + 0.138767163330924 * 2.71828183^(-
(0.0341952559501701 * (R - 6.42857142857143) ^ 2 +
0.0177803313628377 * (T -1.85714285714286) ^ 2 +
0.00835368531666321 * (h - 5.57142857142857) ^ 2
+0.000248841071006035 * (L - 5.85714285714286) ^ 2 +
0.00724650933494119 * (V -1.57142857142857) ^ 2)) + -
2.63622282837113 * 2.71828183^(-(0.0341952559501701 * (R - 8) ^ 2 +
0.0177803313628377 * (T - 4.71428571428571) ^ 2 +
0.00835368531666321 * (h - 4.71428571428571) ^ 2 +
0.000248841071006035 * (L - 4.14285714285714) ^ 2 +
0.00724650933494119 * (V - 2.85714285714286) ^ 2)) +
4.61266741098594 * 2.71828183^(-(0.0341952559501701 * (R -
5.71428571428571) ^ 2 + 0.0177803313628377 * (T -
        4.42857142857143) ^ 2 + 0.00835368531666321 * (h -
3.85714285714286) ^ 2 +0.000248841071006035 * (L - 1) ^ 2 +
0.00724650933494119 * (V - 3.42857142857143) ^ 2)) + -
3.35698394004858 * 2.71828183^(-(0.0341952559501701 * (R -
4.42857142857143) ^ 2 + 0.0177803313628377 * (T -5.28571428571429) ^
2 + 0.00835368531666321 * (h - 4.42857142857143) ^ 2
+0.000248841071006035 * (L - 4.71428571428571) ^ 2 +
0.00724650933494119 * (V -4.42857142857143) ^ 2)) + -
11.6356368788031 * 2.71828183^(-(0.0341952559501701 * (R -
6.28571428571429) ^ 2 + 0.0177803313628377 * (T -2.14285714285714) ^
2 + 0.00835368531666321 * (h - 3.28571428571429) ^ 2
+0.000248841071006035 * (L - 6.71428571428572) ^ 2 +
0.00724650933494119 * (V -4.71428571428571) ^ 2)) +
10.2982163288411 * 2.71828183^(-(0.0341952559501701 * (R -
4.57142857142857) ^ 2 + 0.0177803313628377 * (T -4.85714285714286) ^
2 + 0.00835368531666321 * (h - 4.57142857142857) ^ 2
+0.000248841071006035 * (L - 7.71428571428572) ^ 2 +
0.00724650933494119 * (V -1.71428571428571) ^ 2)) +
4.16447053809088 * 2.71828183^(-(0.0341952559501701 * (R -
6.71428571428572) ^ 2 + 0.0177803313628377 * (T -1.14285714285714) ^
2 + 0.00835368531666321 * (h - 3.57142857142857) ^ 2
+0.000248841071006035 * (L - 2.85714285714286) ^ 2 +
0.00724650933494119 * (V -2.42857142857143) ^ 2)) +
0.292697254025541 * 2.71828183^(-(0.0341952559501701 * (R -
7.85714285714286) ^ 2 + 0.0177803313628377 * (T - 6) ^ 2 +
0.00835368531666321 * (h - 4.14285714285714) ^ 2 +
0.000248841071006035 * (L - 8) ^ 2 + 0.00724650933494119 * (V -
3.28571428571429) ^ 2)) + -0.371400257096364 * 2.71828183^(-
```

```
(0.0341952559501701 * (R - 1.28571428571429) ^ 2 +
0.0177803313628377 * (T - 5.85714285714286) ^ 2 +
0.00835368531666321 * (h - 7.85714285714286) ^ 2
+0.000248841071006035 * (L - 6.57142857142857) ^ 2 +
0.00724650933494119 * (V - 6) ^ 2)) + -2.18174894439838 *
2.71828183^(-(0.0341952559501701 * (R - 6.14285714285714) ^ 2 +
0.0177803313628377 * (T - 8) ^ 2 + 0.00835368531666321 * (h -
3.14285714285714) ^ 2 + 0.000248841071006035 * (L - 5) ^ 2 +
0.00724650933494119 * (V - 2.57142857142857) ^ 2)) +
5.31815620967638 * 2.71828183^(-(0.0341952559501701 * (R - 1) ^ 2 +
0.0177803313628377 * (T - 3) ^ 2 +
0.00835368531666321 * (h - 4.85714285714286) ^ 2 +
0.000248841071006035 * (L -5.57142857142857) ^ 2 +
0.00724650933494119 * (V - 4) ^ 2)) + 0.489583304271364 *
2.71828183^(-(0.0341952559501701 * (R - 7) ^ 2 + 0.0177803313628377 *
(T - 7.57142857142857) ^ 2 + 0.00835368531666321 * (h -
7.14285714285714) ^ 2 + 0.000248841071006035 * (L -
3.14285714285714) ^ 2 + 0.00724650933494119 * (V -
3.57142857142857) ^ 2
)) + -0.185877278339399 * 2.71828183^(-(0.0341952559501701 * (R -
7.57142857142857) ^ 2 + 0.0177803313628377 * (T -4.57142857142857) ^
2 + 0.00835368531666321 * (h - 6) ^ 2 + 0.000248841071006035 * (L -
3.28571428571429) ^ 2 + 0.00724650933494119 * (V -
6.57142857142857) ^ 2
)) + -3.87305474379277 * 2.71828183^(-(0.0341952559501701 * (R - 2) ^
2 + 0.0177803313628377 * (T - 7.71428571428572) ^ 2 +
0.00835368531666321 * (h - 2) ^ 2 + 0.000248841071006035 * (L - 6) ^ 2
+
0.00724650933494119 * (V - 5.14285714285714) ^ 2));
```

APPENDIX D

REGRESSION MODEL FOR LENGTH OF INSULATOR FOR DIFFERENT VOLTAGES

Following length are mentioned for different *kV* level in literature [11].

Table D-1 Dry arc length of insulators for different *kV*

S No	*kV*	Length
1	230	2000
2	345	2600
3	400	3350
4	500	5000

Based on above data following regression was developed using JMP

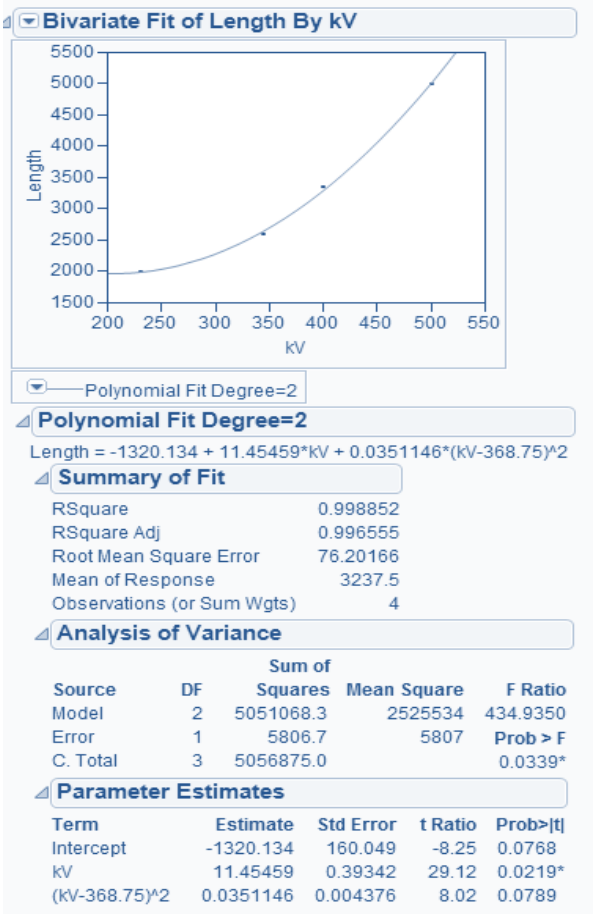

Figure D-1 Regression model for dry arc length of insulator obtained from JMP